POLITECNICO DI MILANO

School of Industrial and Information Engineering

Department of Mechanics

Doctoral Programme in Mechanical Engineering - XXVII Cycle

Human body response to multi-axial dynamical vibrations.

Doctoral Dissertation of:

Stefano SOLBIATI

Supervisor:

Prof. Giovanni MOSCHIONI

Tutor:

Prof. Marco Virginio BONIARDI

The Chair of the Doctoral Programme:

Prof.ssa Bianca Maria COLOSIMO

January 2015

Abstract

Aim of this doctoral dissertation is the study of the nonlinearities affecting the human body response under multi-axial whole-body vibrations (WBV). The research was entirely addressed to the characterization of the response for standing persons using a novel approach for the study of the nonlinearities of the body-transmitted vibrations.
The study of the nonlinearities was performed for both single-axis and multi-axial vibration. The reference parameter for the biodynamic response of the human body was the apparent mass, i.e. the frequency response function between the transmitted force and the applied acceleration.
In the first part of this work, nonlinearities were identified by conditioning the apparent mass deriving from the vertical WBV with a set of nonlinear functions of the acceleration. In the first part of the work both the acceleration and the force were measured only along the vertical direction.
Afterwards, the full (three-by-three) matrix was identified with a purposely-designed excitation system composed by two electrodynamic shakers and a tri-axial force plate. The excitation was initially mono-axial and the force was measured along the three coordinated axes. Both the symmetry of the apparent mass matrix and the effect of the vibration magnitude were assessed with paired t-student and Wilcoxon signed-rank tests. In the last part of the research, the response (forces along three mutually perpendicular directions) was measured with the uncorrelated excitation along two axes. The apparent mass derived in these conditions has been compared with the one obtained upon exciting a single axis.
The contributions of the nonlinear terms to the apparent mass were negligible and the nonlinearity was associated to the variation of the modal parameters in time (low frequency motion during the tests and involuntary muscular actions). The individual's response (i.e. APMS matrix) was more dependent on the vibration magnitude. Magnitude dependent effects may be overlaid by the uncertainty introduced by a large scatter in the population's biometric data. The conditioned APMS matrix (both population and individual) was comparable to that derived using linear estimators. The biodynamic response was influenced by the addition of a secondary transversal acceleration. In case of dual-axis excitations, the overall magnitude had a marginal contribution since dual-axis APMSs did not differ.

Keywords: whole-body vibration; non-linearity; apparent mass; multi-axis.

Acknowledgements

…to my family and all my friends
who had continuously supported me.

List of contents

List of figures

List of tables

Chapter 1

Introduction

The exposure of the human body to direct vibrations may cause serious physical disorders to the lower back also known as low-back-pain (LBP). This chapter aims to introduce the relevance of LBP from a physiological and an epidemiological point of view. The impedance methods for describing the biodynamic response are presented along with a summary of the previous studies about the response due to whole-body vibrations (both seated and standing persons). The scope of the dissertation and its organization by chapters will end this introduction chapter.

1.1 Low-back-pain

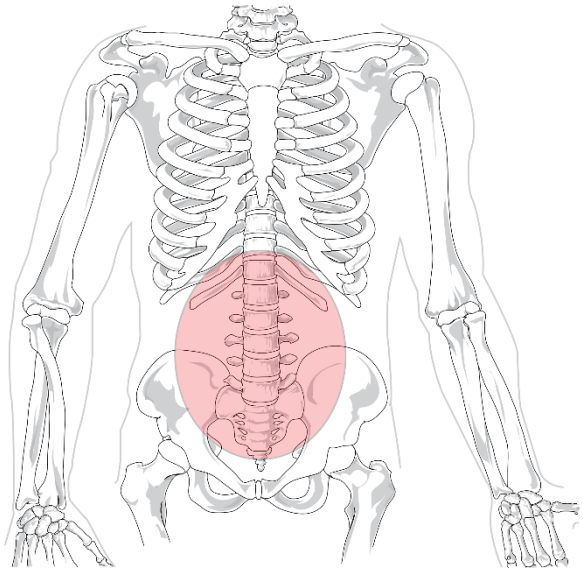

Figure 1.1 Definition-based anatomical location of LBP.

Low-back-pain, hereafter LBP, is the pain or discomfort felt in the area between the inferior margin of the twelfth rib and inferior gluteal folds [1, 2] (Figure 1.1). Despite people tend to underestimate this pathology, many epidemiologic studies evidenced that LBP is a widespread health problem, which everyone may encounter at least once in life [1]. Research on this topic has considerably increased in the recent years, being supported by the latest Global Burden of Disease (GBD) Study (end of 2012) that placed LBP at the top in the ranking

among the globally most disabling diseases [3]. In such study, LBP was presented as the global most invalidating disease with 83 million of years lived with disability (YLDs), about 10.7% of global YLDs. YLDs refers to the "years lived in less than ideal health", i.e. the number of incident cases multiplied by the average duration of the condition [3]. The estimate dramatically rose from previous results (58.2 million YLDs in 1990) such to bring this pathology to the attention of researchers. Besides a huge clinical relevance, LBP was found to determine an identical impact on both society and financial burden of entire countries all over the world. Such transversal impacts include participation restrictions, carer burden, use of health-care resources and financial burden (i.e. direct costs for assessing, treating, medical care, indemnity payment, productivity loss) [1, 4, 5].

1.2 WBV and LBP

Whole-body vibration (WBV) is the mechanical vibration transmitted to the whole body and may entail risks to the health and safety of workers, in particular lower-back morbidity and trauma of the spine [6]. People are normally exposed to whole-body vibrations, at workplace (e.g. trucks or busses drivers) or during their daily life (on board of means of transport), and many categories of workers result at risk since they are exposed to high levels of vibrations many hours a day or during their entire work life.
The link between LBP and exposure to WBV at workplace has been studied since 1960s [7]. In spite the risks from hand-transmitted vibration (i.e. the vibration transmitted to the hand-arm system) have been well assessed and their effects on health also clearly reported, the hazardous nature of WBV was not so evident and the health risks had been initially underestimated [7]. The main reason was the poor quality of the early epidemiologic studies in which there were no information about the exposure (both magnitude and duration), the employers' occupational history and the lack of a control group [7, 8]. On the other hand, epidemiologic studies progressively increased in quality and in the recent years was clear the tendency that long-term occupational exposure to WBV is harmful for the spinal system and a severe risk factor for LBP [7, 8]. Besides LBP, other frequently reported health effects are sciatic pain, early degeneration of the lumbar spine and herniated lumbar disc [7, 8]. Further studies evidenced that driving occupations (e.g. crane operators, tractor drivers, etc…) are specifically associated to LBP due to the continuous exposure to WBV and other ergonomic risk factors (i.e. sitting posture, non-neutral trunk movements, weight lifting and carrying) [2, 8, 9]. Nevertheless, a direct assessment of the role of either WBV or ergonomics on the aetiology of LBP disorders is difficult since their contribution cannot be clearly split.

1.3 EU legislation

Due to the increasing understanding of the disorders caused by LBP, the authorities were forced to bring appropriate proceedings. In September 1990 the European Parliament urged the European Commission to issue a directive in which both noise and vibration managements were directly ruled. In 2002, such final text was issued and the minimum health and safety requirements established in order to ensure basic safety measures against the risks from noise and vibrations at workplace. Such measures were introduced not only with the aim of preserving both the health and safety of individuals but also to create a common reference for all workers within the European Union [6].

1.4 Impedance methods

Instead of the above-mentioned epidemiological studies, body-transmitted vibrations may be treated under a biomechanical approach. In facts, experimental data can be collected under controlled conditions and, afterwards, both the effects and the risk of injury can be studied from the so-obtained mechanical responses [10].
The biomechanical response of human beings can expressed in terms of:

1. impedance methods;
2. transmissibility methods;
3. mathematical models;
4. other mechanical responses (i.e. biomechanical markers, EMG, etc…).

The impedance methods require the measurement of the force and the acceleration at the driving point, the point through which the vibration is transmitted to the body (Figure 1.2). The transmissibility methods allow deriving how the vibration is transmitted from the driving point to different segments of the body: accelerations are directly measured by accelerometers fixed on the skin. Mathematical models imply the use of analytical or physical models (i.e. anthropodynamic dummies) whose responses strongly depend on the data collected using the first two approaches. The other methods are occasionally used in some application and in any case, they have not an immediate usage [10].

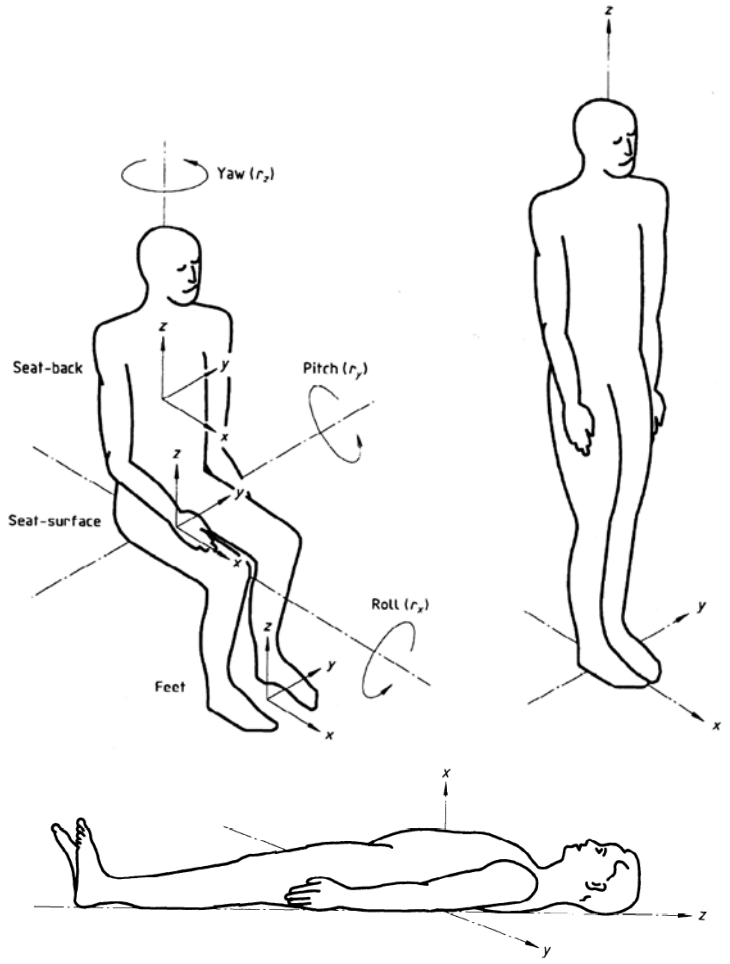

Figure 1.2 Driving point definition for the seated, the standing and the supine persons (Ref. [11]).

Among the four methods, the impedance methods are the most reported in the literature, given that they have relevant applications not only in the study of pathologies related to the vibration exposure but also in the study of interactions between civil structures and the body. Consequently, the human body response is often expressed in terms of mechanical impedance or apparent mass; from these two quantities one may retrieve the resonances of the human body, i.e. the frequencies to which the body is most sensitive to vibrations [10].
The transmitted forces at the driving point are generally measured by load cells supporting a rigid metal plate, whose inertial contribution should be subtracted from the measured forces.
In the field of the biodynamic response of the human body, the driving point mechanical impedance and the apparent mass are computed as transfer functions

(i.e. ratio between spectral quantities) and they can be alternatively computed according to the power spectral density (PSD) method

$$TF_{PSD}(f) = \sqrt{\frac{S_{yy}(f)}{S_{xx}(f)}} \tag{1.1}$$

or to the cross-spectral density (CSD) method

$$TF_{CSD}(f) = \frac{S_{xy}(f)}{S_{xx}(f)} \tag{1.2}$$

The CSD method is preferred to the PSD method because it preserves the phase information and reduces the effect of noise. The extent of correlation between the input and the output is expressed by the coherence function:

$$\gamma^2(f) = \frac{\left|S_{xy}(f)\right|^2}{S_{xx}(f) \cdot S_{yy}(f)} \tag{1.3}$$

The coherence is a value between 0 and 1: the greater the coherence, the greater the correlation between the two signals [10]. In this work the PSD and CSD methods will be compared with the FRF estimators and the conditioned system response, that are commonly used in the study of linear and nonlinear systems [12, 13].

1.5 State-of-the-art

First studies on the human body response to WBV were earlier than the 1990s. When the first standard concerning WBV was published (ISO 5982:1991) it was clearly inadequate due to the lack of a deep knowledge of the phenomenon.
In the last twenty years, the interest in this field rapidly increased because of the global warning launched by many epidemiological studies about the hazardous nature of body-transmitted vibrations. Hence, several studies were carried out with the aim to describe the response, in terms of appropriate functions, and to identify the main influencing parameters.
Among the first studies on WBV, Lundström proposed the vibration energy as a new quantity for risk assessment [14]. He considered this quantity more significant than the acceleration level measured at the vibrating surface (ISO 2631-1:1997) because it accounted for the dynamic forces applied to the body. His work showed that the absorption of energy was related to the frequency of the excitation, its magnitude and direction, the posture of the upper-body, the weight and the gender. Seated subjects were exposed to sinusoidal vibrations maintaining

their upper-body at two distinct postures (erect and relaxed). The absorbed power generally showed a peak in the range 4-6 Hz; females also exhibited a secondary peak at about 9 Hz. A change in the upper-body posture, from erect to relaxed one, increased the resonance in magnitude and decreased it in frequency.

Meanwhile, the mechanical impedance of the seated human body has been characterized along the fore-and-aft and the lateral directions [15]. It was found dependent on frequency, vibration magnitude, upper-body posture (erect and relaxed) and gender. Subjects were submitted to sinusoidal stimuli along both the fore-and-aft and lateral directions; cross-axis mechanical impedances were not characterized. A primary resonance peak was observed in the range 2-5 Hz for both mechanical impedances; a secondary peak, between 5 and 7 Hz, along the lateral direction. They also found that for increasing vibration magnitudes both the resonance frequencies and peaks decreased.

Mansfield and Lundström characterized the apparent mass of the seated human body due to combined fore-and-aft and lateral random vibrations, by exciting subjects along non-orthogonal directions [16]. This method allowed to expose both the x- and y-axis to simultaneous vibrations, but stimuli were evidently correlated to each other. Resonance frequencies along both the x-and y-directions agreed with previous results given by Holmlund [15]. Gender was not found statistically significant as opposed to the direction of vibration which affected the apparent mass. Nonlinearity was retrieved in apparent masses as vibration level increased: resonance frequencies decreased and peaks rose. In addition, the authors proved that the principle of superposition could not be applied when predicting horizontal vibrations.

The mechanical impedance of the seated human body was investigated by exposing subjects to sinusoidal stimuli in the vertical direction [17]. The impedance was found dependent on the frequency and the magnitude of vibration, the upper-body posture (erect and relaxed) and the weight of subjects; gender was not statistically significant. Impedance showed three resonances: the first between 4 and 6 Hz, the second and the third in the range 8–12 Hz and 50-70 Hz, respectively. Nonlinearity with respect to the vibration level was found, the same as previously reported for horizontal vibrations [15].

The apparent masses at different locations on the abdomen, the lumbar spine and the pelvis were evaluated for the seated human body exposed to random vertical WBV [18]. The responses, which generally agreed with previous results in the literature, were found dependent on the vibration magnitude. The resonance frequencies all decreased but, as opposite to [15, 17], their magnitudes increased with the excitation level.

In vehicle measurements, the mechanical impedance of the seated human body was found different from that derived in laboratory [19]. In both cases, the impedance was characterized along the x-, y- and z-axis with different postures (erect and relaxed) and excitations: during in field measurements subjects were exposed to multi-axis vibrations as opposite to in laboratory results, derived by

applying sinusoidal vertical stimuli. The in laboratory mechanical impedance agreed with previous results [15, 17]: the same nonlinearity with respect to the vibration magnitude was also evident. Important cross-coupling effects were found thus avoiding the extension of single-axis data in case of multi-axis excitations.

The apparent mass of the seated human body was strongly influenced by the position of hands and by the weight [20]. Subjects were exposed to random vertical vibrations on a seat provided with an inclined backrest; experiments were performed by varying two sitting postures, hands on laps (passenger) and hands on a steering wheel (driver), and three positions of the feet. When subjects took their hands on laps, the apparent mass showed a primary resonance between 6.5 and 8.6 Hz; when they adopted a driving posture (hands on steering wheel) the apparent mass changed in shape showing two resonances at 5.1-8.25 Hz and 8-12 Hz, respectively. The apparent masses were also different in magnitude: the passenger's one was greater than the other. Nonlinearity with respect to the vibration magnitude was found similarly to [18] while the position of feet slightly influenced the apparent mass. Authors found that resonance frequencies and peaks decreased and increased respectively as the body mass rose. However, such dependence was less evident after normalizing the magnitude with respect to the body weight.

The effects of sitting posture and vibration magnitude were investigated by comparing the apparent masses, due to vertical random vibrations, for nine different upper-body postures [21]. The apparent masses were similar in shape with those previously reported in the literature, affected by the same nonlinearity with respect to the vibration magnitude as stated in [16, 18]. Resonance frequencies were found generally dependent on the vibration magnitude rather than on a change of posture. However, a decrease in the resonance frequencies was observed for postures that provided a large contact area.

Nawayseh presented a study in which he investigated the effect of thigh contact on the apparent mass of the seated human body along with the forces exerted on the seat and footrest during vertical WBV [22]. Subjects were exposed to random vertical vibration on a rigid seat without backrest; postures were changed by varying the height of the footrest thus realizing different extent of thigh contact. The apparent mass in the vertical direction was similar in shape with previous results; nonlinearity with respect to the vibration magnitude was found for all postures as Mansfield [21]. The apparent mass magnitude decreased as the thigh contact reduced while its resonance frequencies were no statistically affected by the postures. The cross-axis apparent masses were evaluated along the fore-and-aft and the lateral directions. Considerable forces were found along the fore-and-aft direction with a resonance peak at about 5 Hz; such resonance shifted to lower frequencies as the vibration magnitude increased. However, the shape of the cross-axis apparent mass in the fore-and-aft direction was found dependent on the posture. The cross-axis apparent mass along the lateral direction was found

negligible in magnitude. The vertical apparent mass at the feet changed in shape with postures and showed a nonlinear behaviour, which reduced as the thigh contact decreased.

The effect of sitting posture on the apparent mass of the seated human body exposed to random vertical vibration has been investigated by Wang [23]. Changes in postures were realized by changing the seat height, the hands position (hands on lap or on a steering wheel) and the inclination of both the backrest and the seat pan. Apparent masses agreed with previous results in the literature either in case of backrest or without a back support; the same dependence on the mass of subjects was found as observed by Rakheja [20]. The static weight at the seat was found affected by the seat height and by the back support (maximum effect with an inclined backrest); the inclination of the seat pan was found negligible. Hands position was found relevant in case of inclined backrest and for those frequencies in vicinity to the primary resonance. The apparent mass was not significantly affected by the seat height although its magnitude at resonance was found slightly reduced at high seat height. Hands position was found statistically relevant for both the resonance frequency and magnitude only in case of inclined back support. Under vertical backrest, hands position was found significant for the only magnitude; no difference was found in case of no back support. Apparent masses were found similar for both genders even if a second resonance peak was found at about 15 Hz for females thus confirming previous observations [14, 15]. Nonlinearity with respect to the magnitude of vibration was retrieved as previously reported in the literature.

A comparison between the responses due to both sinusoidal and random vibrations has been reported by Mansfield [24]. His study aimed to compare the apparent masses derived for seated subject exposed to two types of vertical vibrations; trials were performed without adopting a back support. Results were in agreement with those reported in the literature for both the stimuli. There were no differences between the apparent masses derived from different excitations except for the phases that showed some slightly discrepancy. The work of Mansfield was limited to one level of magnitude without investigating the effect of different levels of excitation. In facts, previous articles have outlined some nonlinearity with respect to the magnitude but results seemed to be in contrast with a change in stimulus. In case of random vibrations, as the magnitude increased the resonance frequency decreased and the peak magnitude rose. As opposite, both the resonance magnitude and frequencies decreased for the sinusoidal stimuli [15, 17].

The effect of backrest and twist of the upper body on the apparent mass of the seated human body was reported by Mansfield [25]. Subjects were exposed to random vertical vibrations under different sitting postures: back without any support, back in contact with a backrest, twist of the upper body, sequential movement of the upper body so as to produce a change in the posture. Both the apparent mass and cross-axis apparent masses were evaluated. Results were in

good agreement with those reported in the literature: the apparent masses showed two resonances at about 5 Hz and 12 Hz except for the moving posture where the first resonance peak was less evident and the second one was totally absent. In this last case, the apparent mass magnitude was always less than those obtained from the other postures and the coherence function was low too. Results from the literature [22] agreed with the experimentally obtained cross-axis apparent masses. For the fore-and-aft apparent mass, the peak at about 6 Hz was found absent for the only moving posture.

The apparent masses at the seat and footrest for the seated human body exposed to fore-and-aft WBV were studied by Nawayseh [26]. Results were given for different magnitudes of vibration and postures: back supported or not by a backrest and four conditions of thigh contact, realized by varying the height of the footrest (feet hanging, maximum, average and minimum thigh contacts). Without a back support, the apparent mass showed three vibration modes at about 1 Hz, 1-3 Hz and 3-5 Hz; the vertical cross-axis apparent mass was found high in magnitude as opposite to the lateral cross-axis apparent mass whose magnitude was negligible. At the footrest, a resonance was found between 3 Hz and 5 Hz in the fore-and-aft direction; in case of backrest the resonance frequency decreased and the apparent mass changed in magnitude across all frequencies. In the vertical direction, a resonance was found at about 1 Hz that in case of backrest increased to 5 Hz. Apparent masses and cross-axis apparent masses have shown nonlinearity with respect to the vibration level, the same reported in case of random vibrations. Nawayseh investigated the forces along the x-, y- and z-axis on the seat and backrest during the fore-and-aft WBV of seated persons [27]. Subjects were exposed to random vibrations under different sitting postures (feet hanging, maximum, average and minimum thigh contacts) obtained by varying the height of the footrest [22]. In the fore-and-aft direction, the response on the seat was found dependent on the thigh contact: the apparent mass had a peak in the range 2-6 Hz, for all posture, and an additional resonance at about 1-2 Hz for the only feet hanging posture. Comparing results with those in [26], the backrest was found to modify the shape of the apparent mass. The apparent mass along the fore-and-aft direction showed two peaks at frequencies less than 2 Hz and in the range 3-5 Hz; it was hypothesized that the second resonance could be related to the tissues of the buttocks. In the vertical direction, the resonance at the seat was in the range 6-8 Hz, depending on the vibration magnitude. The apparent mass was higher in magnitude for the only minimum thigh contact posture while resonance frequencies were not statistically affected by posture changes. The vertical cross-axis apparent mass at the backrest and both the lateral cross-axis apparent masses at the seat and backrest were negligible in magnitude. Forces in all directions, on the seat and backrest, showed nonlinearity with respect to the vibration magnitude.

The effects of vibration magnitude and muscular activity on the apparent mass of the seated humans were investigated under random vertical vibration [28]. The

apparent masses were characterized in case of relaxed upright sitting posture, similar to that described in [26], and in case of periodic movements of the body. Nonlinearity was studied by identifying the parameters of an equivalent 2 DOF model for all the different conditions. The nonlinearity associated to the vibration magnitude reduced greater in case of movement of the body than in case of postural changes.

A comparison between biodynamical responses of the seated humans, in terms of the apparent masses, due to single and dual axis WBVs was proposed by Mansfield [29]. Results were similar to those reported in the literature for both the postures with and without a back support. Cross-axis apparent masses were also in agreement with those stated in previous studies. In general, apparent masses and cross-axis apparent masses were found similar in shape independently on the type of stimulus. Due to this fact, authors stated that models derived from single-axis stimuli could be applied to multi-axis conditions even if they observed a general reduction of the resonance frequencies in case of dual-axis excitations. The major contribute to the cross-axis apparent masses was found between the x- and z- directions.

Nonlinearity in the apparent mass of the seated humans was investigated by Mansfield [30] by exposing subjects to different combinations of stimuli and postures. Nonlinearity with respect to the vibration magnitude and cross-axis apparent masses were in agreement with previous results in the literature involving random vibrations and sitting upright postures. In case of tense postures, the primary resonance frequencies were found higher than those obtained with relaxed postures; however, resonance peaks were not affected by the muscular activity. Cross-axis apparent masses' data suggested that nonlinearity in the vertical direction is partly due to the pitching motion of the upper body. An important finding was that nonlinearity and resonances in the apparent masses were dominated by the magnitude of those frequencies near the peak and not by the overall level of the excitation.

Biodynamical responses of the seated humans under both single and tri-axial random vibrations were characterized by Mansfield [31], similarly to what he previously presented [29]. The direct and the cross-axis apparent masses were derived under different magnitudes of vibration and postures (with backrest and without a back support). Results showed that the apparent masses were primarily affected by the magnitude of vibration along the measuring direction and partly affected by vibrations in the other directions; in any case, this cross-coupling effect had the same extent of nonlinearity due to the vibration magnitude. Statistical analysis confirmed that responses due to multi-axis stimuli were different from those obtained in case of single-axis excitations thus suggesting an improvement of the existing mathematical models.

The absorption of energy for the seated human body was investigated at the seat pan and backrest under horizontal vibrations (fore-and-aft and lateral directions) [32]. Subjects were exposed to uncorrelated random vibrations along both x- and

y-axis directions; the effects of three sitting postures (no back support, vertical and inclined backrest) and three seat heights were investigated. The absorbed energy was strongly influenced by the back support, excitation magnitude and body mass; its spectrum was found similar in shape to the apparent masses derived in the same conditions. The backrest increased the primary resonance frequency while the resonance peak slightly decreased with an inclined back support; an opposite behaviour was found along the lateral direction where the absorbed power increased under inclined backrest.

In the work by Wang [33], a comparison between the vertical apparent mass and the seat-to-head transmissibility, results from the first function were in agreement with previous studies in the literature. However, the apparent mass in case of inclined backrest and seat pan showed a higher resonance frequency with respect to what previously stated [23].

The effect of backrest on the vertical apparent mass of the seated human body was investigated by changing sitting postures (no back support, vertical and inclined backrest), inclination of the back support and thickness of foam backrest [34]. Results agreed with previous studies in the literature for what concerned the resonances without and with a vertical rigid backrest, the decrease in the static apparent mass and the increase in the resonance frequencies in case of back support and of inclined backrest, respectively. They found that the resonance frequencies were little affected by contact with either a rigid or a foam vertical backrest; however, the thickness of foam was found relevant when the backrest had the maximum inclination.

The effect of footrest and of a steering wheel was investigated by varying their position with respect to the seated human body and the applied forces [35]. Subjects were exposed to random vertical vibrations sitting on a rigid seat with a reclined backrest and adopting either a driving or a passenger like posture. The apparent masses were similar to those reported in the literature in case of backrest contact and in case of hands on a steering wheel [23]. Moving the steering wheel far from the body had reduced the primary resonance peak and increased the magnitude of the apparent mass at the 4 Hz secondary resonance; when the feet moved forward, the static mass reduced in magnitude. As a consequence of the forces applied on both the footrest and steering wheel, the apparent mass at resonance and the static mass decreased in magnitude without any change in the resonance frequency.

Nawayseh investigated the power absorbed by the seated human body while exposed to random vertical vibrations [36]. Subjects, similarly to [22, 26, 27], were exposed to vertical vibrations while sitting with and without a backrest and under four postures realized by changing the footrest height. Results were in agreement with previous studies: a primary resonance frequency at about 5 Hz and a secondary resonance between 8 and 10 Hz, more evident in case of increased thigh contact. The absorbed power increased following a quadratic law with respect to the vibration magnitude at the seat, the footrest and at the backrest. The

absorbed power evaluated at the feet was in agreement with previous results in the literature [22]; in particular, the total absorbed power reduced at higher footrest heights. The backrest was observed to reduce the absorbed power at low frequency while increasing that at higher frequencies [27].
The influence of age, gender, weight and body mass index on the apparent mass along with the effect of vibration magnitude and backrest on the inter-subject variability were investigated by Toward [37]. Subjects were exposed to random vertical vibrations under four back support conditions (no backrest, vertical rigid backrest, inclined rigid and foam back supports). The body weight was found the strongest predictor of the modulus of the apparent mass while the primary resonance frequency was correlated to the age and the body mass index: the first increasing and the second decreasing the frequency. Such influences were found more relevant than those associated to changes in posture. The inter-subject variability reduced after normalizing the apparent mass with respect to the sitting weight. Nonlinearity with respect to the vibration magnitude was found affected by the gender and generally coherent with previous findings.
The apparent mass of the seated human body exposed to fore-and-aft, vertical and dual-axis WBVs was derived using two different frequency response estimators (H_1 and H_v) [38]: subjects were exposed to uncorrelated random vibrations under different hand and back support conditions. The responses under single axis excitations were similar for both the estimators while differed for the case of dual-axis excitations: the H_v estimator was able to account for the cross-coupling effects thus producing estimations higher in magnitude. Under dual-axis vibration, supported postures (both hands and back) resulted less coupled and the associated apparent mass in the fore-and-aft direction increased in magnitude with respect to unsupported conditions.
The power absorbed by the seated human body was evaluated at the seat, the footrest and the backrest [39]: subjects were exposed to random fore-and-aft vibration under postures with and without a back support. Results, in terms of resonances and shape, were in agreement with previous findings [14, 32]. Both the footrest and backrest affected the resonance frequency and magnitude of the absorbed power function. In particular, the backrest increased the magnitude at low frequencies and increased it at higher frequencies; the total absorbed power at the backrest was greater than that measured at the seat.
The apparent mass of the seated human body was investigated under single and simultaneous x-, y- and z-axis vibrations [40]. Subjects were exposed to random uncorrelated vibrations along the three axes under different hands support conditions (hands on leaps and on a steering wheel) and back support conditions (without and with a vertical backrest). As in his previous work [38], the responses were evaluated using two different frequency response functions (H_1 and H_v). Results in case of single axis excitations were similar but differed in case of multi-axis excitations: the H_1 estimator tended to suppress the cross-axis couplings

between the body motions [38]. Hands and back support conditions had significant effects on the couplings between body motions.
The effects on the vertical apparent mass of the vibration magnitude and of an additional fore-and-aft vibration were investigated by Zheng [41]. Results, in terms of the vertical apparent mass and the fore-and-aft cross-axis apparent mass, agreed with previous findings [22]: nonlinearity with respect to the vibration magnitude was found for both the apparent masses as the vertical vibration magnitude increased. Similarly, the resonance frequencies decreased in case of constant vertical vibration magnitude and increasing excitation along the fore-and-aft direction. Such nonlinearity was explained by the coupling between the fore-and-aft and the vertical motions of the body.

1.6 Conclusions

Body-transmitted vibrations could lead to serious consequences on health. Vibration transmitted to the body generate cyclic stresses critical for the spine and may lead to musculoskeletal disorders (i.e. low-back pain) besides physical and psychological fatigue.
Many studies focused on understanding the dynamics of the body both in seated and standing postures. These studies evidenced a general nonlinear behaviour which was investigated under different experimental conditions (i.e. vibration magnitude, postures and other anthropometric parameters). Despite the huge amount of material, the variability of the human body dynamics was not still clearly understood, being the issue more complex than expected; the main open issue, is that the variability due to the nonlinear behaviour of the biodynamic response has not been systematically compared to the inter- and intra-subject variability.

1.7 Scope of the dissertation

The research activity was focused on the identification of the nonlinearities affecting the response of the human body exposed to whole-body vibrations. Our study was oriented on the characterization of the response, expressed in terms of the apparent mass, of the standing people. This field was not completely explored and few works were reported in the literature. Besides the lack of material, the largely described nonlinear behaviour was often in contrast or not fully supported by the experimental results: e.g. nonlinearities with respect to the vibration magnitude were found even if the ordinary coherence function was close to unity.
The research activity was carried out according to the following steps:

1. characterization of the apparent mass in case of vertical whole-body vibration;
2. identification of the nonlinearities;

3. design and realization of a suitable excitation system and setup for measuring the apparent masses in the basicentric reference system;
4. characterization of the full (three-by-three) matrix of apparent masses for the standing persons;
5. characterization of the response in case of multi-axial vibrations (no more than two axis contemporarily excited).

1.8 Organization of the dissertation

The thesis was organized in eight chapters, following the main steps above described. The apparent masses of standing people exposed to vertical whole-body vibrations were reported and described in Chapter 2. In Chapter 3, such data were processed to get the conditioned apparent masses so as to outline and study the nonlinearities in the biodynamic response. The design of a dual-axis excitation apparatus and the calibration of the measurement setup were introduced in Chapter 4 and Chapter 5, respectively. The full three-by-three matrix of the apparent masses, due to independent excitations along each axis of the basicentric reference system, was derived in Chapter 6. The effect of a second axis of excitation was presented in Chapter 7. At Chapter 8, conclusions and main suggestions for further works.

Chapter 2

Apparent mass variability

In this chapter, the apparent mass for standing people under vertical whole-body vibration was derived using the cross-spectral density method. A brief introduction of the state of the art, with regard to the apparent mass of standing subjects, the method and the results were provided along with their discussion.

2.1 Introduction

The biodynamic response of the human body has been extensively investigated in the sitting posture, analysing the effect of anthropometric angles and of the vibration magnitude. On the contrary, the number of studies focused on the characterization of the response for standing subjects is more limited [42-48].
Previous studies evidenced a dependence of the apparent mass on the adopted posture [45, 46, 48]. For instance, the main resonance frequency significantly decreased when passing from straight to bent knees. An additional dependence was found with respect to the vibration magnitude [45, 46]: resonances shifted to lower frequencies for increasing acceleration levels. Matched paired tests between the medians revealed significant differences in both the resonance frequency and amplitude. Consequently, the mathematical models developed for predicting the biodynamic response of the human body accounted for both the posture and the vibration magnitude [49, 50]. Linear lumped parameter models consisted of either simple inertial equivalent systems [49] (i.e. single or two DOFs) or more complex anatomical models, with the aim of representing the motion of each segment (i.e. the upper body, the pelvic region, the shanks, the thighs, the visceral region, the legs, etc…). For the anatomical models, both inertial and geometric parameters were generally retrieved from previous studies and anthropometric data [50]. In both cases, the parameters were calculated after fitting the analytical results with the experimental data (i.e. by minimizing a proper error function). The model parameters (i.e. stiffness and damping) changed with the vibration magnitude: they tenderly reduced in value at higher accelerations [50].
Aim of this chapter is to derive and to evaluate the effect of posture and of the vibration magnitude on the apparent masses derived for standing subjects exposed to vertical whole-body vibrations.

2.2 Experimental method

2.2.1 Apparatus

The experimental setup is shown in Figure 2.1; an electrodynamic shaker (Table 2.1) generated the required vertical vibration, which was transmitted to standing subjects by a rigid metallic plate (500 x 500 mm in size). Structure's resonances occurred above 60 Hz, i.e. the first natural frequency of the supporting surface, which was generally far enough from the investigated range of frequencies (2 - 20 Hz). The force transmitted through the shaker-plate interface was measured by three piezoelectric load cells PCB 212B (Table 2.2), whose sensitivity has been identified with a fit-to-purpose calibration procedure, and the plate acceleration was measured by a piezoelectric accelerometer (Table 2.3). Anyway, the acceleration was not measured at the driving point but near an edge of plate (Figure 2.2) because it behaves as a rigid body in the frequency range of interest. Both the acceleration and force signals were filtered and amplified by two B&K Nexus conditioning units (band-pass filter between 0.1 Hz and 100 Hz) and eventually sampled by two NI 9234 acquisition modules (24 bits A/D converter, sampling frequency of 2500 Hz). Signals were digitized and stored on a personal computer; the collected time histories were afterwards processed off-line.

Figure 2.1 Snapshot of the laboratory instrumentation for the characterization of the apparent mass.

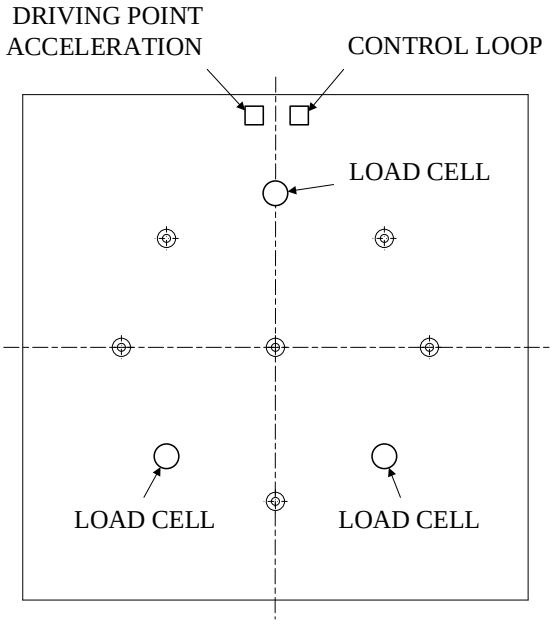

Figure 2.2 Transducers' placement on the force plate.

Table 2.1 Electrodynamic shaker's specifications.

Company	LDS Test and Measurements
Model number	V830/335
Maximum stroke	± 50.8 mm
Random force	9.81 kN RMS
Usable frequency range	0 – 3000 Hz
Maximum acceleration (random)	588.4 m s^{-2} RMS (60 g)

Table 2.2 Load cells' specifications.

Company	PCB Piezotronics, Inc.
Model number	212B
Type	In-line (uniaxial)
Sensitivity (± 15%)	4047 pC/kN
Measurement range (compression)	≤ 44.48 kN
Maximum static force (compression)	66.72 kN
Upper frequency limit	60 kHz
Non-linearity	≤ 1%
Preload	8.896 kN

Table 2.3 Accelerometer's specifications.

Company	Brüel & Kjær
Model number	4508B
Sensitivity	9.87 mV/(m s^{-2})
Frequency range	0.3 – 8000 Hz
Measuring range	±700 m s^{-2}

2.2.2 Subjects

Eight male subjects (students and staff of the Politecnico di Milano) were involved in the experiments, which were carried out in compliance with both the EU legislation on workers' vibration exposure [6] and with the Politecnico di Milano ethics guidelines. Subjects' biometric data are summarized in Table 2.4.

Table 2.4 Subjects' biometric data.

Subject	Age (years)	Height (cm)	Weight (kg)	BMI (cm^2/kg)
1	28	170	66	23
2	27	167	55	19
3	25	171	67	23
4	26	181	73	22
5	30	176	72	23
6	29	173	78	26
7	18	165	60	22
8	18	176	70	23
Average	25.1	172.4	67.6	22.6
SD	4.7	5.2	7.4	1.9
Median	26.5	172	68.5	23

2.2.3 Stimuli

Subjects were exposed to Gaussian white noise signals (bandwidth 2 - 20 Hz) at three different vibration magnitudes (0.5 m s^{-2}, 1.0 m s^{-2} and 1.5 m s^{-2} RMS; PSD functions at Figure 2.3). Input signals were synthetized each time, by changing the settings of the control software (LMS Virtual.Lab Rev 7). This method should provide for more information with respect to the commonly used procedure in which the same three acceleration waveforms were used in each session of trials [46]. The order of presentation for the stimuli was randomized in order to prevent fatigue phenomena.

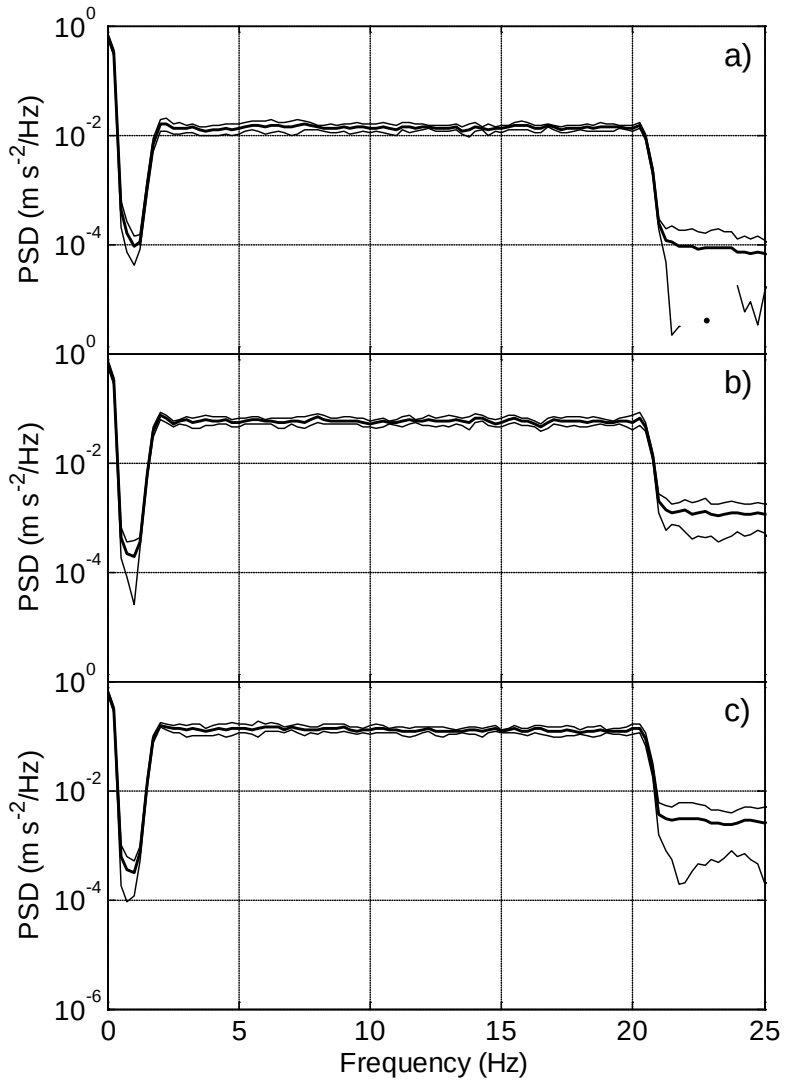

Figure 2.3 Power spectral density functions of the accelerations generated by the electrodynamic shaker: a) 0.5 m s^{-2}, b) 1.0 m s^{-2}, c) 1.5 m s^{-2} RMS.

2.2.4 Postures

During the experiment, subjects stood on the force plate in two different postures: upright posture with straight legs and upright posture with bent legs, with angle of 150° verified with an artefact (Figure 2.4). In both postures, subjects kept their feet 25 cm apart, wearing their own shoes (the apparent mass is weak effected by the feet/plate interface [48]). As for the stimuli, postures were presented randomly and the total exposure duration did not exceed 60 seconds for each configuration (total vibration exposure approximately 360 s). In addition, subjects were advised to look straight to a fixed point during the trial and to maintain the same posture without any involuntary movement of the body.

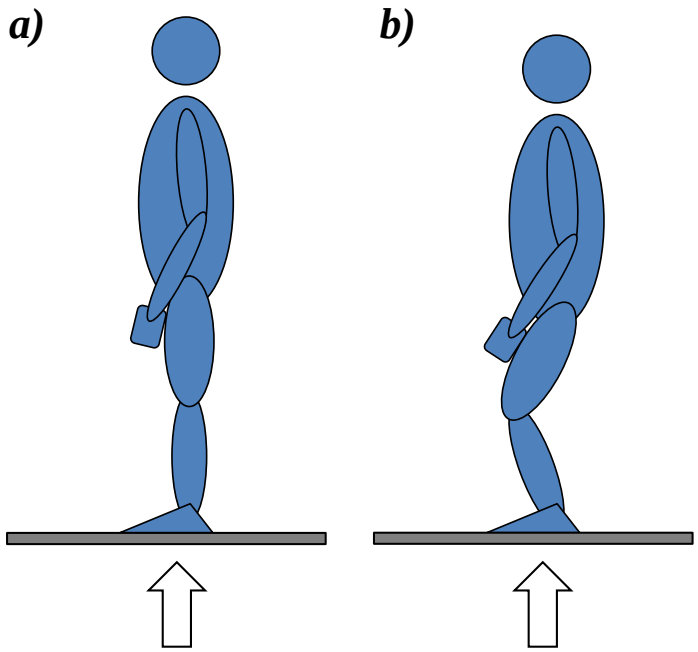

Figure 2.4 Adopted postures: a), upright with straight legs; b), upright with bent legs.

2.3 Data processing

2.3.1 Vertical apparent mass

The biomechanical response of the human body under vertical WBV was expressed in terms of the apparent mass (APMS) which was derived by the use of the cross-spectral density method (CSD). The so obtained apparent mass ($APMS_{CSD}$) was provided with both magnitude and phase information along with

the ordinary coherence function. Results were presented with a frequency resolution of 0.25 hertz.
Before proceeding with the data analysis, the dynamic force introduced by the plate was removed by mass cancellation in the time-domain: from the time history of the load cells was subtracted the product between the acceleration and the static mass of the plate. The apparent masses were also normalized with respect to the subject's weight in order to minimize the inter-subject variability due to the different body masses of the subjects [46, 48].
A typical value of uncertainty was attributed to each APMS (all postures and vibration levels) and expressed in terms of the mean Coefficient of Variation (COV), i.e. the average of the ratio (frequency-by-frequency) between the standard deviation and the mean value:

$$u_{APMS}(f) = \frac{\sigma_{APMS}(f)}{\mu_{APMS}(f)} \tag{1.4}$$

2.3.2 Statistical analysis

Statistical analyses were performed for assessing whether the apparent mass differed under different vibration levels. Both parametric and nonparametric tests on the medians and the means of the apparent masses were applied frequency by frequency.
Non-parametric methods are distribution-free methods, which make no assumption on the population distribution; conversely, parametric methods are derived and applied for a particular parametric family of distributions (e.g. the normal distribution) [51]. When the underlying distribution is known, non-parametric methods are less efficient than the corresponding parametric version because they do not use all the information given by the samples; however, to overcome this drawback in efficiency large sample size is required in order to get the same statistical power [51]. The non-parametric paired Wilcoxon signed-rank test was applied for testing the equality of the medians. The Wilcoxon test was widespread adopted in the literature for testing differences between human responses under different conditions (e.g. the apparent mass magnitude against the excitation level) because the distribution of the experimental data was expected to be not normal [52].
Under the assumption of symmetric and continuous distributions (samples with low skewness), the median is a valid estimate for the mean. Nevertheless, these two estimators have different definitions, which may lead to different results and interpretations in case of low sample size. Non-parametric methods may lose their distribution-free behaviour and become parametric when moderately large samples ($n > 20$) are submitted; in this case, the normal approximation is valid and the test statistic reduces to that of a normal distribution. The paired t-student

test was applied for testing the equality of the means, as an alternative for the paired Wilcoxon signed-rank test. This procedure is parametric (observations are sampled from a normal distribution) and evaluates whether there are differences between the means of paired dependent samples (i.e. one sample tested twice).

2.4 Results

2.4.1 Vertical apparent mass

The normalized apparent mass along with the associated ordinary coherence function were derived for each subject and displayed in Figure 2.5 and Figure 2.6 for the upright and the bent legs posture, respectively.
The vertical apparent mass exhibited a main resonance peak between 4 Hz and 6.5 Hz, when adopting an upright posture; some subjects also showed one or two additional peaks above the frequency of 9 Hz. These findings are coherent with the ones existing in the literature [46] in which a main resonance was evident but only an additional secondary peak resulted in some subjects.
In case of knees bent posture, the vertical apparent mass had a main resonance at a lower frequency (between 2.5 Hz and 4 Hz) while a secondary resonance peak was also evident from 6 Hz to 14 Hz; some subjects also exhibited an additional third resonance peak at frequencies higher than the secondary one. These results partially matched with those derived by Subashi [46] where only a secondary peak was evident besides the main resonance.
For both postures, the inter-subject variability of the measured data (apparent masses and ordinary coherence functions) was displayed (Figure 2.7 and Figure 2.8) and then highlighted by the coefficient of variation (i.e the ratio between the standard deviation and the mean) in Figure 2.9. For the upright posture, the apparent mass was characterized by large scatters, about the 20% of the static mass, around the main resonance peak (4-6.5 Hz). For the bent legs posture, the coefficient of variation increased up to 50% of the static mass in the frequency range comprising both the main peak and antiresonance (2-7 Hz). In both postures, there was a positive trend in the variability of the apparent mass up to 10 Hz.

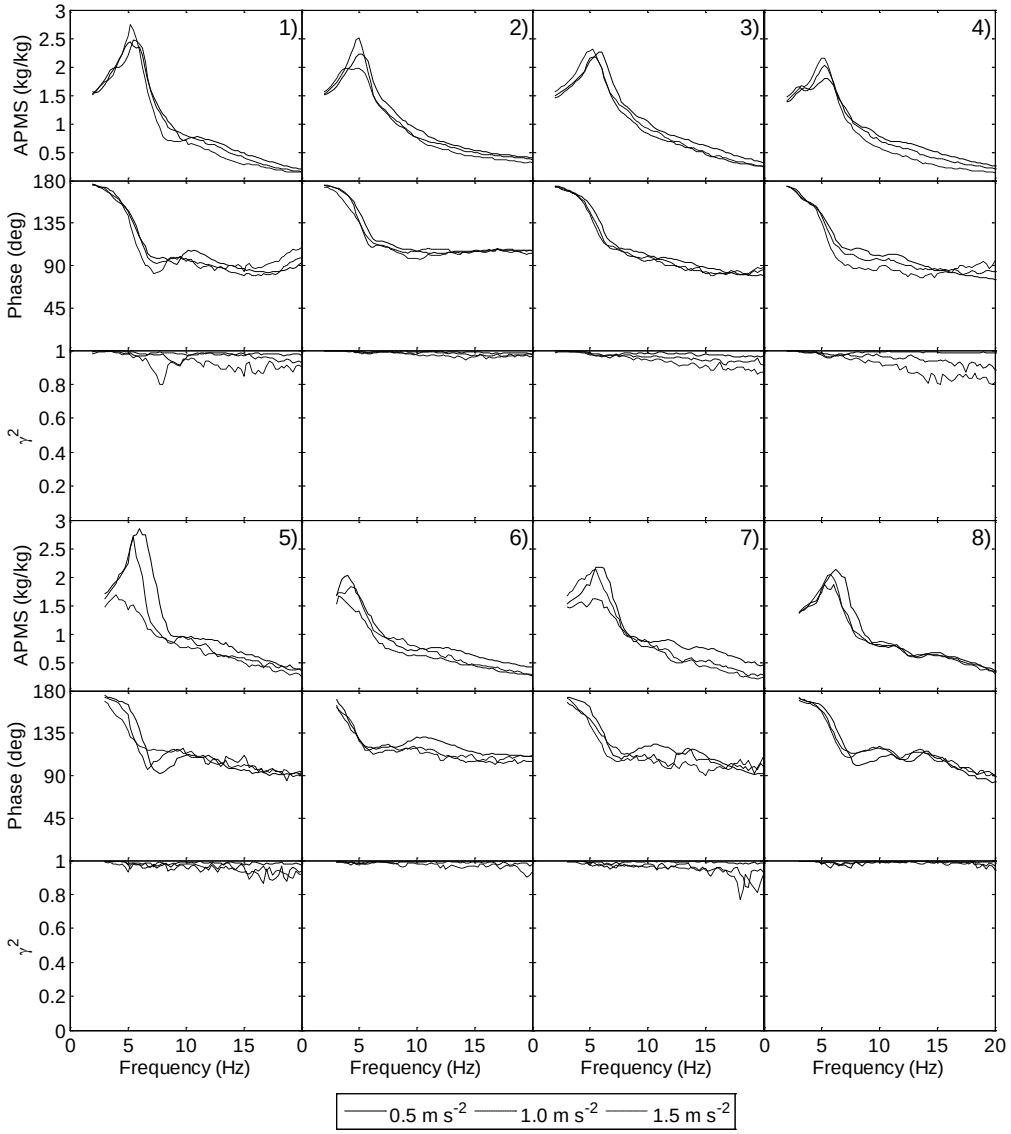

Figure 2.5 Normalized apparent masses of eight subjects (modulus, phase, ordinary coherence function): upright posture.

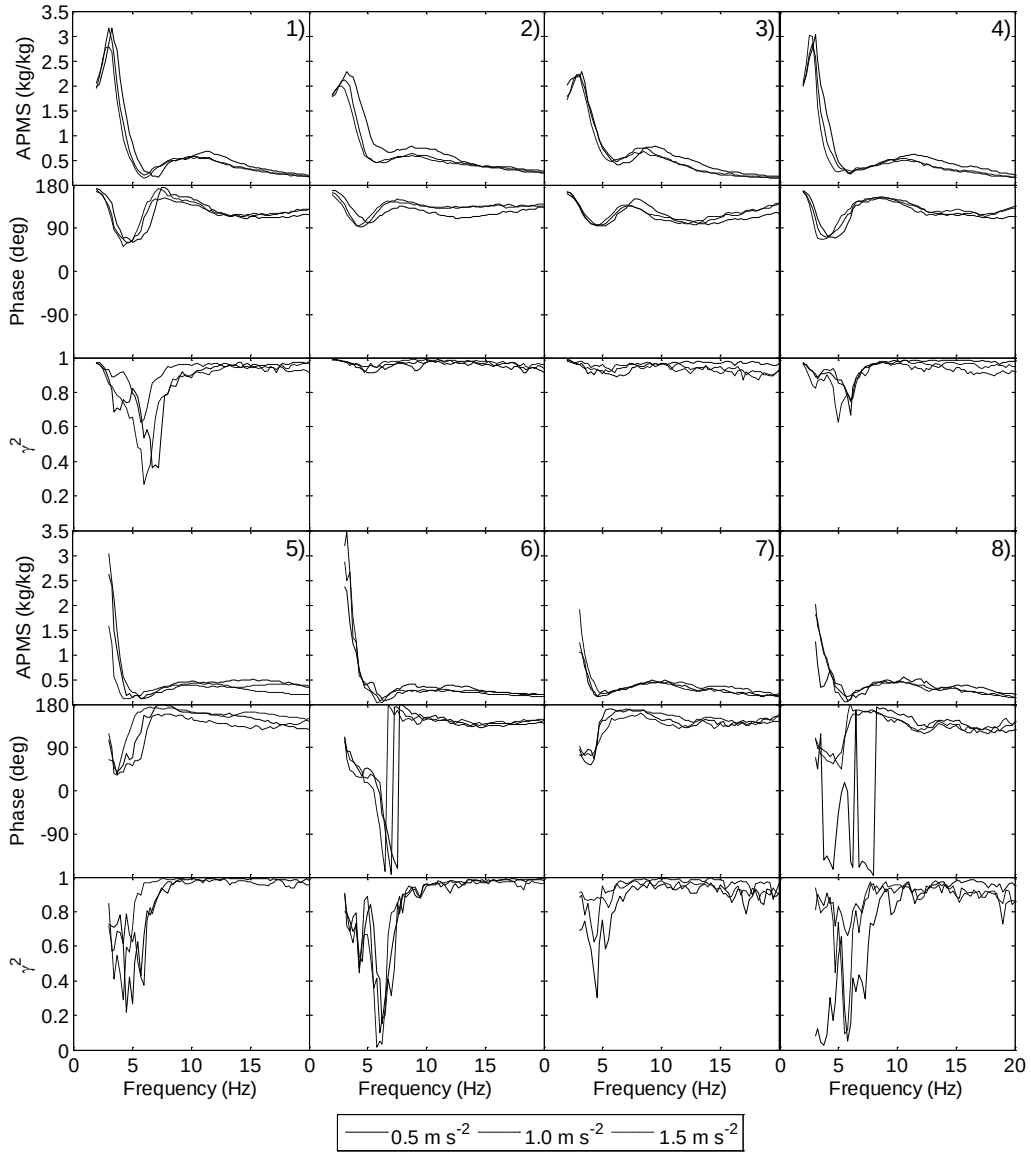

Figure 2.6 Normalized apparent masses of eight subjects (modulus, phase, ordinary coherence function): bent legs posture.

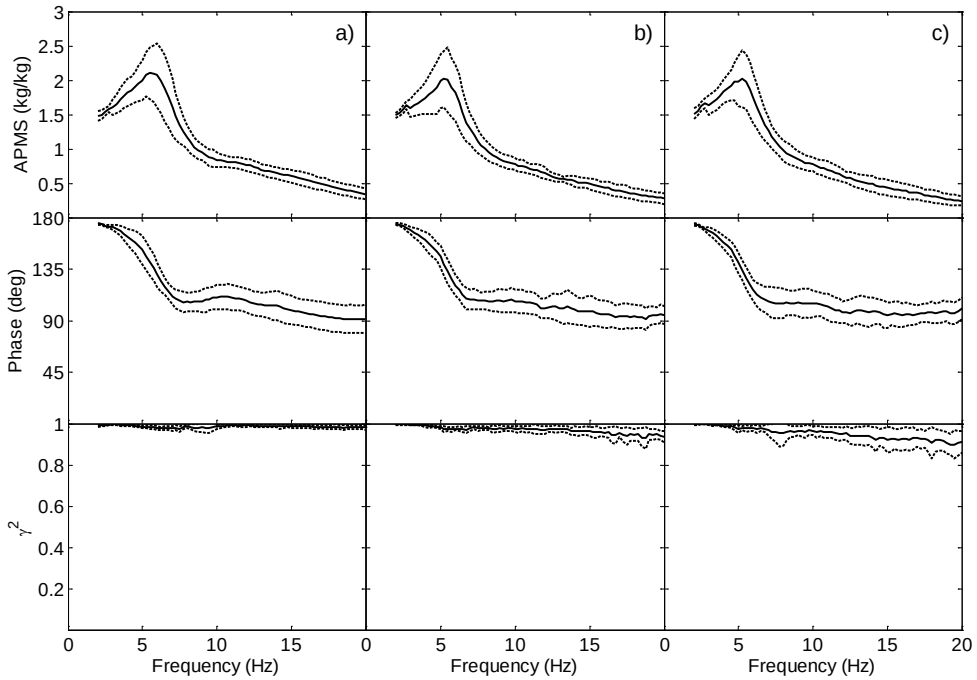

Figure 2.7 Apparent mass, phase and ordinary coherence function (mean ± standard deviation) for the eight subjects in case of upright posture: a) 0.5 m s^{-2}, b) 1.0 m s^{-2}, c) 1.5 m s^{-2} RMS.

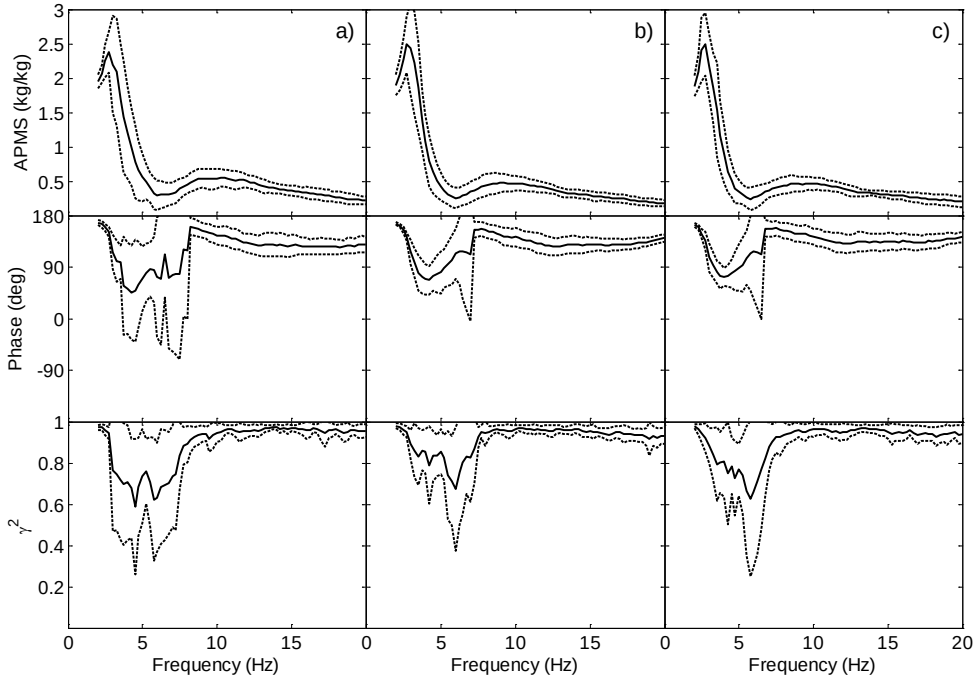

Figure 2.8 Apparent mass, phase and ordinary coherence function (mean ± standard deviation) for the eight subjects in case of legs bent posture: a) 0.5 m s^{-2}, b) 1.0 m s^{-2}, c) 1.5 m s^{-2} RMS.

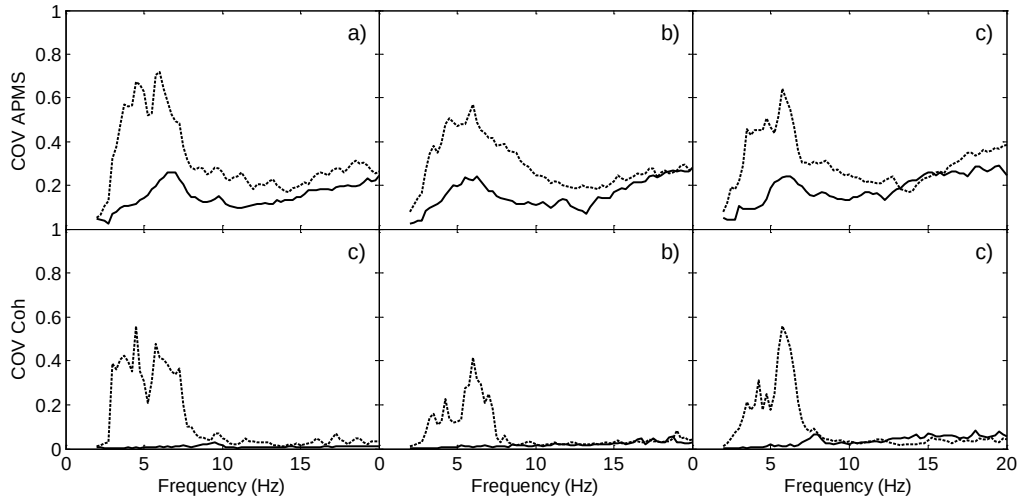

Figure 2.9 Coefficients of variation for the normalized apparent masses and ordinary coherence functions of eight subjects (___ upright posture, _ _ _ bent legs posture): a) 0.5 m s^{-2}, b) 1.0 m s^{-2}, c) 1.5 m s^{-2} RMS.

The ordinary coherence function in the upright posture was almost equal to unity except in correspondence of the second resonance (12 Hz), where the coherence decreased to lower values; moreover, a large variability at high frequencies was observed as the vibration magnitude increased. In case of bent legs posture, some subjects exhibited high coherences over the whole range of excitation and some others marked deep drops in the ordinary coherence function around the main resonance and antiresonance. Thus, higher coefficients of variations were observed in this frequency range while the variability at higher frequencies remained substantially unchanged.
Since for the bent legs posture the ordinary coherence function assumed values much lower than unity, a comparison between the CSD and the PSD methods was necessary in order to assess the amount of noise on the response. In the range 2-8 Hz, the two estimators differed by producing two distinct peaks at the main resonance and antiresonance. Moreover, the difference decreased in magnitude for increasing excitation levels with a marked trend for the peak around the main resonance.

2.4.2 Effect of vibration magnitude

The effect of vibration magnitude on the apparent masses of the eight subjects was checked by the application of both the paired Wilcoxon signed-rank test and paired t-student test for which the results are displayed in Figure 2.10 and Figure 2.11, respectively.

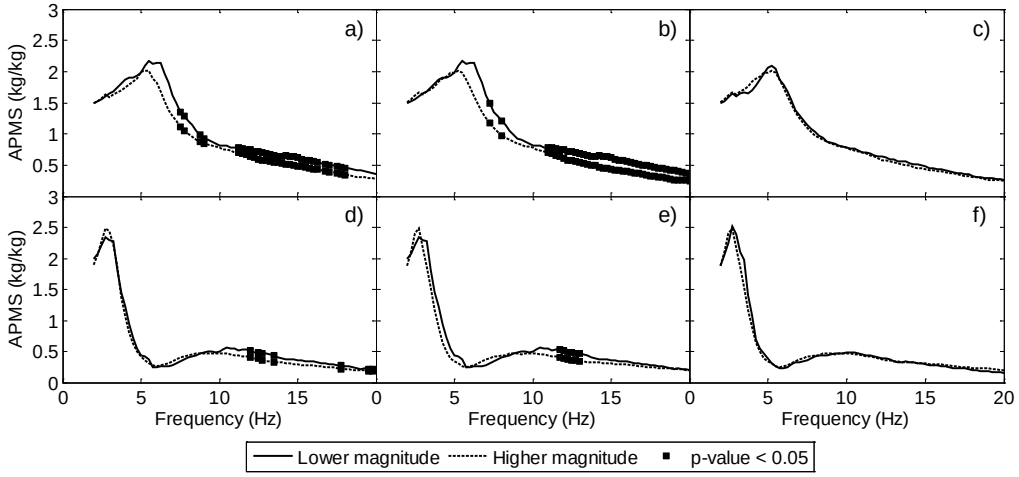

Figure 2.10 Results of the paired Wilcoxon signed rank test; upright posture: a) 0.5-1.0 m s^{-2}, b) 0.5-1.5 m s^{-2}, c) 1.0-1.5 m s^{-2}; bent legs posture: d) 0.5-1.0 m s^{-2}, e) 0.5-1.5 m s^{-2}, f) 1.0-1.5 m s^{-2}.

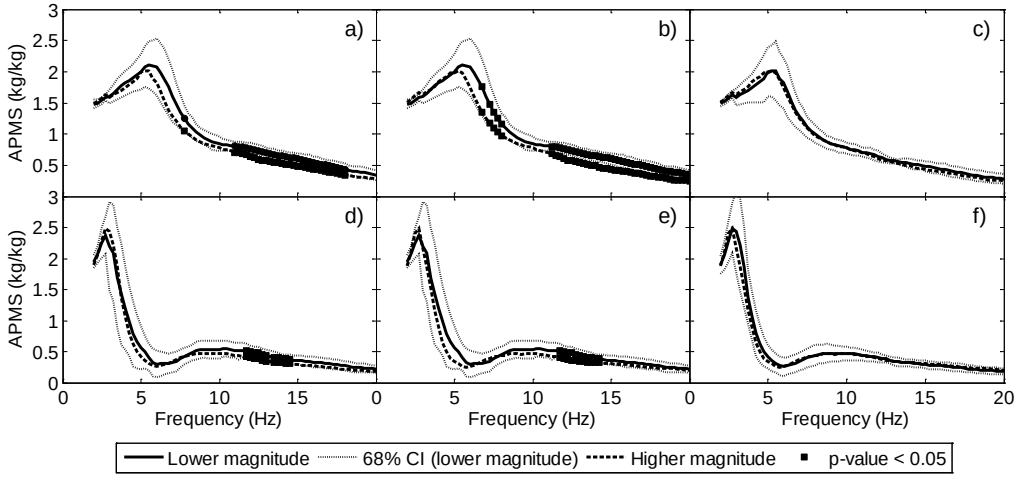

Figure 2.11 Results of the paired t-student test; upright posture: a) 0.5-1.0 m s^{-2}, b) 0.5-1.5 m s^{-2}, c) 1.0-1.5 m s^{-2}; bent legs posture: d) 0.5-1.0 m s^{-2}, e) 0.5-1.5 m s^{-2}, f) 1.0-1.5 m s^{-2}.

With regard to the paired Wilcoxon sign-rank test (Figure 2.10), for the upright posture significant differences in the magnitudes ($p < 0.05$, Wilcoxon) were found above 10 Hz between apparent masses taken at 0.5 m s^{-2} and 1.0 m s^{-2} and between the apparent masses at 0.5 m s^{-2} and 1.5 m s^{-2}. Conversely, few differences were found between the magnitudes of the apparent masses below 10 Hz and, in any case, the shape of the apparent masses resulted not affected by the vibration magnitude ($p > 0.05$, Wilcoxon). For the bent legs posture, a perfect match

between the apparent masses occurred at all frequencies except in the range 11-14 Hz ($p < 0.05$, Wilcoxon) for the pairs 0.5-1.0 m s^{-2} and 0.5-1.5 m s^{-2}. There was a perfect match ($p > 0.05$, Wilcoxon) between the apparent masses measured at 1.0 m s^{-2} and 1.5 m s^{-2}.
Results from paired t-student test are shown in Figure 2.11 where the apparent masses were compared in pairs (the one derived for the lowest magnitude of vibration is provided with its uncertainty bands). Statistically significant differences ($p < 0.05$, t-test) were found at all frequencies above 10 Hz, at about the second broad resonance, for both pairs 0.5-1.0 m s^{-2} and 0.5-1.5 m s^{-2}. In the main resonance region (4-6.5 Hz) there were significant differences in magnitude ($p < 0.05$, t-student) only for the couple 0.5-1.5 m s^{-2}, for those frequencies higher than the resonance. There were no differences between the two apparent masses derived at 1.0 m s^{-2} and 1.5 m s^{-2}, being the latter completely contained within the uncertainty bands provided with the first. For the bent legs posture, significant differences ($p < 0.05$) in the magnitude of both pairs 0.5-1.0 m s^{-2} and 0.5-1.5 m s^{-2} occurred in the range 11-15 Hz, slightly above the frequency of the second broad resonance. There was no statistical difference between the mean apparent masses at 1.0 m s^{-2} and at 1.5 m s^{-2}.

2.5 Conclusions

The effect of vibration magnitude on the apparent mass for both postures was tested by the use of the paired Wilcoxon sign-rank test and paired t-test.
Results, in terms of apparent masses, generally agreed with those previously reported [46] except for the rising of further broader resonances at higher frequencies, maybe due to the different investigated vibration magnitudes or experimental conditions (i.e. posture was constrained by handling a rigid frame), or maybe both.
For the upright posture, both paired match statistical analysis indicated no significant differences between each pair of apparent masses except at higher frequencies (above 12 Hz) for pairs with the lowest magnitude of vibration (i.e. 0.5 m s^{-2}) while there was no difference between the other two apparent masses (i.e. at 1.0 m s^{-2} and 1.5 m s^{-2}). Statistical significant differences were found for the knees bent posture, above the second broad resonance (between 11 Hz and 14 Hz) between the apparent masses at the lower excitation magnitude and the other two for which there were no differences.
This comparison method differs from that previously adopted because it compared point-by-point the whole apparent masses and the scatter between observations was also considered (i.e. the t-test assumed a normal distribution for the samples).
Since resonances remained unchanged in both postures, in terms of frequency and amplitude, and significant differences occurred above 12 Hz, where the amplitude

is less than the static mass, it was reasonable that the extent of the inter-subject variability was such to reduce the effect of the vibration magnitude. In the resonance region, the most critical when dealing with vibration assessment, the apparent masses behaved in the same manner.
This finding was in contrast with previous studies in which both the frequencies and peak magnitudes depended on the vibration magnitude. Some concerns over the statistical analysis rose because in such studies the median resonance frequency and the amplitude of the median apparent mass at each vibration magnitude was submitted to statistical tests (i.e. paired match Wilcoxon sign-rank test). In the introduction to the statistical methods (2.3.2) the difference between the median and the mean values was discussed along with their drawbacks.
As already mentioned, the Wilcoxon sign-rank test is a non-parametric method which uses the plus and minus signs of the differences between paired observations. Since there are no assumptions on the distribution of the population, information such as the standard deviation are not directly involved in the estimation procedure. Thus, the statistical test results less robust than the corresponding parametric procedure (e.g. paired t-test) and more samples are needed in order to get the same power.
In the literature, the Wilcoxon signed-rank test was adopted for testing the medians because the real distribution of the samples was considered unknown and the few number of samples avoided the use of normality tests (e.g. Shapiro-Wilk normality test). In reality, the means have the property to belong to normal distributions as stated by the central limit theorem and the assumption of gaussianity holds.
When samples are distributed asymmetrically (i.e. no zero skewness), the median becomes insensitive to outlier data and results may not correspond to the submitted sample. In other words, the use of the median leads to a rejection of some values, similarly to what stated in [33, 53] where low coherence trials or outlier FRFs were excluded from the analysis.
For this study, both statistical tests agreed since distributions were symmetric, but this condition is seldom satisfied. Thus, it is recommended a detailed preventive analysis of the data set, taking more attention to those aspects which may void the whole results and lead to wrong interpretations.

Chapter 3

Conditioned apparent mass

Nonlinearities in the apparent masses of the previous chapter has been studied by conditioning the transmitted force with the input acceleration and some of its nonlinear transformations. Results were presented in terms of the conditioned apparent mass and of the multiple coherence function. The effect of the vibration magnitude was also evaluated along with some considerations about the model accuracy introduced by the conditioning procedure.

3.1 Introduction

In the existing studies, the response of the human body to vibration has been analysed using the driving-point apparent mass or impedance and the vibration transmissibility, i.e. linear estimators of the frequency response function (FRF). The techniques for the analysis of nonlinear systems were described in many different textbooks [13, 54, 55]; we report in the following a short summary in order to ease the method understanding. The response *y(t)* of a generic system to an input *x(t)* is:

$$y(t) = H\{x(t)\} \tag{3.1}$$

H is the system operator, defined as a mapping of the possible outputs *y(t)* to the possible inputs *x(t)* (e.g. how the human body converts a vertical force stimulus into an acceleration). A mechanical system is linear if the operator *H* is linear, i.e. if *H* is homogeneous, additive, time invariant, causal, and stable. The existing literature studies evidenced that the human body behaviour is:

- not homogeneous: it was shown that the apparent mass depends on the vibration level, hence if the input is scaled by a factor Φ the output is not scaled by a factor Φ;
- not additive, given that response to random excitation was found to be different from the response to swept sine;
- not time invariant, because involuntary muscle tension may change the body FRF;
- causal, because in absence of mechanical stimulus the body does not (unintentionally) generate forces in the frequency range typical of WBV; and
- stable: if the input vibration level is finite, the inertial forces or the vibration at different positions is also finite.

At the current state of the art, the human body has always been analysed with FRF, which rely on the hypothesis of system linearity. In a linear system, the output *y(t)* is the convolution between the input time history *x(t)* and the time-domain response of the system to the Dirac function (impulse response) *h(t)*:

$$y(t) = x(t) \otimes h(t) \tag{3.2}$$

Thanks to the convolution theorem, the above equation can be written, in frequency domain, as:

$$Y(f) = X(f)H(f) \tag{3.3}$$

where *H(f)* is the so-called frequency (*f*) response function. In the specific case of the apparent mass (*APMS*), for instance, *X(f)* is the acceleration *a(f)* and *Y(f)* is the force *F(f)*, while for vibration transmissibility *X(f)* and *Y(f)* are the vibration spectra measured at different positions.
Equation (3.3) is meaningless in presence of nonlinearities; there are different ways to check the hypothesis of linearity, but the most common is the coherence function $\gamma(f)$ [10]:

$$\gamma^2(f) = \frac{\left|S_{xy}(f)\right|^2}{S_{xx}(f) \cdot S_{yy}(f)} \tag{3.4}$$

where $S_{xx}(f)$ and $S_{yy}(f)$ are the power spectra of the input and the output, respectively, and $S_{xy}(f)$ is the cross-spectrum between the input and the output signals. Equation (3.4) is always 1 if the spectral quantities are computed by Fourier transforming the input and output time histories. Assuming that *x(t)* and *y(t)* are random phenomena, their spectra can be estimated using the Welch method, i.e. by splitting the signals into *N* overlapped segments and computing the average of the *N* resulting spectra. If equation (3.4) is computed using spectral density estimators, the coherence function drops below unity if there is contaminating noise on the measured signals, if there are leakage errors not reduced by windowing, if there are non-measured inputs affecting the output or if the system *H(f)* is nonlinear. In the investigation of the human body response to vibration the measurement chain noise is usually limited and the only vibration input is the one measured by the acceleration sensor. The leakage is usually negligible and therefore low coherence values should be only endorsed to a nonlinear response of the system.
The common practice in WBV analysis for the identification of system nonlinearity is the comparison between the power spectral density (*PSD*) and the cross-spectral density (*CSD*) estimators. In the first case, the FRF is obtained as the ratio between the power spectral densities of the input and output signals ($S_{xx}(f)$ and $S_{yy}(f)$, respectively). In the specific case of the apparent mass:

$$APMS_{PSD}(f) = \sqrt{\frac{S_{yy}(f)}{S_{xx}(f)}} \tag{3.5}$$

The CSD method involves the evaluation of the cross-spectrum between the input and output signals:

$$APMS_{CSD}(f) = \frac{S_{xy}(f)}{S_{xx}(f)} \tag{3.6}$$

Equation (3.6) is known as the H_1 linear estimator, which has the twofold advantage, as opposed to eq. (3.5), of preserving the information on the phase and of removing the noise in the measurement system output [12, 13]. The comparison between $APMS_{PSD}$ and $APMS_{CSD}$ is equivalent to the analysis of coherence, given that $\gamma^2(f)$ is the ratio between the *CSD* and the *PSD* estimators of the transfer function.

3.1.1 Analysis of nonlinear system

If the coherence drops below unity, the system may be nonlinear. The origin of nonlinearity can be the lack of homogeneity or additivity or the variation of the modal parameters. In the first case, the nonlinear system can be investigated with the procedure developed by Bendat and Piersol [12], while if the modal parameters are not constant the system can be modelled as a linear system with uncertainty.
The procedure described by Bendat consists in modelling a nonlinear single input, single output (*SISO*) system as a multiple input, single output (*MISO*) system with nonlinear inputs. In other terms, if the human body response to vibration is nonlinear, the response (inertial force) to the stimulus (vibration) is the sum of one linear function of the input and *M-1* linear response to nonlinear functions of the input:

$$Y(f) = H_{1y}(f) \cdot X(f) + \sum_{i=2}^{M} H_{iy}(f) \cdot \mathcal{F}_i(X(f)) + N(f) \tag{3.7}$$

$H_{1y}(f)$ is the linear FRF associated to the input $X(f)$. Similarly, $H_{iy}(f)$ is the linear FRF associated to a nonlinear function $\mathcal{F}_i$ of the input, for instance the input squared or the input square-root. $N(f)$ is the noise, accounting for the non-modelled nonlinearities and for the uncorrelated measurement noise. With this scheme (graphically summarized in Figure 3.1), a linear system with transfer function $H_{1y}(f)$ is in parallel with *M-1* nonlinear systems $g_2(x)$ ... $g_n(x)$ followed

by linear transfer functions $H_{2y}(f)$ … $H_{My}(f)$. The model fully describes the nonlinear system behaviour (if the system is not homogeneous and additive), while the FRF estimator $H(f)$ would only point out the linear component of the model $H_{1y}(f)$.

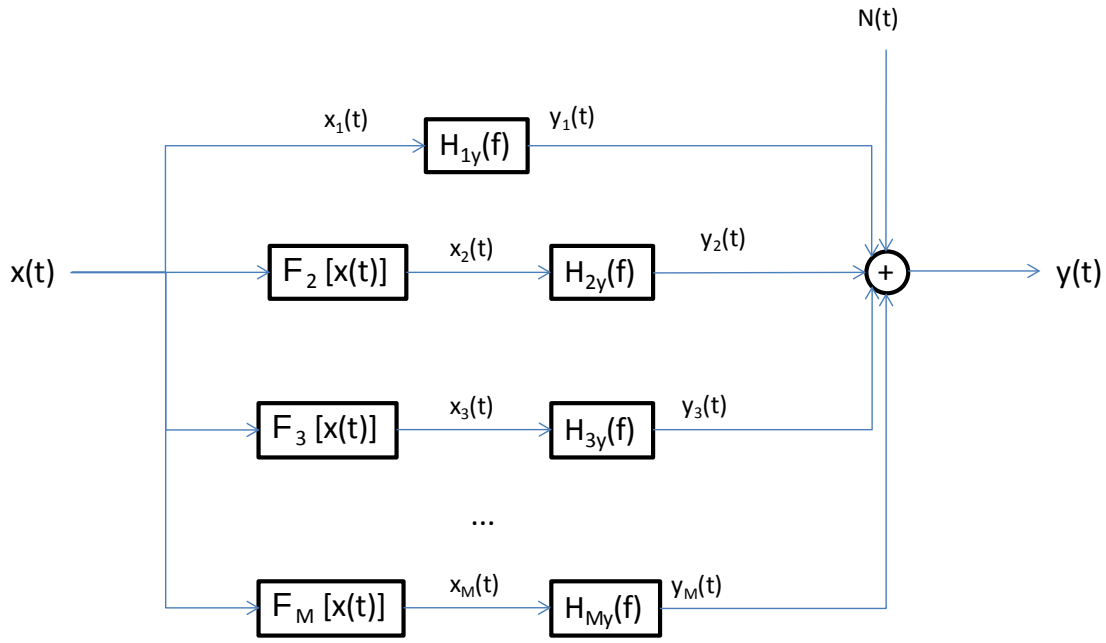

Figure 3.1 Single input-single output nonlinear model of a linear system in parallel with n nonlinear systems.

Neither the linear FRFs nor the noise are known a priori or directly measurable; after the identification, all the model parameters are completely defined along with other useful conditioned quantities (the conditioned output spectra and the multiple coherence functions). The set of linear FRFs $\{H_i(f)\}$ relates mathematically each input to the total output (their physical meaning is often awkward). The identification procedure needs that inputs are stationary (ergodic) or transient random signals, even correlated but not perfectly. The four compulsory conditions for a correct system identification are [12]:

1. the ordinary coherence function between any pair of inputs must be different from unity, which means no redundant information;
2. the ordinary coherence function between any input and the output must not equal to unity, otherwise the other inputs have no contributions to the output and the system is described by a single input/single output model;
3. the multiple coherence function between any input and the others should not equal unity (i.e. the input is redundant and then eliminated); and

4. the multiple coherence function between the output and the given inputs should be close to unity; conversely, some inputs are omitted or nonlinearities have large effects.

As previously evidenced, the validity of the nonlinear model is checked using the conditioned outputs, computed by modifying the generally correlated set of inputs $\{X_i(f)\}$ using the conditioned spectral density techniques [56], in order to obtain an equivalent set of inputs $\{U_i(f)\}$ in which all the inputs are uncorrelated. With this new set of inputs, it is possible to identify a new set of frequency responses $\{L_i(f)\}$, generally different from $\{H_i(f)\}$, which relate each conditioned input to the total output. The product between the inputs $\{U_i(f)\}$ and the frequency responses $\{L_i(f)\}$ is a set of linearly independent outputs $\{Y_i^*(f)\}$, referred to as conditioned outputs. The best linear system estimator is $L_1(f)$ which differs from $H_1(f)$ if the nonlinear effects are important [57].

Ordinary coherence functions $\gamma^*_i(f)$ can be computed between the conditioned output and conditioned inputs in order to assess, at each frequency, the percentage of the output due to each uncorrelated input. The multiple coherence function between the input and the output is computed by combining all partial coherence functions $\gamma^*_i(f)$:

$$\gamma^2_{y:\mathrm{M}}(f) = 1 - \prod_{i=1}^{M}\left(1 - \left[\gamma_i^*(f)\right]^2\right) \tag{3.8}$$

The multiple coherence function can be used to assess the validity of the proposed nonlinear model, whilst the comparison between the conditioned output and the output can be used to assess to which extent the output is correctly modelled by the nonlinear system. Given that, in our case, the conditioned output is the force spectrum, the latter can be used to compute the conditioned apparent mass. With reference to the scheme of Figure 3.1, assuming that *y* is the measured force and *x* measured the acceleration:

$$APMS_{COND}(f) = \frac{S_y(f) - S_n(f)}{S_x(f)} \tag{3.9}$$

In order to ease the comparison with the existing literature works, the apparent masses of equations (3.5), (3.6) and (3.9) have been normalized with respect to the static mass.

If the system is not “fixed parameter” the above described procedure does not reduce the measurement variability, and it is more convenient to describe the human body behaviour using a linear model with uncertainty. Uncertainty can be evaluated analysing the data dispersion in different postures and with different

vibration levels, computing the Coefficient of Variation (the ratio between the standard deviation and the mean apparent mass):

$$u_{APMS}(f) = \frac{\sigma_{APMS}(f)}{\mu_{APMS}(f)} \tag{3.10}$$

This quantity is frequency dependent and has been summarized with the RMS between 2 and 20 Hz (hereinafter u_{APMS}). The computation of u_{APMS} on the non-normalized *APMS* of the entire data set (8 subjects in upright and legs bent posture, 0.5, 1.0 and 1.5 m s^{-2} RMS) using a linear model provides for an indication of the expected *APMS* variability in uncontrolled conditions. This parameter indicates the model uncertainty for the evaluation of the effect of people on structures, where the posture, the vibration level, and the subjects' masses are unknown. Conversely, the computation of u_{APMS} of the normalized *APMS* on a data set that includes only a specific posture, a single vibration level using the conditioned response model provides for an indication of the *APMS* variability in controlled condition. The parameter is indicative of the modelling uncertainty for subjects with known body mass in a given posture.

3.2 Data analysis

The responses for the standing people derived in the previous chapter were conditioned according to the diagram of Figure 3.1. Results were provided in terms of both the linear estimators and of conditioned quantities (i.e. $APMS_{COND}$ and the multiple coherence function). All spectral quantities were presented with a frequency resolution of 0.25 hertz.
As usual, before proceeding to the data analysis the inertial force due to the plate was removed by mass cancellation in the time-domain. Afterwards, the conditioned apparent masses were normalized with respect to the subject's weight. A typical value of uncertainty was attributed to each conditioned APMS (all postures and vibration levels) and expressed as in equation (3.10).

3.3 Nonlinear model

The biodynamic response of standing subjects to vertical whole-body vibration was computed including in equation (3.7) the input acceleration, the absolute value of the acceleration and the squared power of the acceleration time history. The complexity of the model might be increased with the addition of other nonlinear functions, but the ones selected are the most common in typical nonlinear model identification problems [54]. Furthermore, preliminary tests evidenced that the addition of cubic and high-order powers of the acceleration time history did not increase the modelling accuracy.

The constant-parameter FRFs in upright and legs bent postures are shown in Figure 3.2 and Figure 3.3, respectively. The first (linear) FRF is very similar to that identified with the H_1 estimator used to derive the apparent masses. Subsequent linear FRFs (describing the response to the nonlinear inputs acceleration modulus and squared acceleration) decreased in magnitude with the order of estimation (i.e. $\max(|H_{1y}|) > \ldots > \max(|H_{3y}|)$). The three FRFs are characterized by a dominant peak in the frequency range 3-5 Hz and by decreasing amplitudes above 5 Hz.

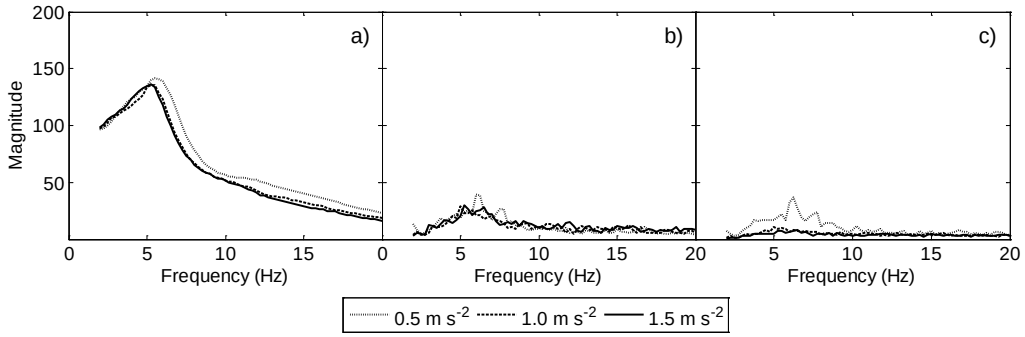

Figure 3.2 Mean constant-parameter linear functions (upright posture): a), H_{1y} (kg); b), H_{2y} (N/|m s^{-2}|); c), H3y (N/(m s^{-2})^2).

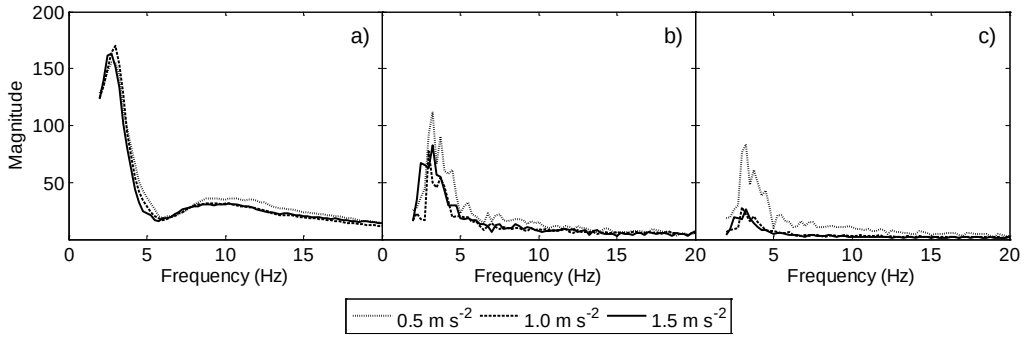

Figure 3.3 Mean constant-parameter linear functions (legs bent posture): a), H_{1y} (kg); b), H_{2y} (N/|m s^{-2}|); c), H_{3y} (N/(m s^{-2})^2).

As already outlined [54], the numerical values of the linear functions of Figure 3.2 and Figure 3.3 were irrelevant, given that their physical meaning did not have a straightforward interpretation.

3.4 Conditioned apparent masses

The conditioned apparent mass of the eight subjects was compatible with the results of existing literature studies, with a dominant peak between 3 and 6 Hz. The biodynamic response in upright position differed from the one with legs bent, in terms of both resonance frequency and amplitude. Similarly, the coherence function depended on the posture and on the subject. The coherence was almost one in upright position, while with legs bent varied from subject to subject: in 3 cases both the ordinary and the multiple coherence functions were close to one, thus evidencing the validity of the linear system approximation (as for instance, in part *b* of Figure 3.4). In the remaining tests, the ordinary and the multiple coherence functions decreased to values below 0.5 at frequencies close to 6 Hz as in part *a* of Figure 3.4. The difference between the ordinary coherence and the multiple coherence function, in each of the 8 subjects that underwent the tests, was limited. The largest differences were noticed in subjects with bent legs between 4 and 8 Hz.

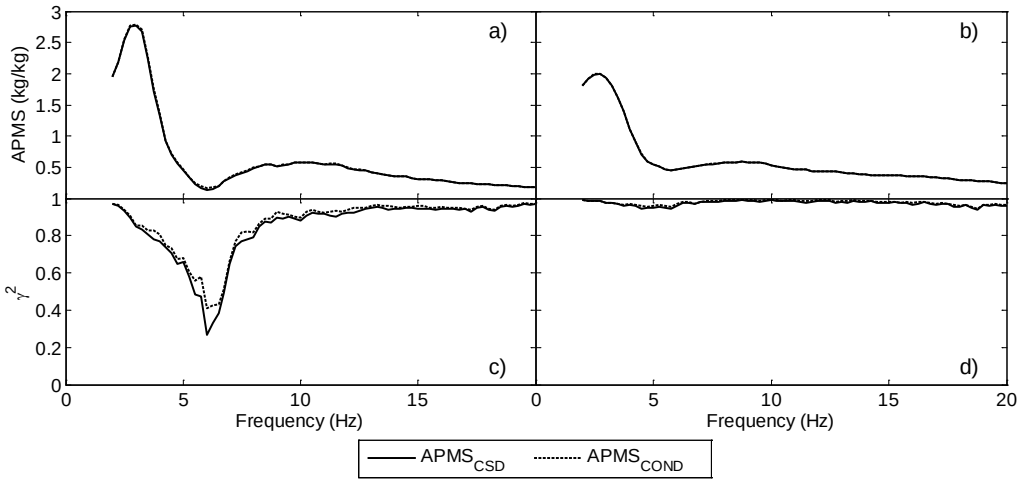

Figure 3.4 Subject nr. 1: a), normalized apparent masses, c) coherence functions; subject nr. 2: b), normalized apparent masses, d) coherence functions.

The (limited) benefits deriving from the adoption of a nonlinear model were also evidenced by the analysis of the average apparent masses (Figure 3.5 and Figure 3.6). The plots show the linear and the conditioned APMS of standing subjects in upright and legs bent postures with vibration levels between 0.5 and 1.5 m s^{-2}. The differences between the apparent masses obtained using a linear and a nonlinear model were low in comparison with the tests repeatability. In the same way, the difference between the ordinary and the multiple coherence functions was negligible, independently from the posture and from the vibration level.

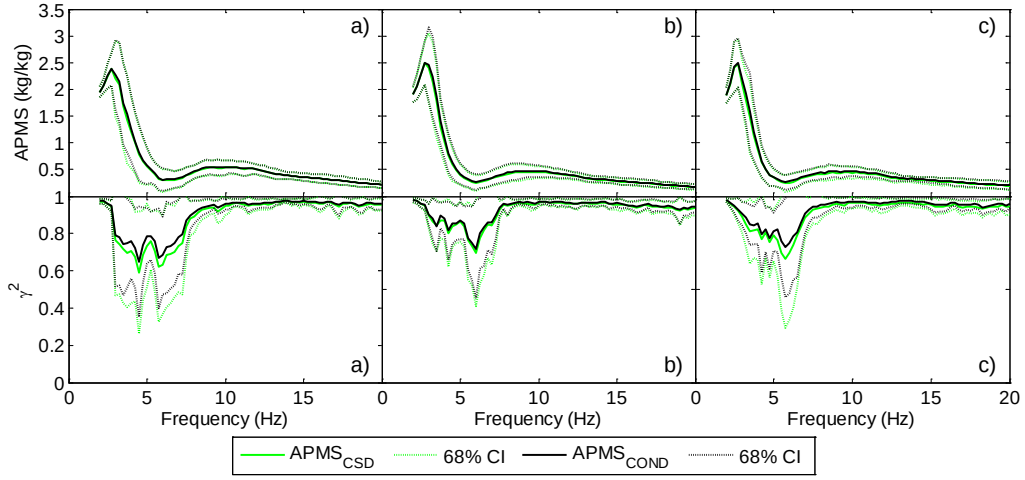

Figure 3.5 Normalized apparent masses and coherence functions (average and 68% confidence interval of eight subjects in legs bent posture): a) 0.5 m s^{-2}, b) 1.0 m s^{-2}, c) 1.5 m s^{-2} RMS.

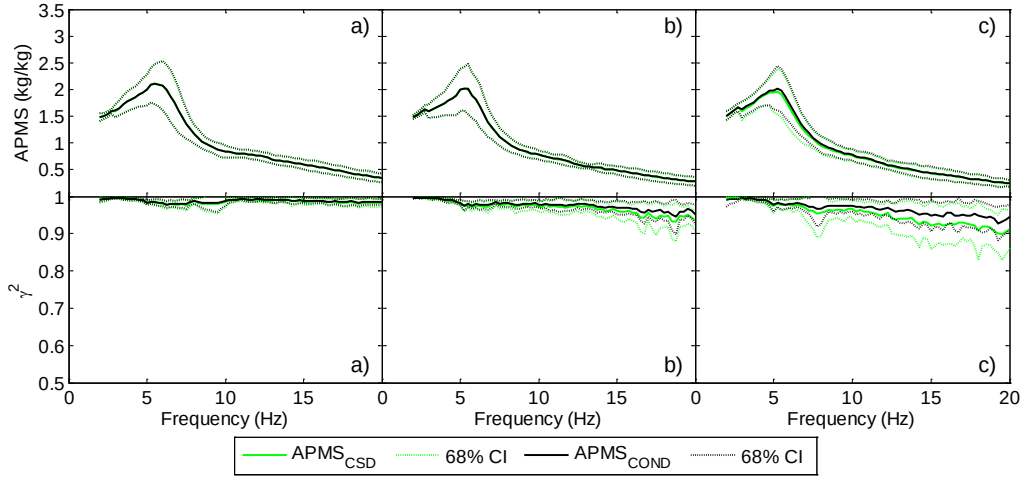

Figure 3.6 Normalized apparent masses and coherence functions (average and 68% confidence interval of eight subjects in upright posture): a) 0.5 m s^{-2}, b) 1.0 m s^{-2}, c) 1.5 m s^{-2} RMS.

Uncertainties associated to the APMS of Figure 3.5 and Figure 3.6 are summarized in Table 2. u_{APMS} of the entire data set was approximately 40 %, uncertainty in controlled condition ranged from 15 to 19% in the upright posture, and from 28 to 30% when subjects stood with their legs bent. The effect of vibration magnitude on the measurement data dispersion was small (uncertainty changes smaller than 5%) and the differences between the linear and the conditioned models were negligible (less than 3%).

Table 3.1 Uncertainty associated to the experimental APMS.

Posture	Vibration level ($m\ s^{-2}$ RMS)	Mean COV (%) ($APMS_{COND}$)	Mean COV (%) ($APMS_{CSD}$)
All postures	**All magnitudes**	/	40.2
Upright	**0.5**	15.1	15.1
Upright	**1.0**	16.1	16.1
Upright	**1.5**	18.7	18.9
Legs bent	**0.5**	30.3	31.5
Legs bent	**1.0**	27.9	29.2
Legs bent	**1.5**	27.6	30.6

The relevance of the vibration level in the conditioned biodynamic response of the human body was investigated with parametric and nonparametric hypothesis tests. Both the paired Wilcoxon signed-rank test (Figure 3.7) and the paired t-student test (Figure 3.8) evidenced that, either in the standing or legs bent postures, there was no difference between the biodynamic response measured at 1.0 and 1.5 m s^{-2}. Conversely, the apparent mass measured with a stimulus of 0.5 m s^{-2} was different from the ones measured at 1.0 and 1.5 m s^{-2} at frequencies above 10 Hz, both in standing and legs bent postures.

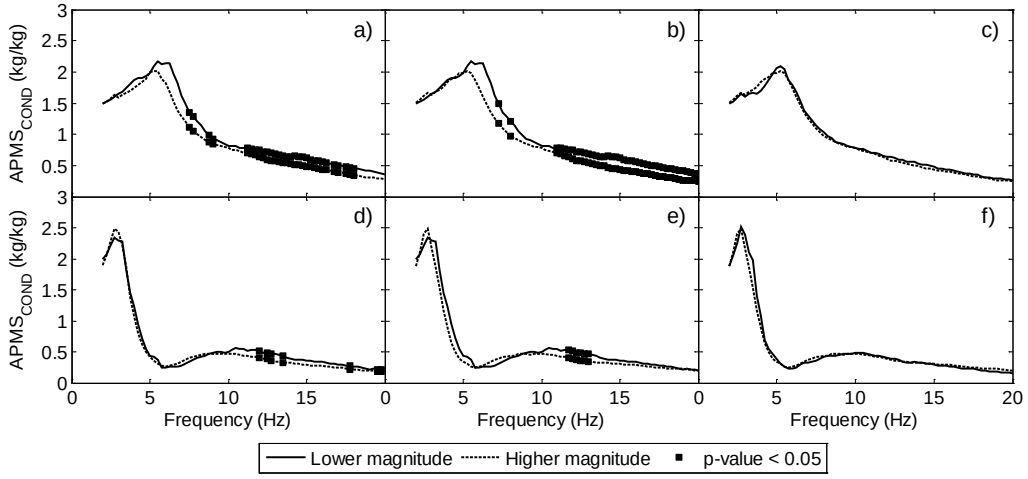

Figure 3.7 Results of the paired Wilcoxon signed-rank test; upright posture: a) 0.5-1.0 m s^{-2}, b) 0.5-1.5 m s^{-2}, c) 1.0-1.5 m s^{-2}; legs bent posture: d) 0.5-1.0 m s^{-2}, e) 0.5-1.5 m s^{-2}, f) 1.0-1.5 m s^{-2}.

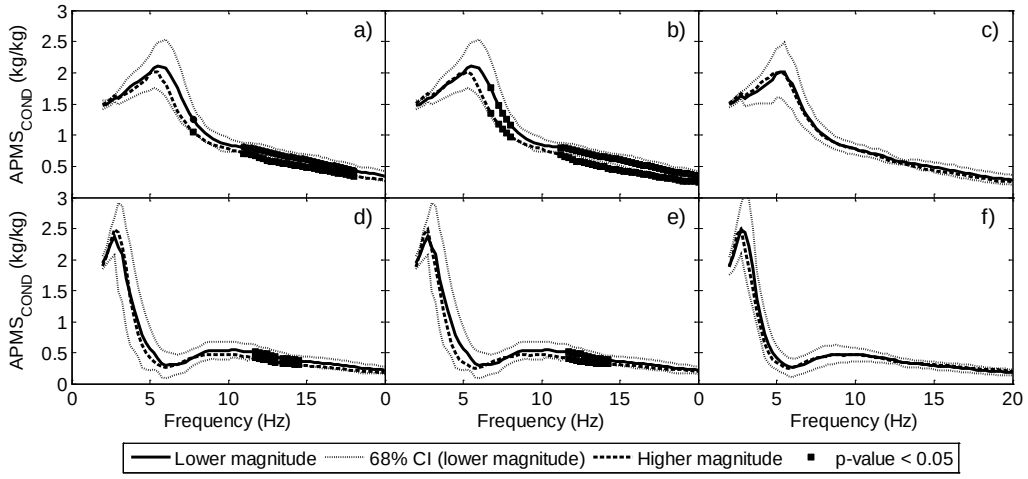

Figure 3.8 Results of the paired t-student test; upright posture: a) 0.5-1.0 m s^{-2}, b) 0.5-1.5 m s^{-2}, c) 1.0-1.5 m s^{-2}; legs bent posture: d) 0.5-1.0 m s^{-2}, e) 0.5-1.5 m s^{-2}, f) 1.0-1.5 m s^{-2}.

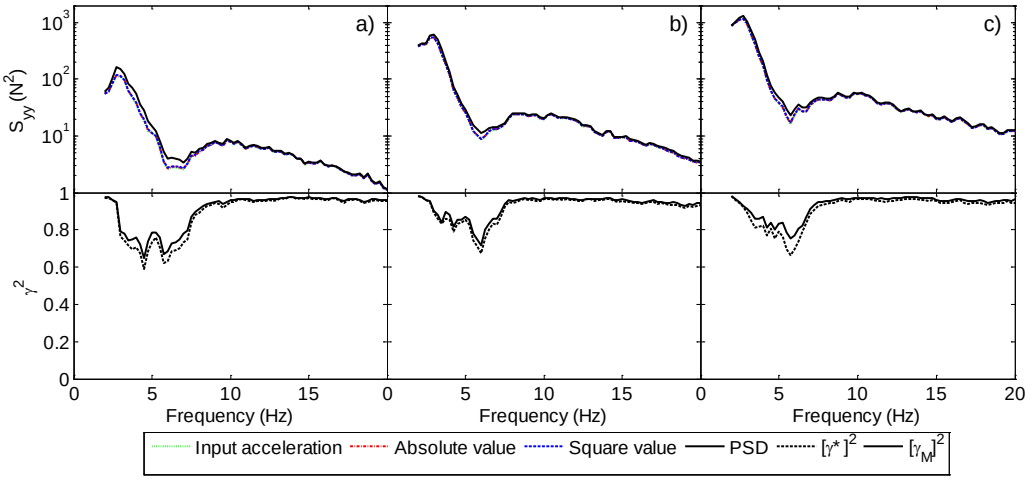

Figure 3.9 Conditioned autospectrum of the transmitted force (legs bent posture); a) 0.5 m s^{-2}, b) 1.0 m s^{-2}, c) 1.5 m s^{-2} RMS.

A snapshot of the differences between the adoption of linear and nonlinear models was provided by the conditioned force autospectra, i.e. the inertial forces generated by subjects estimated from the acceleration spectra. The conditioned force autospectra for vibration levels of 0.5, 1.0 and 1.5 m s^{-2} are shown in Figure 3.9. The linear and the nonlinear models were accurate at frequencies above 10 Hz (differences between the measured and the predicted response lower than 5%), while the modelling accuracy between 2 and 10 Hz was lower (maximum difference between the measured and the predicted response 20-40% at 5 Hz).

Nevertheless, the responses estimated using conditioned and linear models were compatible, and the multiple coherence was, at most, 10% larger than the ordinary coherence function (at 6 Hz with the stimulus of 1.5 m/s²). Such a value was comparable to the intra-subject variability identified in similar conditions [48].

3.5 Coherence function

The ordinary coherence function has different behaviours in upright and legs bent postures. In the upright posture, coherence is close to unity for all subjects in the whole range of frequencies. When the lower limbs were bent, the average coherence function decreased between 2 and 8 Hz, with a minimum value around the antiresonance frequency (approximately 6 Hz). In the existing studies, the information provided by the ordinary coherence function was mainly used for assessing whether a system was linear or not. High coherence values were interpreted as linear indicators and the adoption of linear identification techniques (i.e. cross-spectral density method) was fully justified. However, experimental results were in contrast with the assumption of linearity since the response of the human body exhibited a nonlinearity with respect to the vibration magnitude. Besides linearity, the coherence function may indicate whether there is correlation between the output and the input signals: high coherence values are retrieved in case of good signal-to-noise ratio, as clearly exposed by Hinz [58]. However, this aspect was considered of marginal importance because under controlled conditions and laboratory instrumentation (i.e. conditioning units, shielded cables, etc.) the signal-to-noise ratio is always adequate.
The low coherence therefore indicates the presence of non-measured inputs or that the mechanical system is nonlinear (i.e. that the system is not additive, homogeneous, time invariant, fixed parameter or causal). Since the only input in the frequency range of interest was the one provided by the stimulus and that a nonlinear model did not increase the coherence value, the nonlinearity was reasonably caused by the variation of the modal parameters in time. This is consistent with what was evidenced in literature [25], where the authors investigated the apparent mass of seated subjects in case of repeated movements of the upper body: subjects twisted their torso to the left and right with accompanied arm movements. In this situation, the coherence was lower than that derived for the static posture; it was hypothesized that the twisting motion was responsible of the whole drop off in the coherence function at low frequencies.
In some of the existing studies, authors rejected trials with low coherence [33, 53]. Results evidenced that the low coherence might be associated with low frequency motion during the tests and involuntary muscular actions, given that the nonlinearity in the response and the measurement noise were proven trivial. The stationarity of the response has been verified dividing the time history into sub-records using the Welch approach and computing the apparent mass on each

of them (Figure 3.10). The analysis returned the state of the apparent masses as a function of time and the FRFs were then statistically analysed. Coherence is low where the apparent mass exhibited large coefficients of variation and both the lower and the upper envelopes showed significant misalignments in the shape (peaks and drops occurred at different frequencies).

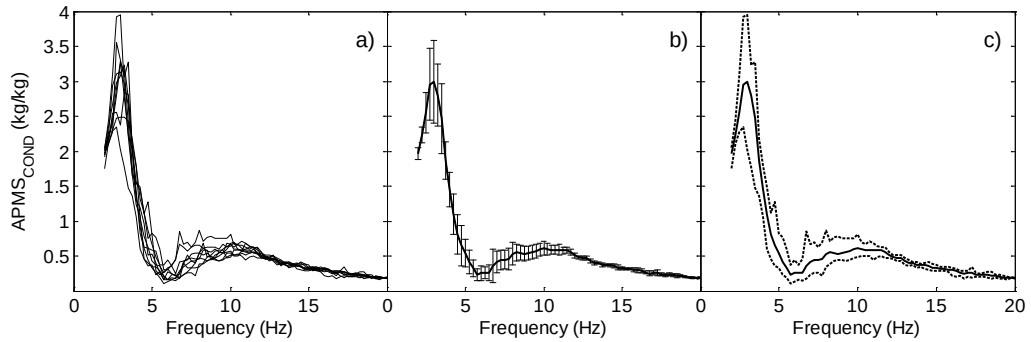

Figure 3.10 Normalized conditioned apparent mass for subject nr. 1: a), intra-subject variability; b), mean and standard deviation; c), upper and lower envelopes.

3.6 Conclusions

3.6.1 Discussion

The contributions of the nonlinear terms to the apparent mass are negligible in the whole range of frequencies. This means that the nonlinear terms (quadratic, square root, and absolute value) did not take part in the definition of the response and other mechanisms were responsible of the low coherence at frequencies below 10 Hz. To our knowledge, it is the first time that the human body biodynamic response is modelled with a parallel nonlinear system and, consequently, there is no material for comparisons. The noise term, which accounted for the non-modelled nonlinearities and the uncorrelated noise on the measurement chain, decreased as the vibration magnitude rose and was always lower than 40% of the apparent mass. The largest error occurred in the antiresonance region, where the apparent mass is approximately 0.5 times the (static) body mass.

3.6.2 Effect of vibration magnitude

Both the parametric and the nonparametric tests evidenced that the conditioned biodynamic response to vertical whole-body vibration was affected by the vibration magnitude only at frequencies larger than 10 Hz. In this frequency range, the apparent mass was lower than the static mass and the effect of

modelling inaccuracy was less critical than the one deriving from an error in the resonance region.
In the existing studies [45, 46], the effect of vibration magnitude on the apparent mass resonance frequency and amplitude have been investigated using the paired Wilcoxon sign-rank test (a non-parametric method); results evidenced that both the resonance frequency and amplitude were magnitude dependent. Since the apparent masses were normally distributed, the differences between the Wilcoxon test and the paired t-test outlined that the effect of vibration magnitude was comparable to the intrinsic phenomenon variability; also in this case, it is convenient to adopt a linear system with uncertainty rather than to use frequency dependent models.

3.6.3 Model accuracy

Experimental results confirmed that the normalized APMS of standing subjects is influenced by the posture and, in specific frequency ranges, by the vibration level; consequently, the adoption of posture, vibration level and body mass dependent APMS models provides for the best description of the biodynamic response to WBV. Results evidenced that the effect of the vibration magnitude on the normalized APMS was definitely smaller than that of the posture and that the effect of vibration magnitude on the non-normalized APMS was negligible in comparison with the effect of the body mass. The benefits deriving from the adoption of the nonlinear models (parallel of linear systems) were negligible. After the correction of all the nonlinear effects (i.e. using nonlinear, vibration magnitude dependent models), the modelling uncertainty (15 to 30 %) was governed by the subjects' posture and body mass. The uncertainty augmentation deriving from the adoption of a unique linear model (3%, Table 3.1) was tolerable, similarly to what happens in the case of hand-arm vibration [59]. This consideration is particularly useful in the identification of the response of mechanical structures in presence of crowds. From this perspective, the body can be modelled with a linear system with uncertainty, thus easing the numerical modelling of man interaction with lightly damped structures (metallic bridges, slender staircases, and similar structures).

Chapter 4

Design of a tri-axial force plate

This chapter describes the design of the tri-axial force plate used to measure the transmitted forces along the three orthogonal axes. General considerations on the design were initially provided; then, a finite element model was used to design the supports with the desired frequency pass-band. At the end, each mechanical component was realized and then mounted in the final configuration. Results from the experimental modal analysis confirmed the absence of resonance frequencies within the frequency range of interest.

4.1 Introduction

The apparent mass is the frequency response function between the transmitted force and the acceleration at the driving point, both measured in the same direction. If the transmitted force is taken along other directions than the excitation axis, the resulting frequency response function is usually referred to as "cross-axis" apparent mass (the first is referred to as the "direct" or the "in-line" apparent mass). In order to investigate the response of the human body (for standing persons) in the basicentric reference system, a tri-axial force plate is needed for measuring the transmitted forces along the three orthogonal directions.

4.2 Constraint configuration for the tri-axial force plate

The tri-axial force plate should be designed in order to measure the force transmitted by the feet of the subjects at the driving point, along each of the three orthogonal axes. Basically, every mounting configuration might be valid in order to derive the transmitted forces but an isostatic mounting eases the measurement operations. In facts, with a hyperstatic mounting, (a setup in which the number of constraints is larger than the degrees of freedom DOF), additional forces will sum to those due to the subjects' inertial forces. These additional contributions are associated to the bending moments which rise at the links between the plate and the supports. Besides the cardinal equilibrium equations, some additional equations are necessary for expressing the relationships between the reaction bending moments and the forces to subtract from measurements. On the contrary, in case of isostatic configuration, the subjects' transmitted forces are simply obtained by summing the measurements along each axis without the need for any correction.

4.3 Draft design of the tri-axial force plate

In order to measure the transmitted inertial forces, the design of the tri-axial plate should undergo the following requirements:

1. the supports must realize the above discussed isostatic configuration;
2. the supports' longitudinal stiffness should be higher than that of the load cells;
3. the supports should guarantee an appropriate stiffness in order to reproduce the ideal joints.

Since a body in the free space has six degrees of freedom, the plate results statically determined by blocking all the translational movements and rotations (i.e. all the DOF are reduced), no matter if the joints introduce redundant constraints (e.g. reaction forces in the same directions).

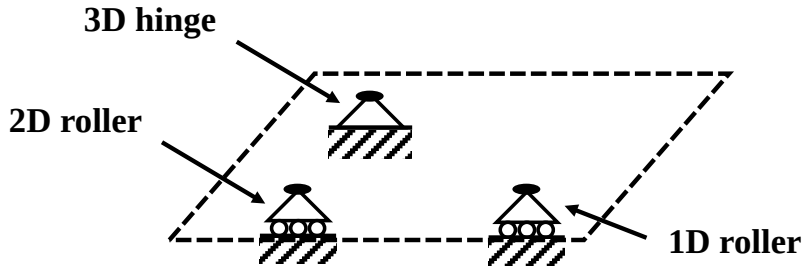

Figure 4.1 Joints' configuration for the tri-axial force plate.

As shown in Figure 4.1, the adopted joints were chosen as follow:

- a three-dimensional hinge (3 degrees of constraint (DOC)),
- a mono-dimensional roller (1 DOC),
- and a two-dimensional roller (2 DOC),

which completely reduced to zero the DOF of the whole structure.

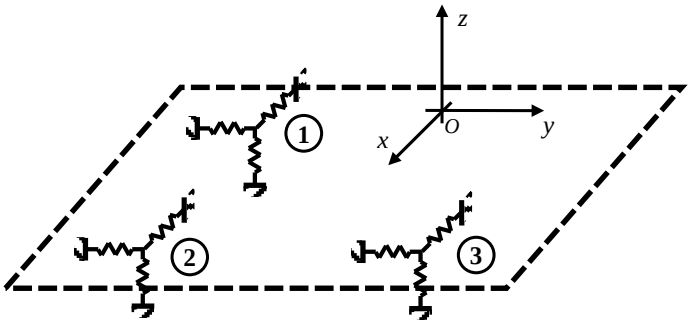

Figure 4.2 Joints' equivalent spring model.

Generally, each joint was modelled with a set of three springs, one along each direction (see Figure 4.2), whose stiffnesses had a proper value in order to realize the desired DOC. For instance, a low value of stiffness was assigned to the spring whose axis corresponded to a translational DOF.
The translational DOFs in the xy-plane of the two-dimensional roller (joint number 2 of Figure 4.2) were obtained with two springs whose stiffnesses were considerably smaller than those of the three-dimensional hinge (joint number 1) in the same directions. Even for the mono-dimensional roller (joint nr. 3) the stiffness along the y-axis was small compared to the others. In this way, the supports' design was fully dominated by the ratio between the stiffness values.

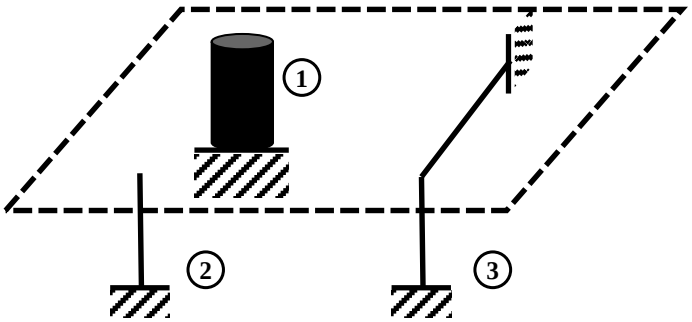

Figure 4.3 Joints' definitive design.

A draft design, which defines the approximate geometry of the supports, was given after substituting each spring of Figure 4.2 with a proper mechanical element (Figure 4.3). The three-dimensional hinge was well represented by a cantilever beam (element nr. 1 of Figure 4.3) while the two-dimensional roller, whose reaction force lies along the z-axis, was adequately represented by a second thin cantilever (element nr. 2). The difference between the two cross-sectional areas was necessary in order to provide the required stiffness ratio. Stiffnesses in the xy-plane were provided by the flexural bending stiffnesses of each beam; the smaller the cross-sectional area was, the smaller became the associated flexural stiffness. Thus, displacements in the xy-plane were greater for the thin cantilever. Finally yet importantly, the second cantilever should be thin enough even for providing that the inertial forces, which lie in the xy-plane, could be entirely transmitted to the hinge for a correct force measurement. This aspect will be relevant once the load cells will be applied to the supporting frame.
Based on the same considerations, the mono-dimensional roller was designed for providing enough compliance only along the y-axis. As depicted in Figure 4.3, element number 3 consisted in two connected beams lying in the xz-plane. The

cross-sectional areas were dimensioned so that the stiffness along the y-axis is smaller than that of element 1 along the same axis.
However, the compressional stiffness provided by each support should be higher than the load cells' axial stiffness. This is to avoid that the axial force deforms the beam instead of the sensing element inside the load cell; if this would occur, no force measurement were produced.

4.4 Load cells and force measurement

Four piezoelectric load cells are used to measure the inertial forces transmitted to plate along each of the three orthogonal axis. Correct estimations are expected if the supports are designed according to the guidelines listed in the previous section.

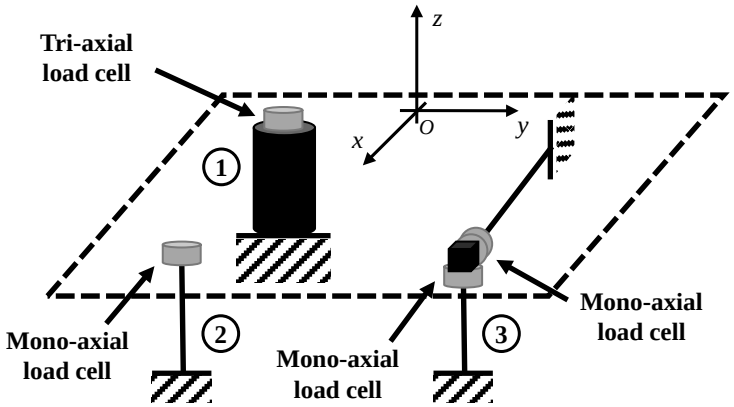

Figure 4.4 Load cells' positioning.

The four load cells are positioned on the supporting frame as Figure 4.4 shows. A tri-axial load cell (PCB 260A11) is located between the first support and the plate with the aim of measuring the forces along the three axes. One mono-axial load cell (PCB 211B) is mounted on the top of the second support in order to measure the reaction force on the z-axis. Finally, two of mono-axial load cells (PCB 211B) are fixed at the end of each beam of the third support, close to the junction with the plate; these two force sensors measure the forces along the x- and the z-axis.
After sampling the measure of each load cell, the inertial force along each direction (due to the subject's body and the plate) is the summation between the signals taken on the same direction:

$$F_{x,tot} = F_{1,x} + F_{3,x} \tag{4.1}$$

$$F_{y,tot} = F_{1,y} \tag{4.2}$$

$$F_{z,tot} = F_{z,1} + F_{z,2} + F_{z,3} \tag{4.3}$$

The above equations are valid if the plate is statically determined and the supports are designed in order to reproduce the ideal joints configuration (Figure 4.1).

4.5 FE model of the force plate

A Finite-element (FE) model was built using the modelling software PTC Creo Parametric, version 2.0, with the aim of solving the following tasks:

- give a proper dimensioning for the supports;
- design the geometry of the plate;
- providing the force plate's natural frequencies (modal analysis);
- solve for the internal stress distribution (static stress analysis).

4.5.1 Load cells modelling

The load cells were introduced in the FE model as three-dimensional springs whose stiffnesses were set to proper values depending on the type of transducer (i.e. mono-axial or tri-axial load cell).
Stiffnesses were ordered in a three-by-three matrix with non-null elements on the main diagonal (i.e. only direct terms were considered and the extra-diagonal values were equal to zero). Table 4.1 shows the numerical values for each modelled load cell; the indexes are referred to the basicentric reference system. For the mono-axial load cells (PCB 211B) the producer provided for only the stiffness along the measuring axis (i.e. k_{zz}). Since the piezoelectric element should be insensitive to any deformation along the other axes, the cross-axis stiffnesses (k_{xx} and k_{yy}) were set to values much higher than the nominal stiffness.

Table 4.1 Load cells' stiffness matrices.

Model	k_{xx} (N mm^{-1})	k_{yy} (N mm^{-1})	k_{zz} (N mm^{-1})
211B	$1.0 \cdot 10^{12}$	$1.0 \cdot 10^{12}$	$2.1 \cdot 10^{6}$
260A11	$7 \cdot 10^{5}$	$7 \cdot 10^{5}$	$1.75 \cdot 10^{6}$

The use of the only springs was not sufficient for the modelling of the load cells' behaviour. In fact, the transducers also introduce a finite contact area and some additional cinematic constraints should be provided. Hence, rigid links were introduced in order to avoid all relative rotations between the contact surfaces

(Figure 4.5). In this way, ones assumes that the load cells have infinite flexural stiffness which is a more realistic condition.

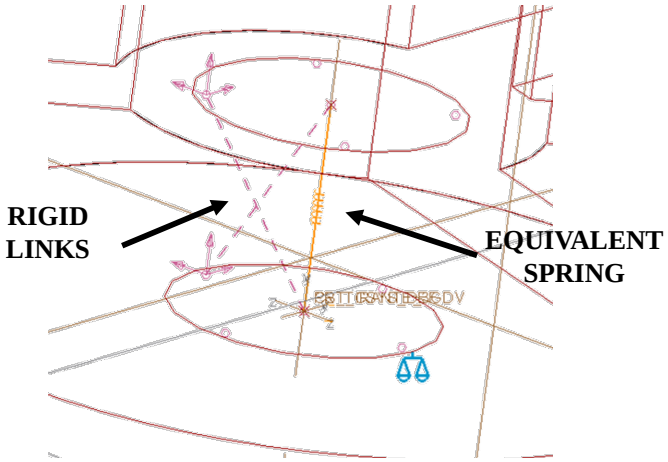

Figure 4.5 Rigid links applied to both the contact surfaces.

4.5.2 Supports

Both the supports' lengths and cross-sectional areas were dimensioned according to the following procedure:

1. imposition of an external force of 1 kN along each axis;
2. computation of the resulting reaction forces at the interface load cell-support and of the corresponding displacements.

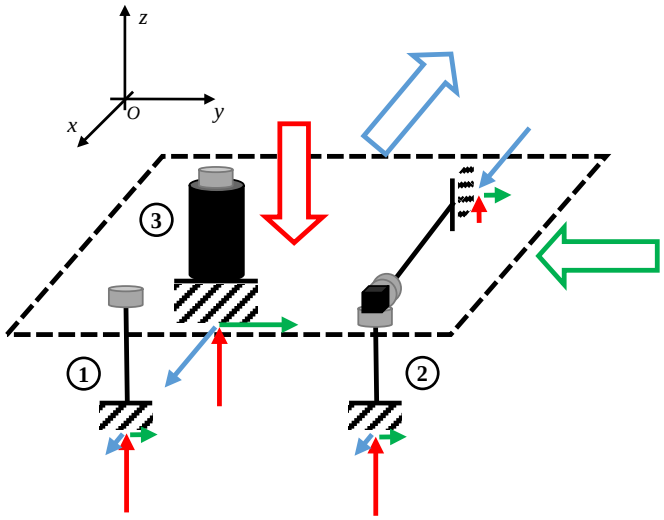

Figure 4.6 External forcing procedure for the dimensioning of the supports.

Stiffnesses along the forcing directions were computed as the ratio between the estimated reaction force and the displacement. Supports without load cells along the forcing direction were dimensioned so as their stiffness was about 1% of that of the load cell in the considered direction. A further reduction in stiffness was reached by providing each thin cantilever with a throat on both the extremities (Figure 4.7). In addition, it was ensured that the total force measured by the load cells was at least the 95% of the total applied load.

Figure 4.7 Proposed geometry for the mono-axial support.

Supports were made of steel (Fe 540) and since they are fixed to a vibrating surface (i.e. a shaker), they were designed with proper interfaces for a secure mounting.

4.5.3 The plate

The plate originally consisted in a 500 by 500 mm thin plate (5 mm thick) made of steel. Such a plate was previously used for measurements along one axis (i.e. the z-axis as in Chapter 2) and its design needed to be modified in order to agree with the new constraints' configuration. In particular, the lowest resonance frequency should be high enough in order to do not fall within the bandwidth of interest (i.e. 1 - 20 Hz).
In order to accomplish with the above mentioned condition, the plate's stiffness was increased by introducing ribs as in Figure 4.8. The ribs were positioned in three specific areas:

1. along the perimetral edge;
2. around the load cells, as the vertexes of a triangle;
3. along the main diagonals, with an additional frame in correspondence of the vertex with the highest distance from the load cells (i.e. the higher the distance from the constraints, the lower the equivalent flexural stiffness).

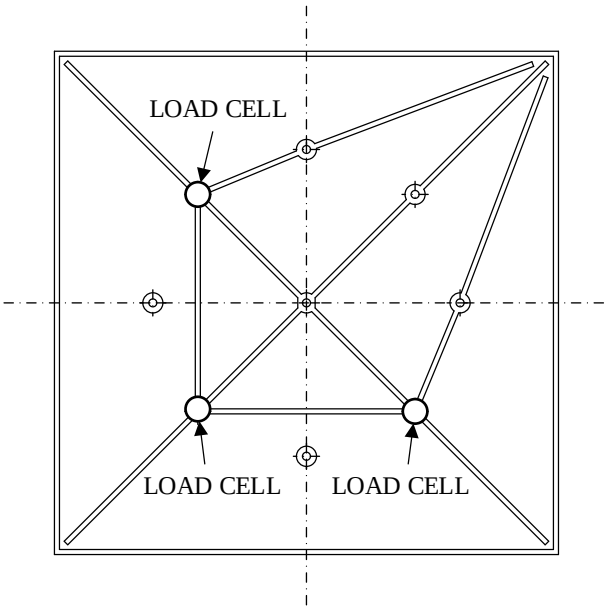

Figure 4.8 Plate (bottom view): ribs' configuration.

4.5.4 Modal analysis

A modal analysis is required to assess if there are resonances of the force plate within the range of characterization of the apparent masses (i.e. for frequencies below 20 Hz).
The first two vibration modes were identified for the unloaded force plate. In this configuration, the force plate is constrained to the shaker's head and without any applied load. The mode with the lowest resonance frequency was identified at about 96 Hz (Figure 4.9) and consists in a rotation of the plate around the support below the tri-axial load cell and a bending of the plate, with maximum displacement at the free corner (the one with the highest distance from the supports). The second vibration mode (145 Hz) is a rotation of the plate that also bends around the supports (Figure 4.10). In this case, the two movements are in counterphase with respect to the previous mode.

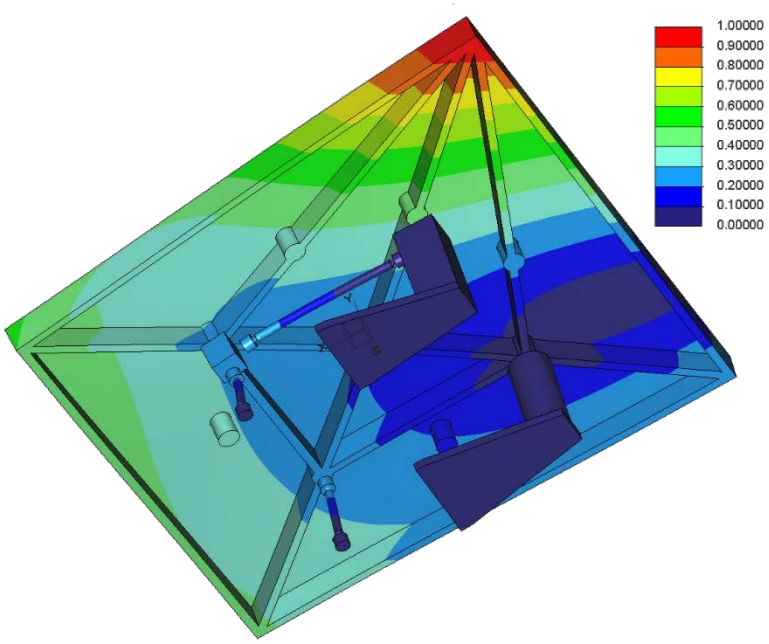

Figure 4.9 First vibration mode at 96 Hz for the unloaded force plate.

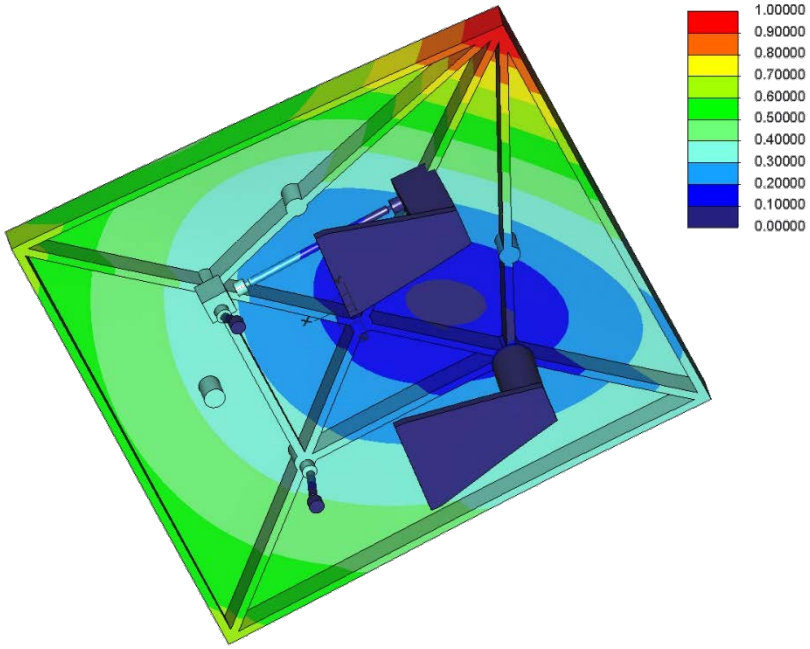

Figure 4.10 Second vibration mode at 145 Hz for the unloaded force plate.

4.5.5 Static stress analysis

The static stress analysis consists in applying the inertial force due to a standing person accounting for the maximum acceleration imposed to the plate. From the second chapter, the normalized apparent masses for the standing person (all postures and acceleration magnitudes) were sketched together in Figure 4.11.

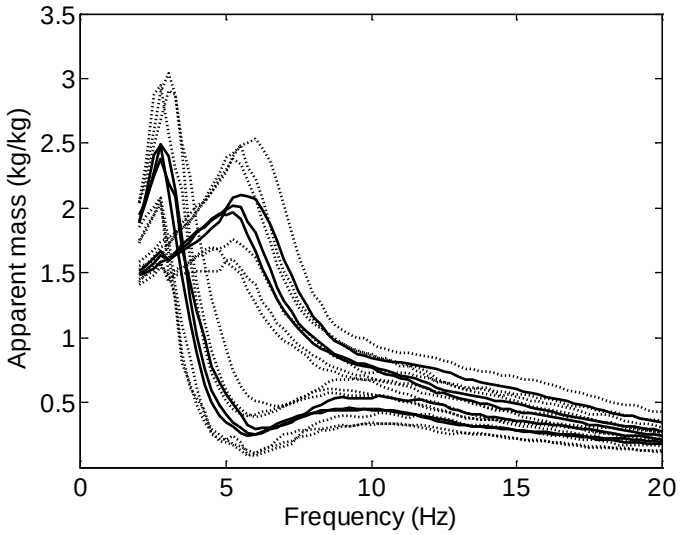

Figure 4.11 Apparent masses for the standing person (all magnitudes and postures).

The maximum magnitude does not exceed three times the subject's static mass, if one considers also the uncertainty bands (CI of 68 %). Thus, if the subject's body mass is 75 kg , the resulting inertial force is given as follows:

$$F_{in} = m \cdot k_{APMS} \cdot (g + a_{plate}) \tag{4.4}$$

where m is the subject's body mass, k_{APMS} is the maximum value reached by the APMS of Figure 4.11, g is the acceleration of gravity and a_{plate} is the imposed acceleration which sums to the gravity. The last condition would consider the most unfavourable situation in which the two accelerations are in phase.
From equation (4.4), the total applied load is equal to 2800 N (a_{plate} = 1.5 m s^{-2} RMS) which will be applied directly to the plate's surface. A reliable result will be provided by applying the load to two footprints which reproduce the contact area between the subject's feet and the plate.

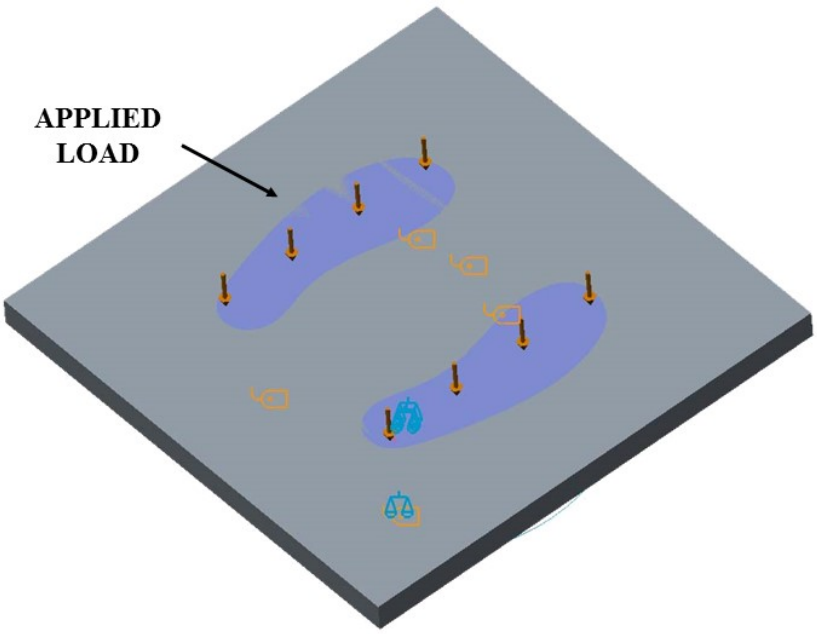

Figure 4.12 Modelling of the applied load on the plate.

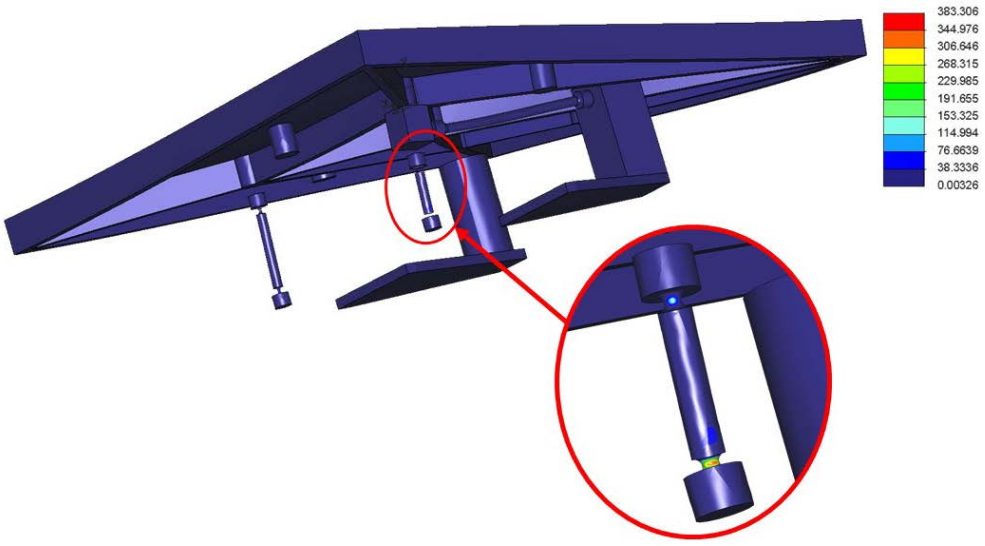

Figure 4.13 Static stress analysis of the force plate.

The equivalent von Mises stress was 385 MPa, localized in correspondence of both the throats of the cantilever supporting the bi-axial load cells (Figure 4.13). Such value is lower than the limit stress of the material (450 MPa for the yield strength and 540 MPa for the ultimate strength) and it is localized on the central

part of the throat. Thus, the force plate resulted verified for an applied load consisting in a standing person exposed to vertical WBV at the magnitude of 1.5 m s^{-2} RMS.

4.6 Dual-axis interface

The apparent masses due to excitations in horizontal directions have been identified with the use of a secondary electrodynamic shaker. The shaft of the secondary vibration source has to be aligned to the plate plane in the x- or the y-axis of the basicentric reference system.
The force plate described in the previous section has been mounted onto an interface, designed to be compliant along the secondary direction of excitation.
The interface consists in two discs of aluminium joined together through two thin plates of spring steel (C72) (i.e. the plates will be aligned perpendicularly to the direction of translation). The aluminium provides for reduced weight of the whole structure while the spring steel the necessary mechanical resistance and elasticity, even under large displacements.
Hence, the design should respond to the following requirements:

1. no resonance frequencies within the bandwidth of interest (1-20 Hz);
2. mechanical resistance in case of maximum displacement in the lateral direction (about 12 mm);
3. mechanical resistance of the whole structure under the inertial forces due to either vertical or lateral vibrations (accounting for the apparent mass of subjects).

Even in this case, the maximum stress should not exceed the limit stress of the material under the expected inertial forces. The final design of the interface was obtained using the software PTC Creo parametric (version 2.0). A 3D parametric model was built with the following parameters:

- distance between the upper and lower discs (i.e. the same as the height of the iron steel plates);
- width of the spring steel plates (the height directly corresponds to the distance between the upper and lower discs);
- distance between the two plates;
- thickness of the plates.

These parameters were changed for satisfying the above mentioned requirements (points from 1 to 3) and dimensions were finally determined (Table 4.2).

Table 4.2 Main dimensions for the dual-axis interface.

Parameter	Dimension
Distance between the upper and the lower discs	140 mm
Width of the spring steel plates	200 mm
Distance between the two spring steel plates	240 mm
Thickness of the spring steel plates	0.8 mm

4.6.1 Static stress analysis

The first static stress analysis was computed by imposing to the upper disc the maximum displacement at the highest acceleration magnitude, which was estimated being 1.4 mm (in the range 1 – 20 Hz, at 1.5 m s^{-2} RMS). The resulting maximum stress was 67 MPa (von Mises equivalent stress), much lower than the limit stress (1800 MPa).
A second internal stress analysis was performed on the whole assembly force plate/dual-axis interface. As for the case of the force plate, it was imposed a load equal to the inertial force exerted by a standing person.

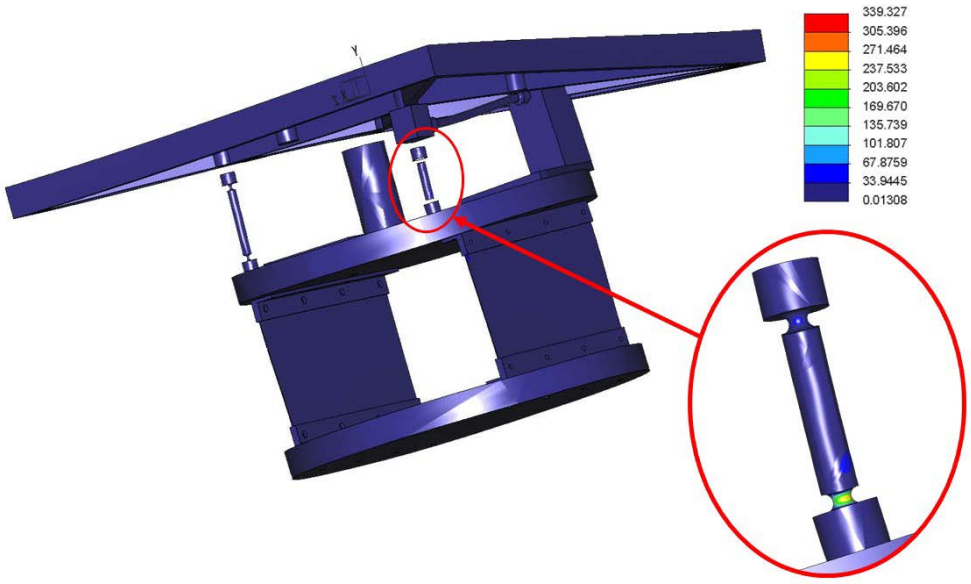

Figure 4.14 Static stress analysis of the force plate mounted on the dual-axis interface.

The resulting equivalent von Mises stress was 340 MPa (yield strength equal to 450 MPa). The maximum stress was always localized at both the throats of the supports in correspondence of the bi-axial load cell (Figure 4.14).

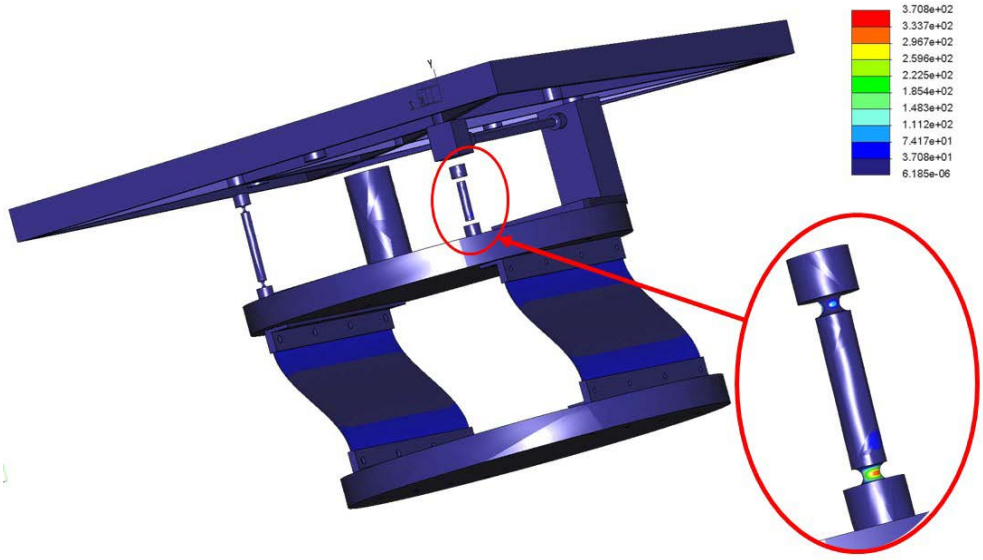

Figure 4.15 Static stress analysis due to a combination between the transversal displacement and the maximum inertial load.

Finally, if the maximum transversal displacement and the maximum inertial load were combined, the resulting maximum equivalent von Mises stress was 370 MPa (Figure 4.15). The whole measuring system resulted verified even in case of the most possible unfavourable condition.

4.6.2 Modal analysis

The first two vibration modes were identified for both the unconstrained and the constrained models (i.e. the dual-axis interface mounted on the shaker's head with the force plate fixed on the upper disc). For the unconstrained model, the first two modes were identified at about 25 Hz and at 423 Hz. The first modal shape consisted in a roto-translation which basically reduced to a relative translation between the two discs. The second modal shape corresponded to a flexural vibration mode of both the steel plates and it was too high in frequency to be considered. If the interface was fixed to the shaker's head, the first mode reduced to about 13 Hz whilst the second to 377 Hz. Again, the first mode corresponded to a mutual translation of the two discs with the lower one fixed (Figure 4.16). This mode is not practically relevant, given the constraint provided by the secondary shaker in the lateral direction. The total displacement halved and this

was the reason the resulting resonance frequency reduced by a factor of two. The second mode consisted in a high frequency flexural vibration mode of the lower disc and, even in this case, it was not reported because largely out of the band of interest.

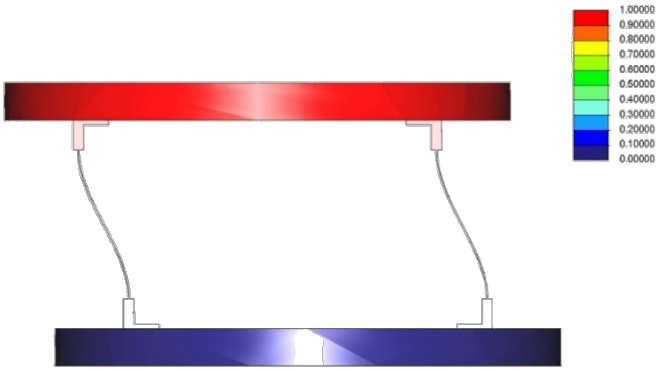

Figure 4.16 First modal shape for the constrained dual-axis interface.

In case of dual-axis interface provided with the force plate mounted onto the upper disc, two resonance frequencies rise below 100 Hz. The first, always associated to the translation of the upper plate, reduced to about 6.5 Hz (Figure 4.17) while the second was at about 92 Hz. This last modal shape was a torsional movement of the force plate where the upper plate also spun due to a deformation of the spring steel plates.

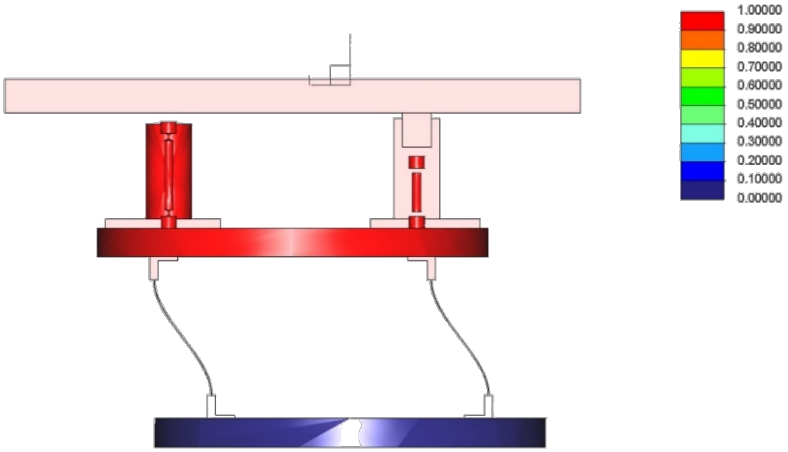

Figure 4.17 First modal shape for the constrained system force plate/dual-axis interface.

4.7 Setup assembling

Once that all requirements were satisfied, each mechanical component was manufactured. Some detailed view of the force plate and of the dual-axis interface are shown in Figure 4.18. The final setup is shown in Figure 4.19: the force plate (with the load cells) was fixed to the dual-axis interface, which was mounted on the shaker's head.

a) 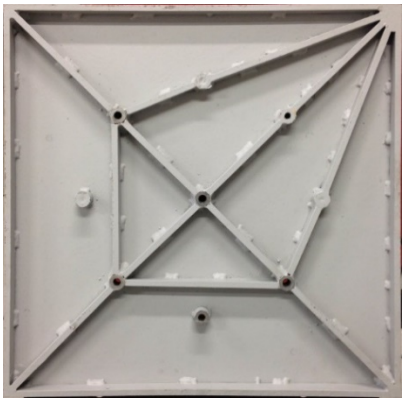 b) 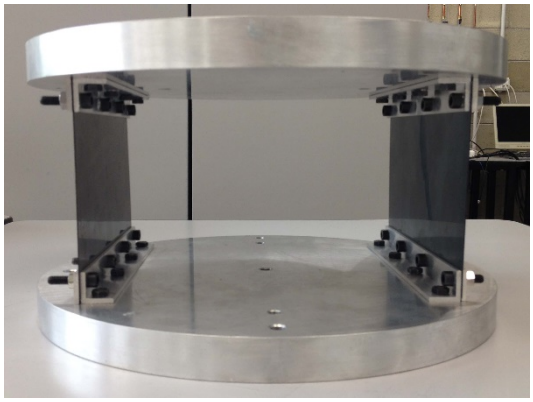

Figure 4.18 Realized components: a) plate provided with ribs; b) dual-axis interface.

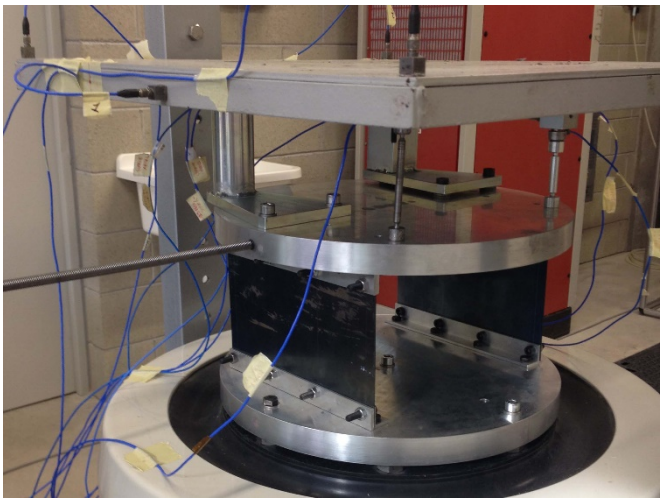

Figure 4.19 Final setup: force plate mounted on the dual-axis interface.

4.8 Experimental validation of the design

4.8.1 Modal analysis of the dual-axis interface

The results given by the FE model were experimentally verified for the unconstrained dual-axis interface. The interface was suspended to a rigid frame using two elastic belts and it was excited by hammering the centre of the lower disc, the centre of the upper disc and its edge along the direction of the allowed degree-of-freedom. A set of four accelerometers was put in order to measure the response based on the modes given by the FE model. The resulting first mode was at 21 Hz, very close to the theoretically computed.

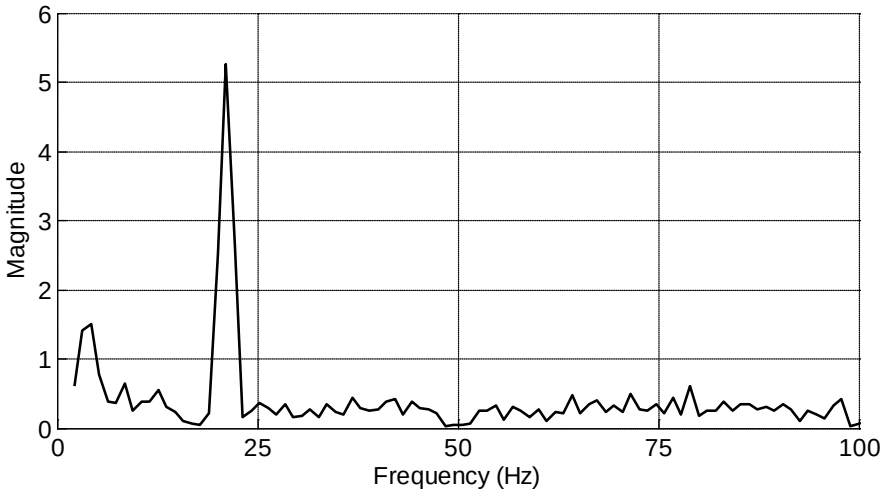

Figure 4.20 Experimental FRFs (1 – 100 Hz) for the unconstrained dual-axis interface.

A second modal analysis was performed by mounting the dual-axis interface on the head of the electrodynamic shaker. In this configuration, the lower disc was avoided to translate and the resulting total displacement was consequently halved so that the first resonance frequency dropped to about 10 Hz.

4.8.2 Modal analysis of the force plate

The results from the modal analysis of the FE model were checked by mounting the force plate onto an electrodynamic shaker with the aim of identifying the first two resonance frequencies (i.e. previously estimated in 96 Hz and 145 Hz). Hence, the force plate was submitted to random vertical vibrations at the same acceleration magnitude (1.5 m s^{-2} RMS) in the bandwidth 1-150 Hz. The experimental setup is shown in Figure 4.21: five accelerometers (four mono-

axials and one tri-axial) were fixed on the force plate, the chassis and the supporting frame of the shaker. The resulting frequency response functions (FRFs) were derived with respect to the vertical acceleration taken from another accelerometer (not shown in Figure 4.21) placed in the centre of the shaker's head. Results confirmed that the force plate had two main resonances at 100.3 Hz and 124.2 Hz (the first was very close to the one estimated by the FE model); other three secondary resonances rose at 10 Hz, 32 Hz and 62.5 Hz. This last resonance was associated to a rotation of the force plate around the shaker's pins because the peak was evident for the only accelerometers placed on the plate's edge (the tri-axial accelerometer had no resonance along both the x- and y-axis).

A second configuration was chosen for understanding the origin of both the unexpected resonance frequencies (10 Hz and 32 Hz). In the new configuration, the shaker's supports were deflated and the supporting frame rest on four blocks of steel. The resulting FRFs are shown in Figure 4.22, where there are two main resonances at 102.8 Hz and 126.6 Hz and minor resonances rose at 50.5 Hz, 61 Hz and 72 Hz. These resonances were related to rotations of the plate since they did not appear in the FRFs derived from the tri-axial accelerometer (placed in the centre of the plate). Then, the lowest resonance frequency at 10 Hz was associated to a movement around the pins since the peak disappeared when they were deflated. An additional peak appeared at 26 Hz, while the resonance at 32 Hz was the same as the suspension conditions changed. On the other hand, the FRFs for the supporting frame and the shaker's chassis were null within all the bandwidth of excitation (for convenience they were not reported in the drawings).

In general, results confirmed the goodness of the FE model and the non-ideal behaviour of the excitation device. In facts, the shaker was effected by unexpected transversal resonances that fortunately rose quite out from the range of interest (i.e. 1–20 Hz).

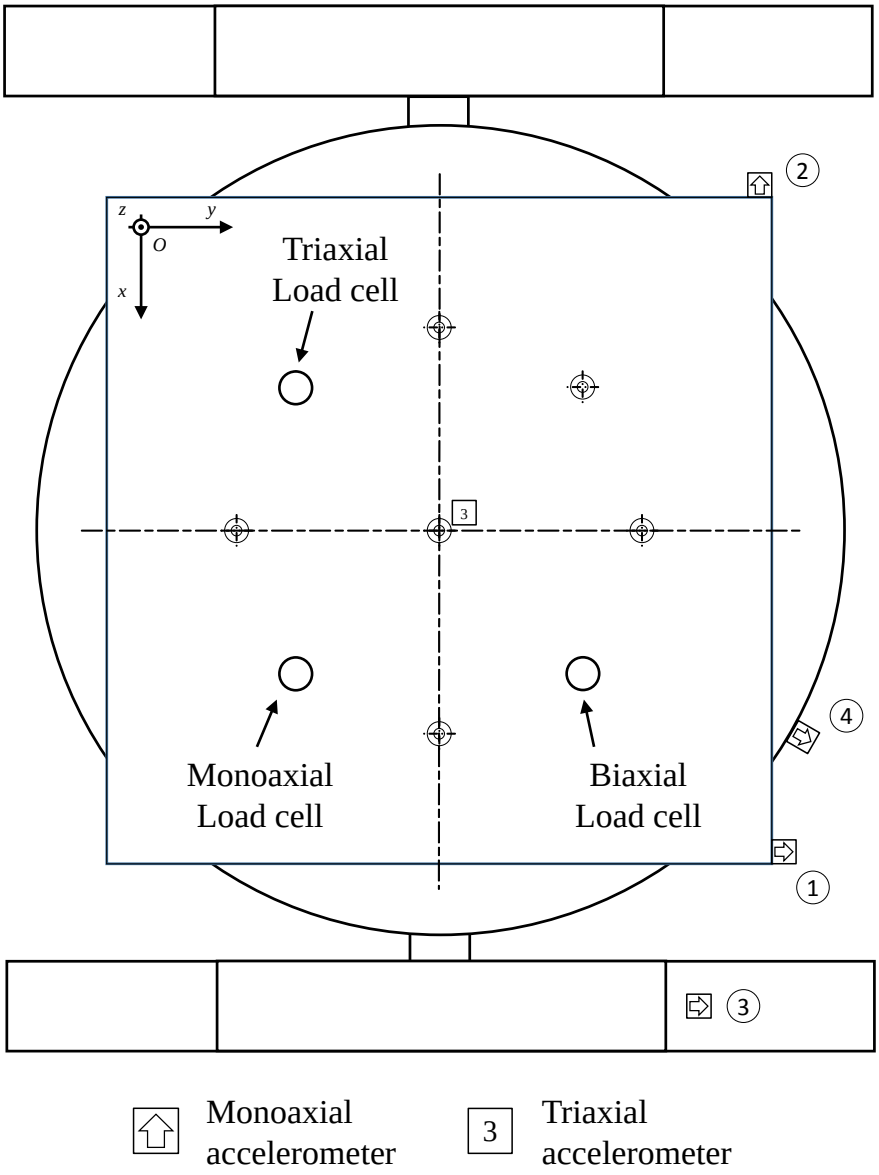

Figure 4.21 Position of the accelerometers for the experimental modal identification.

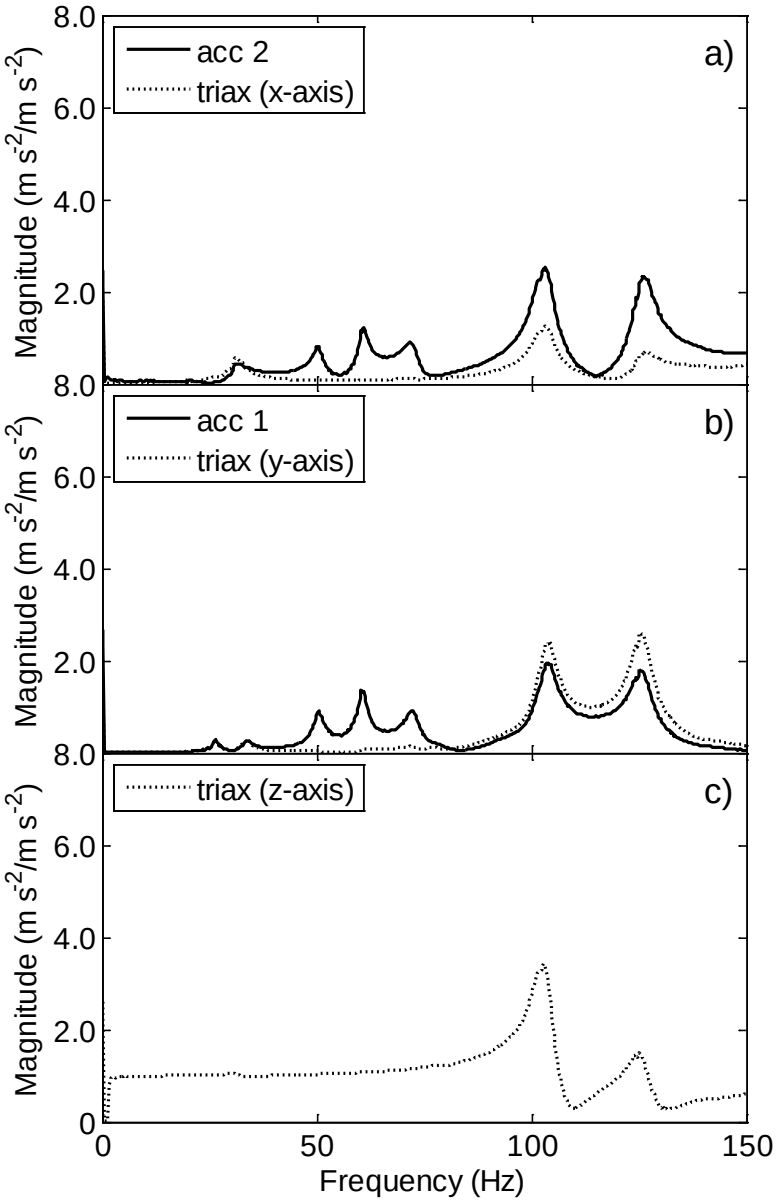

Figure 4.22 Measured FRFs (1 – 150 Hz) for the unloaded force plate (flat supporting pins): a) x-axis, b) y-axis, c) z-axis.

Chapter 5

Calibration of the tri-axial force plate

This chapter deals with the calibration of the tri-axial force plate. After an introduction to the calibration and its challenges, the procedures for calibrating the load cells along the z-axis and in the xy-plane are presented along with the results expressed in terms of the reverse sensitivity matrix. The chapter ends with some considerations on the uncertainty obtained for the measured forces.

5.1 Introduction

The previous chapter described the design of the tri-axial force plate along with the modal and static analysis performed on each mechanical element. At this point, a calibration of the whole force plate is necessary to ensure that measurements are a good representation of the transmitted forces; this is an essential issue for deriving the apparent masses along the x-, y- and z-axes.
The force plate was designed to be isostatically fixed to the shaker head; in the actual working conditions, the constraints are different because of the finite contact area between the load-cells and the plate and the not negligible flexural stiffness of the force sensors. Furthermore, the transverse sensitivity of the piezoelectric crystal induces readings on axes perpendicular to the one in which the load is applied, and additional forces derive from the bending torques rising at the interface between the plate and the load-cells.
The calibration is targeted to the identification of the sensitivity matrix, expressing the relationship between the forces - torques and the voltage. From the measurement theory, the sensitivity is defined as the first derivative of the calibration curve:

$$k_i = \left[\frac{\partial y(\mathrm{x})}{\partial x} \right]_{x=x_i} \tag{5.1}$$

Equation (5.1) is not used in practice and the sensitivity is identified by interpolating the experimental calibration data in a least square sense. If the input-output dependence is linear, the sensitivity is constant and is coincident with the slope of the interpolating line. High order curves (quadratic or cubic functions) can be used if the linear interpolation leads to a large residual uncertainty or if the residuals are not randomly distributed.
It is well known that the use of nominal sensitivity may lead to biased measurements in presence of non-ideal piezoelectric cells constraints. For current purposes, the load cells sensitivity can be identified using a dynamometric

hammer or by measuring the inertial forces of calibrated masses put on an electrodynamic shaker.
These methods are operatively different, but are in principle equivalent. With the first method a dynamometric hammer is used to hit the surface of the force plate; this is a non-stationary method because the analysis is performed on the transient response due to an impulsive excitation. With the second method, a set of calibrated masses is directly applied to the plate surface and the inertial force under a known acceleration are measured by the force platform.
In order to identify the deviation from the nominal sensitivity, the result of calibration was a matrix of correction coefficients minimizing the calibration residuals. The coefficients magnitude indicate whether the isostatic constraint condition is reached or not.

5.1.1 The sensitivity vector

Piezoelectric transducers are almost insensitive to angular rotations but the sensitivity on the plane parallel to the mounting surface could be significant. This is due to the misalignment of the sensitivity vector with respect to the measuring direction (Figure 5.1) [60]. Such a misalignment could lead to huge errors in presence of non-negligible transverse inputs (e.g. shear forces in case of load-cells).

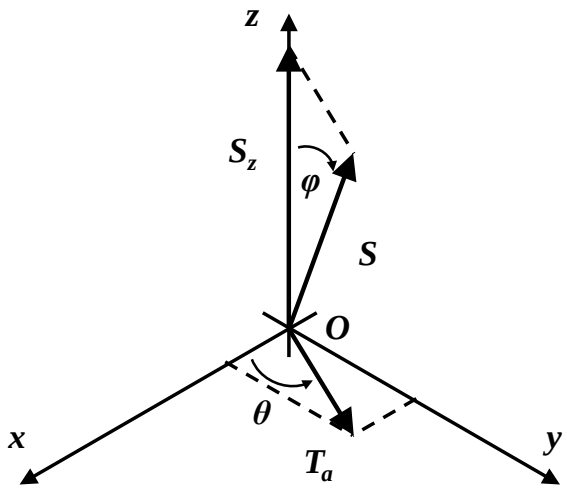

Figure 5.1 Sensitivity vectors and reference coordinate system.

Generally, the sensitivity vector *S* is not aligned to the z-axis but it is tilted by an angle φ and it could be also decomposed in the three orthogonal components S_x, S_y and S_z. The z component, S_z, is normally referred as the transducer's sensitivity

while the absolute transverse sensitivity T_a is the vectorial composition between S_x and S_y:

$$T_a^2 = S_x^2 + S_y^2 \tag{5.2}$$

$$\theta = \arctan\left(\frac{S_y}{S_x}\right) \tag{5.3}$$

Transverse inputs along the θ direction will produce the maximum transverse outputs while there are no outputs if they are applied at $\theta \pm 90°$ [60].
The absolute transverse sensitivity (T_a) is expressed in the same units of the transducer sensitivity and it is generally reported as a relative value, with respect to the nominal sensitivity:

$$T_r = \frac{T_a}{S_z} \cdot 100 \tag{5.4}$$

The ratio of equation (5.4) is commonly referred to as the *cross-talk* and its value is typically between 1% and 3% (sometimes up to 5%) even if some applications demand for transverse sensitivities less than 1%: e.g. in case of simultaneous inputs (e.g. triaxial accelerations or forces) or for transducers of low sensitivity. However, the cross-talk is not the main source of uncertainty in a measurement chain and the accuracy with which it should be known is not stringent [60].
Neglecting the transducer random noise, the output from a piezoelectric transducer is given by:

$$V = a_z \cdot S_z + a_x \cdot S_x + a_y \cdot S_y \tag{5.5}$$

where a_x and a_y are the accelerations on the mounting surface (xy-plane)[60].

5.1.2 LMS method for deriving the sensitivity matrix

The calibration coefficients in the sensitivity matrix are derived by solving the calibration problem:

$$\hat{y} = \mathbf{A} \cdot \hat{x} \tag{5.6}$$

In equation (5.6), the vector $\hat{y}$ contains the values of the loads applied during the calibration procedure while vector $\hat{x}$ refers to the loads measured by the load-cells

with their nominal sensitivity. Matrix $\mathbf{A}$ is the sensitivity matrix, the unknown term in equation (5.6).
In order to determine the calibration matrix A at minimum a set of linearly independent calibration conditions equal to the number of rows of the calibration matrix would be needed.
Instead of determining the exact solution, it is preferable to find a solution, which minimizes the vectorial difference $\mathbf{Ax - b}$ [61] for a set of conditions larger than the minimum required.
The general solution for the problem of equation (5.6) is given by:

$$\mathbf{x} = \mathbf{A}^{\mathbf{g}}\mathbf{b} + \left(\mathbf{I} - \mathbf{A}^{\mathbf{g}}\mathbf{A}\right)\mathbf{w} \tag{5.7}$$

which is valid either if the system is consistent or not; in this second case, the solution provided by equation (5.7) is meant to be a least-squares solution.
Matrix $\mathbf{A}^{\mathbf{g}}$ is any generalized inverse matrix but in many practical situations corresponds to the Moore-Penrose generalized inverse matrix (sometimes called "pseudoinverse") which minimizes the Euclidean norm of the solution vector.
The Moore-Penrose inverse matrix satisfies the following four conditions:

1) $\mathbf{A}\mathbf{A}^{\mathbf{g}}\mathbf{A} = \mathbf{A}$;
2) $\mathbf{A}^{\mathbf{g}}\mathbf{A}\mathbf{A}^{\mathbf{g}} = \mathbf{A}^{\mathbf{g}}$;
3) $\left(\mathbf{A}\mathbf{A}^{\mathbf{g}}\right)^{\mathbf{T}} = \mathbf{A}\mathbf{A}^{\mathbf{g}}$;
4) $\left(\mathbf{A}^{\mathbf{g}}\mathbf{A}\right)^{\mathbf{T}} = \mathbf{A}^{\mathbf{g}}\mathbf{A}$.

The proof of equation (5.7) is given if one considers the Euclidean norm of the residual vector $\|\mathbf{Ax - b}\|$. In facts, this is a minimum if and only if the solution vector is given by the formula:

$$\mathbf{x} = \mathbf{A}^{\mathbf{g}}\mathbf{b} + \left(\mathbf{I} - \mathbf{A}^{\mathbf{g}}\mathbf{A}\right)\mathbf{w} \text{ for any arbitrary } \mathbf{w} \in \mathbb{R}^n \tag{5.8}$$

The residual vector $\mathbf{Ax - b}$ is also given as follows:

$$\mathbf{Ax - b} = \mathbf{Ax - AA}^{\mathbf{g}}\mathbf{b} - \left(\mathbf{I - AA}^{\mathbf{g}}\right)\mathbf{b} \tag{5.9}$$

being $\mathbf{AA}^{\mathbf{g}} = \mathbf{I}$.
If one proves that vectors $\mathbf{Ax - AA}^{\mathbf{g}}\mathbf{b}$ and $\left(\mathbf{I - AA}^{\mathbf{g}}\right)\mathbf{b}$ are orthogonal, the generalized Pythagoras's theorem may be applied:

$$\|\mathbf{Ax - b}\|^2 = \left\|\mathbf{Ax - AA}^{\mathbf{g}}\mathbf{b}\right\|^2 + \left\|\left(\mathbf{I - AA}^{\mathbf{g}}\right)\mathbf{b}\right\|^2 \geq \left\|\left(\mathbf{I - AA}^{\mathbf{g}}\right)\mathbf{b}\right\|^2 \tag{5.10}$$

The lower bound on the right side of equation (5.10) is attained if and only if $\mathbf{Ax} = \mathbf{AA^g b}$ and by the James's theorem this occurs for

$$\mathbf{x} = \mathbf{A^g}\left(\mathbf{AA^g}\right)\mathbf{b} + \left(\mathbf{I} - \mathbf{A^g A}\right)\mathbf{w} = \mathbf{A^g b} + \left(\mathbf{I} - \mathbf{A^g A}\right)\mathbf{w} \tag{5.11}$$

In equation (5.11) the matrix $\mathbf{A^g}$ may not satisfy the four conditions of the Moore-Penrose inverse matrix. Equation (5.11) reduces to:

$$\mathbf{x} = \mathbf{A^g b} + \left(\mathbf{I} - \mathbf{A^g A}\right)\mathbf{w} \tag{5.12}$$

where the vectors $\mathbf{A^g b}$ and $\left(\mathbf{I} - \mathbf{A^g A}\right)\mathbf{w}$ are orthogonal to each other:

$$\left(\mathbf{A^g b}\right)^{\mathbf{T}}\left(\mathbf{I} - \mathbf{A^g A}\right)\mathbf{w} \tag{5.13}$$

$$\left(\mathbf{A^g AA^g b}\right)^{\mathbf{T}}\left(\mathbf{I} - \mathbf{A^g A}\right)\mathbf{w} \tag{5.14}$$

$$\left(\mathbf{A^g b}\right)^{\mathbf{T}}\mathbf{A^g A}\left(\mathbf{I} - \mathbf{A^g A}\right)\mathbf{w} \tag{5.15}$$

$$\left(\mathbf{A^g b}\right)^{\mathbf{T}}\mathbf{A^g}\left(\mathbf{A} - \mathbf{AA^g A}\right)\mathbf{w} = \mathbf{0} \tag{5.16}$$

Hence, by applying the Pythagoras's theorem

$$\left\|\mathbf{A^g b} + \left(\mathbf{I} - \mathbf{A^g A}\right)\mathbf{w}\right\|^2 = \left\|\mathbf{A^g b}\right\|^2 + \left\|\left(\mathbf{I} - \mathbf{A^g A}\right)\mathbf{w}\right\|^2 \geq \left\|\mathbf{A^g b}\right\|^2 \tag{5.17}$$

If $\mathbf{A}$ is a m-by-n rectangular matrix and its rank is equal to m or n, the general inverse is given by:

$$\mathbf{A^g} = \mathbf{A^T}\left(\mathbf{AA^T}\right)^{\mathbf{-1}} = \left(\mathbf{A^T A}\right)^{\mathbf{-1}}\mathbf{A^T} \tag{5.18}$$

Finally, the least mean square solution of the calibration problem is provided as follows:

$$\hat{y}\cdot\hat{x}^T = \mathbf{A}^{\dagger}\cdot\left(\hat{x}\cdot\hat{x}^T\right) \tag{5.19}$$

$$\mathbf{A}^{\dagger} = \hat{y}\cdot\hat{x}^T\cdot\left(\hat{x}\cdot\hat{x}^T\right)^{-1} \tag{5.20}$$

where $\mathbf{A}^{\dagger}$ is Moore-Penrose inverse matrix.

5.1.3 The sensitivity matrix

As already mentioned, the sensitivity matrix multiplies the generalized force vector to obtain the transducer outputs. Generally, it appears as a full matrix since it accounts for the relationships between each channel and the measured quantities. The elements on the main diagonal are the sensitivities along the desired directions, while other elements are the transverse-axes sensitivities.
Dealing with force platforms, the input quantities should be either forces or torques, both evaluated with respect to a given Cartesian reference system. Since during the measurement process the reference parameter is the inverse of the sensitivity matrix, in the following the latter has been addressed as reverse sensitivity, which is a six-by-N matrix, where N is the number of channels to calibrate:

$$\left[\{F\}_{1\times 3}\{M\}_{1\times 3}\right]^T = [S]_{6\times N}\cdot\{V\}^T_{1\times N} \tag{5.21}$$

When the bending torques are null or neglected the sensitivity matrix $[S]$ of equation (5.21) reduces to a three-by-N matrix. The three forces measured along the basicentric reference system can be derived from the sensitivity matrix and the measured voltages:

$$\{F_x \quad F_y \quad F_z\}^T = [S]_{3\times N}\cdot\{V\}^T \tag{5.22}$$

$\{V\}^T = \{V_1 \quad V_2 \quad \dots \quad V_N\}^T$ is the array composed by the voltages provided by each load cell.

5.2 Calibration

As already stated in the introduction, the calibration can be performed using either the inertial forces due to calibrated masses under known accelerations or a dynamometric hammer. In this application, the force plate was calibrated using both the techniques since a third axis of excitation was not available. So, calibrated masses were used for calibrating the channels in the vertical direction and the dynamometric hammer for those in the xy-plane.

5.2.1 Calibration in the z-axis direction

The calibration was carried out on the same setup for the measurement of the apparent mass. The procedure consisted in:

1. placing the masses on the force plate in different positions (in order to generate different moments on the platform);

2. generating vibration at different acceleration magnitudes (0.5 m s^{-2} and 1.0 m s^{-2} RMS) in the vertical direction;
3. acquiring the force and acceleration signals.

Both masses and accelerations were randomized in their ordering and magnitude. The above-described procedure was repeated three times in order to assess:

- the experiments repeatability, evaluated by repeating measurements with the masses in different positions;
- the experiments reproducibility, analysed by changing the orientation of load cells to evaluate the impact of the transversal sensitivity and mounting imperfections on the measurement uncertainty.

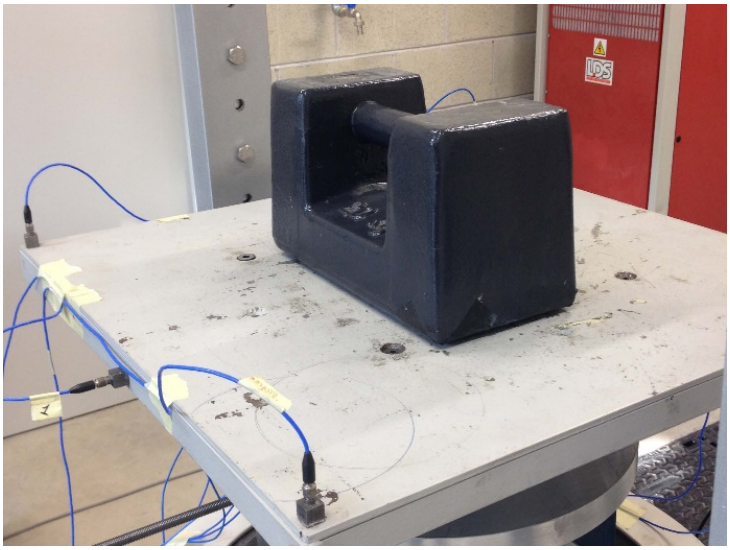

Figure 5.2 Example of calibration in the z-axis direction with a calibrated mass of 20 kg.

The masses consisted in a set of cast iron calibrated masses (5 kg, 10 kg and 20 kg); mass in the range 10-40 kg were realized by combining the calibration masses. The uncertainty of each calibration mass was lower than 0.1%.
Data were collected from each trial: the nett FRFs of each load cell were derived by subtracting, in the complex domain, the FRF of the unloaded force plate from that in case of applied calibration mass. The nett FRFs represent the apparent mass measured by each load cell whose summation in magnitude (accounting for the sign deriving from the relative phase) should theoretically correspond to the applied mass.
With large masses positioned far from the plate centre, the influence of a transverse (lateral) resonance of the shaker in the bandwidth of interest was not negligible. The sensitivity was therefore derived in the range 2-15 Hz where the

FRF was constant in magnitude; this limitation does not affect the experiments, where subjects stood always in a central position on the plate.

5.2.2 Calibration in the xy-plane

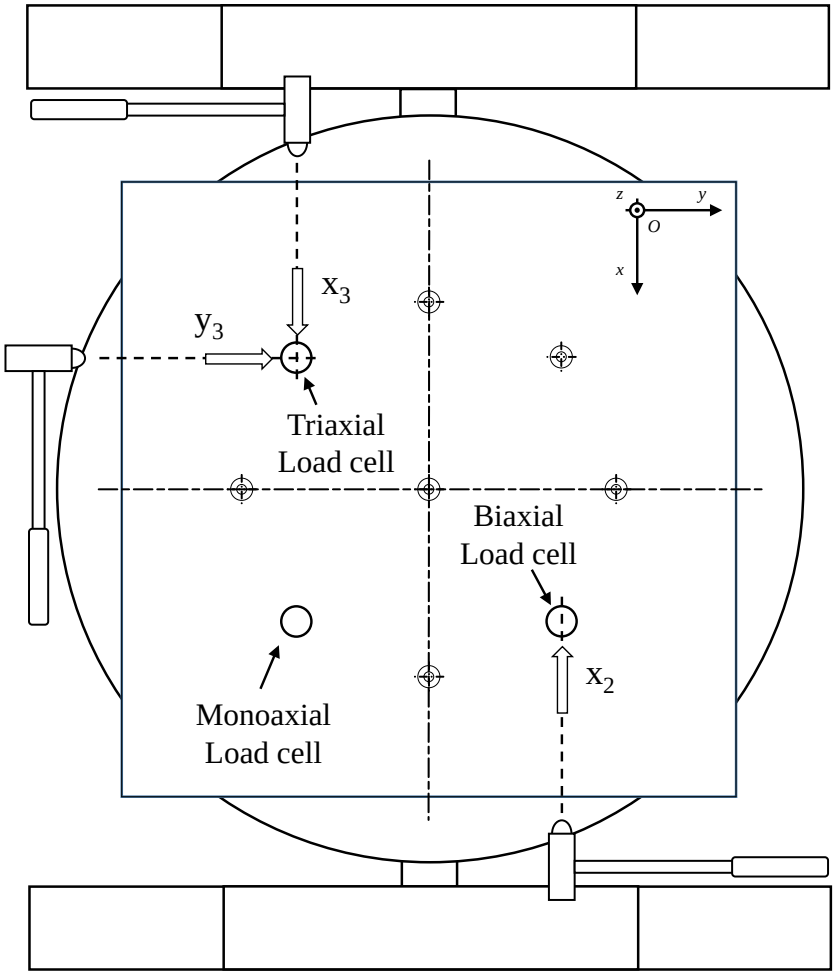

Figure 5.3 Hammering of the load cells in the xy-plane.

The calibration of the load cells measuring forces in the xy-plane was performed by hitting the edge of the force plate with a dynamometric hammer along the measuring directions shown in Figure 5.3. The location of the hammering points was carefully selected to limit the bending moments as much as possible. Of no less importance was the alignment of the hammering hit: in case of small impact angles, the load cells underestimate the force applied by the dynamometric hammer with a consequent underestimation of the sensitivity coefficients. Even

the resulting uncertainty will be effected: ten degrees of inclination are enough to produce a decrease of 1%.
Both the hammer's force and the output signals from the load cells were analysed in the frequency domain. A typical value for the signals was computed as the average of the spectral quantities within the bandwidth of interest (i.e. 1-20 Hz). In some cases, such bandwidth was further reduced because of a lack of energy at frequencies below 5 Hz, due to the small dynamometric hammer used.

5.3 The sensitivity matrix

The data were ordered to compose the matrix equation:

$$\begin{bmatrix} F_{x,1} & F_{x,2} & \cdots & F_{x,M} \\ F_{y,1} & F_{y,2} & \cdots & F_{y,M} \\ \vdots & \vdots & & \vdots \\ M_{z,1} & M_{z,2} & \cdots & M_{z,M} \end{bmatrix} = [S]_{6\times 6} \cdot \begin{bmatrix} O_{1,1} & O_{1,2} & \cdots & O_{1,M} \\ O_{2,1} & O_{1,2} & \cdots & O_{1,M} \\ \vdots & \vdots & & \vdots \\ O_{6,1} & O_{6,2} & \cdots & O_{6,M} \end{bmatrix} \tag{5.23}$$

On the left side of equation (5.23) there are the forces and the torques along the three directions while, on the right side, matrix $[O]$ contains the measurements from each load cell. In our case, the output in the vertical direction was given in terms of the APMS while in the xy-plane as forces. For the bending torques, both the positions of masses and of the hammering points were recorded for computing the equilibrium to rotations. Consequently, matrix $[S]$ is not properly the sensitivity matrix but its inverse.
The calibration problem was solved by directly applying to equation (5.23) the definition of pseudoinverse matrix. The resulting sensitivity matrix was:

$$\begin{bmatrix} 0.05 & 1.13 & 0 & 1.15 & 0.17 & 0.02 \\ 0.09 & 0.15 & 0 & 0.23 & 1.22 & 0.04 \\ 0.98 & 0 & 1.03 & 0 & 0 & 1.41 \\ 3.80 & 0 & 225.76 & 0 & 0 & 18.54 \\ 244.21 & 0 & 219.55 & 0 & 0 & 7.37 \\ 22.42 & 293.38 & 2.81 & 25.82 & 22.72 & 7.60 \end{bmatrix} \tag{5.24}$$

The matrix accounts for both the non-ideal behaviour of the transducers and for the cross talk between the measurement axes. It can be split into two three-by-six submatrices: the first allows to compute the three forces (i.e. F_x, F_y and F_z) while the second the torques with respect to the reference system (i.e. M_x, M_y and M_z). In the first submatrix, the terms out of axes are close to zero (i.e. less than 1% and consequently considered nulls) which means that their contribution is negligible.

The same happens for the torques sub-matrix were low coefficients indicate a low sensitivity; since the moment arms were taken in millimetres, the coefficients for the bending torques were higher than that of the forces.

5.4 Uncertainty

The uncertainty on the vertical loads has been evaluated by applying masses of 25 kg on the force plate. Ten trials were performed and the applied loads were estimated by using the above derived sensitivity matrix (equation (5.24)). The uncertainty was computed as the standard deviation of the estimated masses with respect to the nominal value and it was equal to 3.4 %. Conversely, the uncertainty in the xy-plane was derived as the experiments' standard deviation (Table 5.1) of additional hammerings.

Table 5.1 Sensitivities and their uncertainty.

Load cell	Mean correction factor	Uncertainty
Biaxial x-axis	1.13	2.2 %
Tri-axial x-axis	1.15	2.3 %
Tri-axial y-axis	1.22	2.0%

* Directions are referred to the basicentric reference system.

5.5 Conclusions

The force plate was calibrated according to different methods:

1. calibration masses for the load cells deployed along the z-axis;
2. external forces imposed by a dynamometric hammer for the load cells in the xy-plane.

The calibration problem was solved for the sensitivity matrix by the use of a least-mean-square technique (i.e. pseudoinverse matrix). Such matrix contained the correction factors to apply to the nominal sensitivities since the calibration was carried out under a nominal configuration.
Nevertheless, the so-obtained correction coefficients were derived under not real exercise conditions but their validity was extended by making some further assumptions. This was the case of the vertical load cells for which it was assumed that

1. the force plate behaved linearly independently of the applied mass;
2. the coefficients were valid even for masses bigger than 40 kg (the maximum mass applied during the calibration).

However, the uncertainties obtained for the correction coefficients were all below 5% and for the case of the load cells in the xy-plane less than 3%, despite the drawbacks due to use of the hammer.

Chapter 6

Apparent mass in the basicentric reference system

The apparent mass matrix has been derived for a single subject; statistics have then been performed on 8 subjects. In both cases, the effect of the vibration magnitude has been evaluated with paired statistical tests (i.e. t-student and Wilcoxon matched paired tests). In addition, the reciprocity property has been verified.

6.1 Introduction

The number of studies focused on the characterization of the response for standing subjects is more limited [42-48] than those for seated postures. Among these, few works have directly focused on the characterization of the response along each excitation axis (vertical, fore-and-aft and lateral) [45-47]. Matsumoto characterized the human body response in terms of both the apparent mass and the transmissibility at different locations to assess whether the posture or the vibration magnitude have some remarkable effects. Subjects were all exposed to vertical WBV and only the in-line transfer functions (i.e. along the vertical direction) were provided in the study [45]. Consequently, Subashi derived the vertical in-line and the fore-and-aft cross-axis apparent mass for subjects still exposed to vertical WBV [46]. The lateral cross-axis apparent mass was intentionally omitted because lateral forces were expected to be negligible in reason to the symmetry of the human body around the mid-sagittal plane. The study aimed to assess the effects of both the vibration magnitude and the muscle tension (i.e. by adopting different upper-body and lower limbs postures) on the human body response. A second study by Matsumoto presented the apparent masses of standing subjects under fore-and-aft and lateral WBVs [47]. Subjects were invited to keep their legs straight under increasing vibration magnitude and distance between the feet. The above mentioned studies were carried out under not homogenous conditions: there was no correspondence between the samples (i.e. different populations each time) and postures always varied because each work focused on the effects of some postural peculiarity (e.g. lower limbs posture, muscle tension, feet distance) on the response. In addition, results were derived under different exposure conditions, especially for the apparent masses under horizontal vibrations [47] where both the vibration levels and the frequency range were incompatible with previous works [45, 46]. At the current state of the art, there is a lack of knowledge: nobody proposed an exhaustive study with the aim

of characterizing the whole impedance matrix of standing subjects and nobody proved if the superposition or the reciprocity principles hold.

6.2 Experimental method

6.2.1 Apparatus

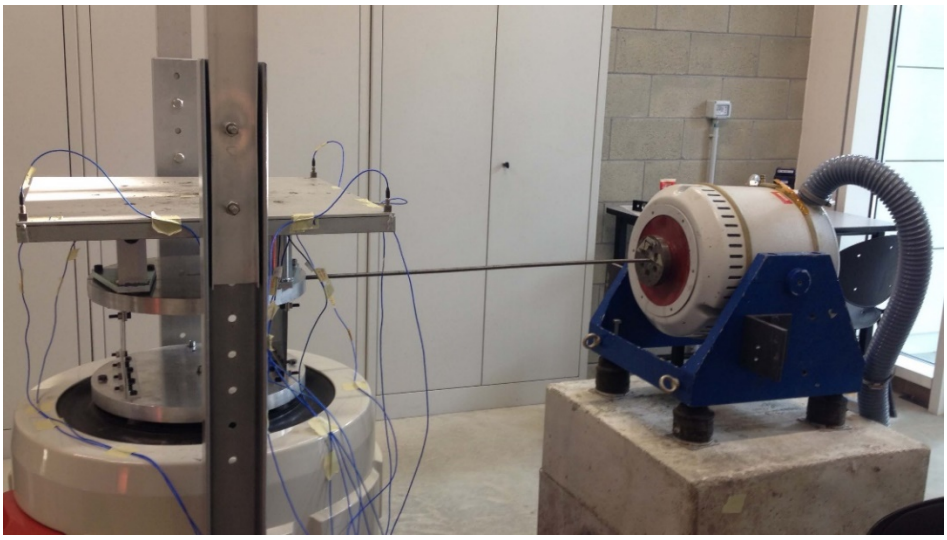

Figure 6.1 Experimental setup for the excitation and the measurement of the human body response in the basicentric reference system.

The experimental setup is composed by two electrodynamic shakers whose heads were connected by a purposely designed connection joint. The tri-axial force plate (Figure 6.1) was mounted on the connection joint. This configuration provides vibrations along each axis of the basicentric reference system. The two shakers allows creating either vertical or lateral vibration by the use of two independent controllers (hereafter, the device that provided vibrations in the vertical direction is called “primary shaker” while the transversal one, “secondary shaker” (Table 6.1).

Table 6.1 Secondary shaker’s technical specifications.

Company	TIRA GmbH
Model	TV 50101-80
Frequency range	1 Hz – 20 kHz
Maximum displacement	25.4 mm (peak-to-peak)
Maximum acceleration	27 g

In addition, due to the compliance of the dual-axis interface, both the primary and the secondary shakers can be driven contemporarily for realizing a dual-axis excitation along two perpendicular directions. This may be useful when studying

the response of the human body if a secondary vibration concurs with the principal one. The primary shaker provided for the required excitation along the vertical direction (z-axis) while the secondary shaker along the horizontal axis. The secondary shaker was placed on three concrete blocks in order to reach the required height and it was fixed to the upper disc of the dual-axis interface by a screwed bar made of steel (8 mm in diameter). Subjects stood on a rigid metallic plate (500 x 500 mm in size) whose structure's resonances were higher than the investigated range of frequencies. For safety purposes, a metallic frame was fixed to the primary shaker's base; in case of emergency, people were able to hang to the frame.

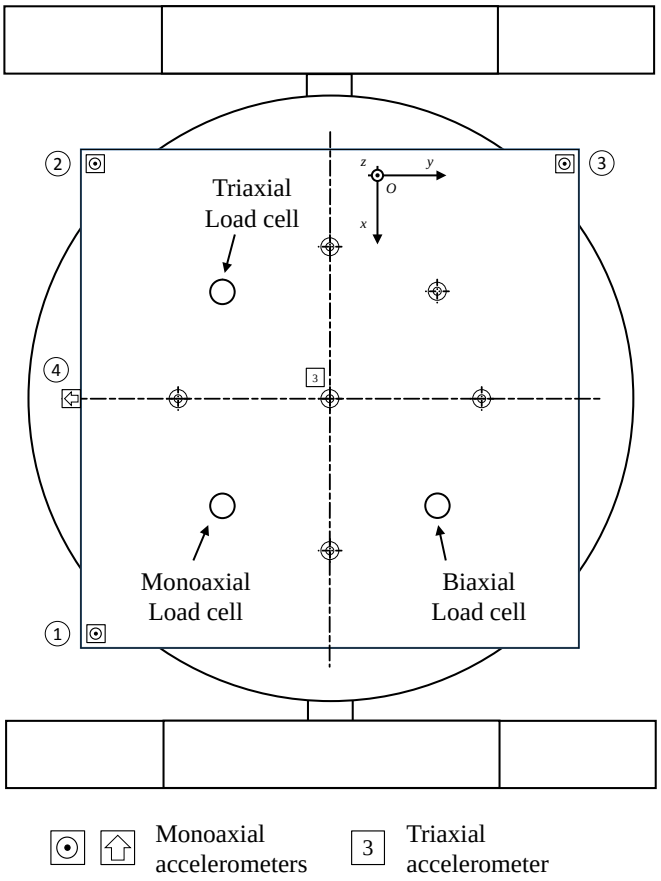

Figure 6.2 Transducers' placement on the force plate.

The forces transmitted along each axis of the basicentric reference system were measured by three piezoelectric mono-axial load cells (PCB 211B) and by a piezoelectric tri-axial load cell (PCB 260A11) which were isostatically fixed to the plate (Figure 6.2); sensitivities were adjusted according to the calibration

procedure described in the previous chapter. The plate acceleration was measured by a piezoelectric tri-axial accelerometer placed close to the centre of the plate. Three mono-axial piezoelectric accelerometers were placed on the plate for the control of the primary shaker while the secondary shaker was controlled by a fourth piezoelectric accelerometer fixed to the plate's edge (see Figure 6.2).
Both the accelerations and force signals were filtered and amplified by four B&K Nexus conditioning units (band-pass filter between 0.1 Hz and 100 Hz) and eventually sampled by two NI PCI-4472 8-channels boards (24 bits A/D converter, sampling frequency of 2000 Hz). Signals were digitized and stored on a personal computer and the collected time histories were afterwards processed off-line.

6.2.2 Subjects

Trials involved eight male subjects picked either from students or staff of the Politecnico di Milano (main biometric data summarized in Table 6.2). The experiments were carried out in compliance with both the EU legislation on workers' vibration exposure [6] and with the Politecnico di Milano ethical guidelines.

Table 6.2 Subjects' biometric data.

Subject	Age (years)	Height (cm)	Weight (kg)	BMI (cm^2/kg)
1	28	180	65	20.1
2	28	167	55	19.7
3	26	171	67	22.9
4	25	184	83	24.5
5	25	174	92	30.4
6	30	180	74	22.8
7	28	173	64	27.7
8	29	178	83	26.2
Average	27.4	175.9	72.9	24.3
SD	1.8	5.6	12.3	3.7
Median	28	176	70.5	23.7

6.2.3 Stimuli

Subjects were exposed to Gaussian white noise signals along each axis of the basicentric reference system. Vibrations were provided at two different magnitudes (0.2 m s^{-2} and 0.5 m s^{-2} RMS) in the range 1 - 20 Hz. The input signals were synthetized each time, by changing the settings of the shakers' control software (the x- and y-axis were excited by a secondary shaker while the z-axis by the primary one). As previously mentioned in Chapter 2, this practice should provide for more information with respect to the commonly used procedure in

which the same acceleration waveforms were used in each session of trials [46]. Stimuli were randomly presented in order to prevent fatigue phenomena.

6.2.4 Postures

During the experiments, subjects stood on the force plate by adopting an upright posture with straight legs. Subjects kept their feet 25 cm apart, wearing their own shoes (the apparent mass is weak effected by the feet/plate interface [48]). The total exposure duration did not exceed 60 seconds for each configuration. In addition, subjects were advised to look straight to a fixed point during the trial and to maintain the same posture without any involuntary movement of the body.

6.2.5 Excitation procedure

The full three-by-three matrix was derived by exposing all subjects to vibration along each axis of the basicentric reference system. Excitations were not simultaneous in order to derive one row each time of the APMS matrix. As an example, the z-axis was first excited and the relating data collected. After the first trial, subjects were exposed to vibrations along the y-axis. Finally, excitations along the x-axis were obtained by inviting the subjects to turn themselves and then looking straight to the secondary shaker. Trials were presented randomly, without a prefixed order of presentation.

a)  b) 

Figure 6.3 Position of the subjects on the force plate: a) frontal and vertical excitations, b) lateral excitation.

6.3 Data processing

The biomechanical response in the basicentric reference system was expressed in terms of the apparent mass (APMS), derived by the use of the cross-spectral density method (CSD). The resulting apparent masses ($APMS_{CSD}$) were provided with both the magnitude and the phase information along with the ordinary coherence function (all spectral quantities were presented with frequency resolution of 0.25 hertz). The inertial contribute due to the plate's mass was removed by mass cancellation in the time-domain; afterwards, the apparent masses were also normalized with respect to the subject's weight as done in the previous chapters.

6.4 The apparent mass matrix

The mean behaviour of the sample was given by aggregating all individuals APMS in a unique matrix of mean quantities (i.e. magnitude, phase and ordinary coherence function), each provided with a proper value of uncertainty (i.e. the standard deviation computed frequency-by-frequency).
The apparent mass matrix is a three-by-three matrix whose columns contain the three APMSs due to independent vibrations along each axis:

$$\begin{Bmatrix} F_x(\omega) \\ F_y(\omega) \\ F_z(\omega) \end{Bmatrix} = \begin{bmatrix} M_{xx}(\omega) & M_{xy}(\omega) & M_{xz}(\omega) \\ M_{yx}(\omega) & M_{yy}(\omega) & M_{yz}(\omega) \\ M_{zx}(\omega) & M_{zy}(\omega) & M_{zz}(\omega) \end{bmatrix} \cdot \begin{Bmatrix} a_x(\omega) \\ a_y(\omega) \\ a_z(\omega) \end{Bmatrix} \qquad (6.1)$$

The main diagonal terms of the matrix are the direct APMSs (i.e. the APMSs along the excitation directions) while the extra-diagonal terms are the so-called cross-axis APMSs which represent the extra-axis APMSs. According to equation (6.1), the spectra of transmitted forces are given as the product between the APMS matrix and the spectra of the acceleration stimuli.

6.4.1 Frontal excitation

The APMSs due to frontal (i.e. x-axis) WBV are displayed in Figure 6.4. Figure 6.5 shows a detailed view of the direct and the lateral cross-axis APMSs. The direct frontal apparent mass was approximately 0.25 of the subject mass at 1 Hz and rapidly decreased to 0.10 at 2.5 Hz; a secondary minor resonance peak occured at 5 Hz for both the acceleration magnitudes. At frequencies higher than 10 Hz the apparent mass asymptotically tended to the 3% of the static weight. The lateral cross-axis APMS also started from 0.20 and rapidly decreased till values

below 1% of the static weight for frequencies higher than 4 Hz. The vertical cross-axis APMS was about 0.50 at 1 Hz and decreased in magnitude until a secondary resonance at about 5 Hz, where the APMS was 0.20 times the static weight. At larger frequencies, the APMS tended to the asymptotic value of 0.10. However, the vertical cross-axis APMS was higher in magnitude than the direct frontal APMS at all the frequencies.

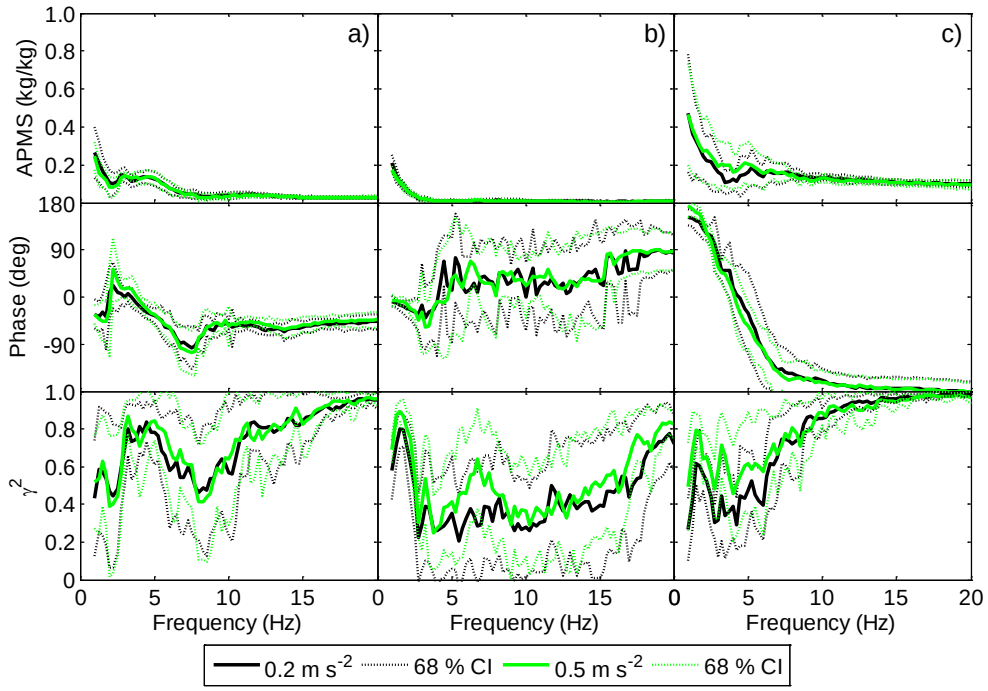

Figure 6.4 APMSs due to frontal WBV: a) M_{xx}, b) M_{yx}, c) M_{zx}.

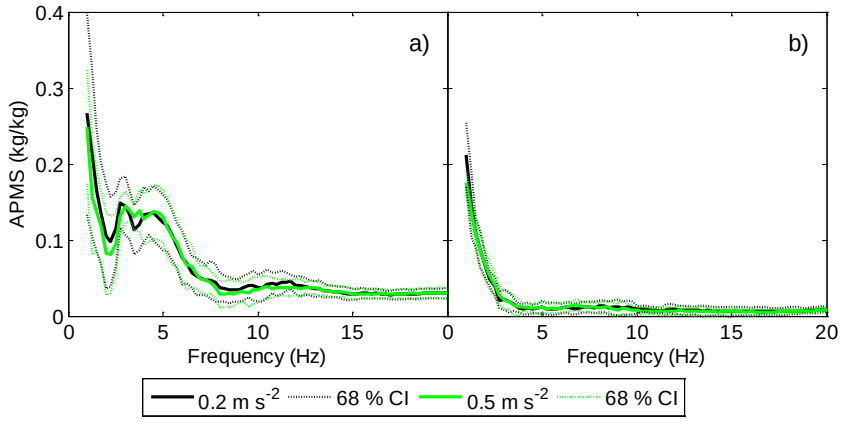

Figure 6.5 Frontal WBV: a) M_{xx}, b) M_{yx}.

The variability of the frontal and the lateral APMSs was almost constant to all frequencies (about 30%). Conversely, the vertical cross-axis APMS was characterized by a coefficient of variation of 60% below 5 Hz; the value reduced to 15% above 10 Hz.
The ordinary coherence function of the frontal apparent mass varied between 0.5 and 0.9 at 15 Hz, with a local maximum at (approximately) 5 Hz. Coherence for the vertical force deriving from the lateral stimulus was characterized by similar values, while the coherence between the force along a horizontal direction and the acceleration in a perpendicular direction was low. In general the coherence was larger above 15 Hz. COVs were usually large at low frequencies, except for the lateral cross-axis APMS, which was characterized by large scatters within the range 1-20 Hz.

6.4.2 Lateral excitation

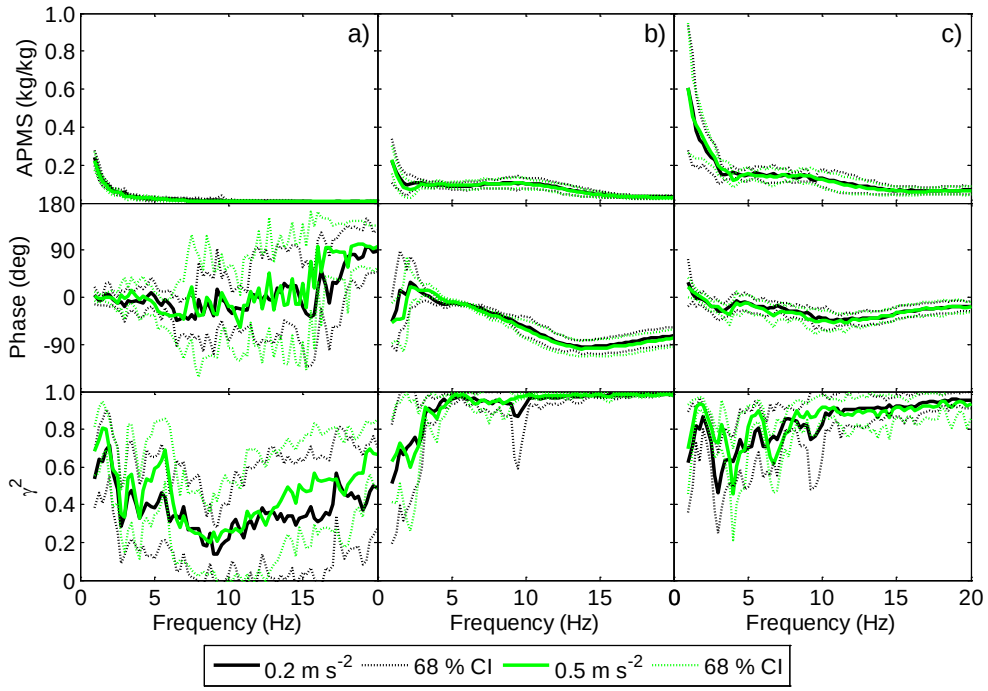

Figure 6.6 APMSs due to lateral WBV: a) M_{xy}, b) M_{yy}, c) M_{zy}.

The APMSs derived in case of lateral (i.e. y-axis) WBV are displayed in Figure 6.6; Figure 6.7 sketches both the direct and the frontal cross-axis APMSs. The frontal cross-axis apparent mass decreased from about 0.25 at 1 Hz to less than 0.01 at about 7 Hz, similarly to the lateral cross-axis APMS in case of frontal excitation. The lateral direct APMS decreased from 0.25 to about 0.10 at 4 Hz

and then increased to a slight secondary resonance peak at 10 Hz; after this frequency, it asymptotically tended to the 3% of the static mass. The APMS was similar in shape for both the acceleration magnitudes with large scatters across the resonance at 10 Hz. The vertical cross-axis APMS was also higher in magnitude than the lateral direct APMS: it decreased from about 0.60 at 1 Hz to 0.20 until 10 Hz; then, the magnitude reduced to the asymptotic value of 0.10. In case of lateral WBV, the vertical cross-axis APMS had large scatters below 4 Hz, but the observed variability was less than the case of frontal excitation.

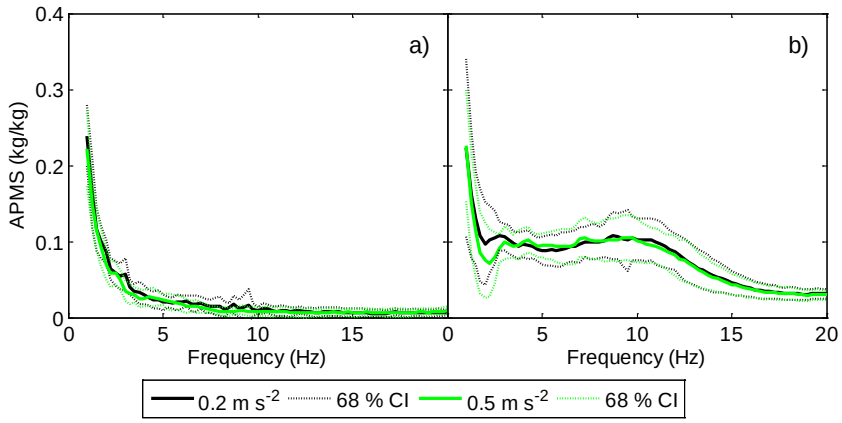

Figure 6.7 Lateral WBV: a) M_{xy}, b) M_{yy}.

For the frontal cross-axis APMS, the ordinary coherence function was minimum at 10 Hz; afterwards, the coherence progressively increased till reaching the value of 0.60 at 20 Hz. Anyway, large scatters in the coherence were found and the variability increased towards high frequencies. For the lateral direct APMS, the coherence function had its minimum at 3 Hz while its highest values (i.e more than 0.90) were reached above 8 Hz. In the vertical direction, the coherence function was lower in value than that along the y-axis for all the frequencies. As in case of frontal WBV, the coherence functions reduced their variability as the frequency increases. This behaviour was particularly evident for the lateral direct APMS where the coherence was close to unity.

6.4.3 Vertical excitation

Figure 6.8 shows the three APMSs derived in case of vertical (i.e. z-axis) WBV; as usual, both the frontal and the lateral cross-axis APMSs are given in Figure 6.9. The direct APMS in the vertical direction exhibited a main resonance peak in the range 5-6 Hz with a peak amplitude twice the static mass.

A main resonance in the same frequency range was also evident in the frontal cross-axis APMS with a peak at about 15% of the static mass. Conversely, no resonances were found for the lateral cross-axis APMS whose magnitude was always below 0.05.

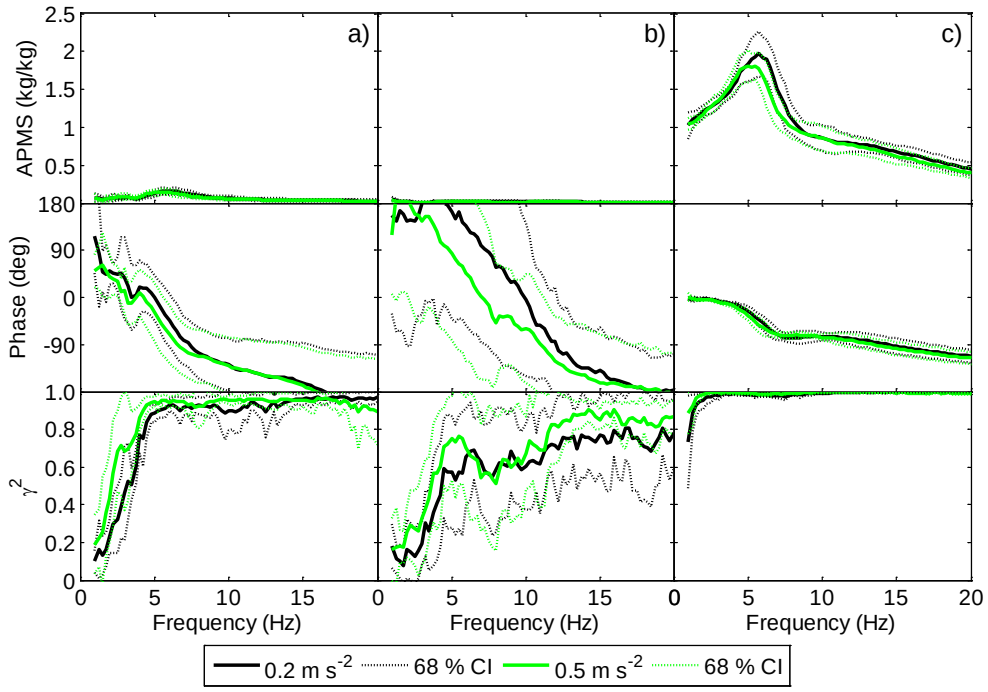

Figure 6.8 APMSs due to vertical WBV: a) M_{xz}, b) M_{yz}, c) M_{zz}.

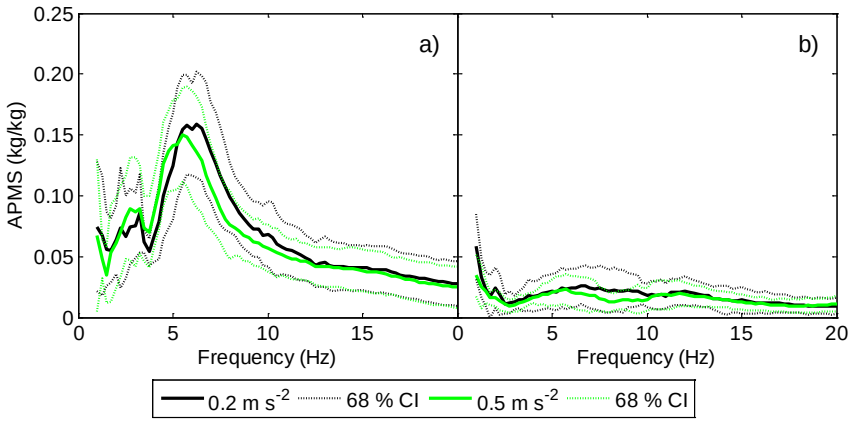

Figure 6.9 Vertical WBV: a) M_{xz}, b) M_{yz}.

The ordinary coherence function for the vertical direct APMS was close to unity over the whole range of frequencies with also a low variability across the subjects. The coherence function for the frontal cross-axis APMS was always larger than the lateral one except for those frequencies below 5 Hz. The lateral cross-axis APMS exhibited the lowest coherence values, with a drop at about 2 Hz, along with the largest scatters within the range 1-20 Hz.

6.5 Conditioned APMS matrix

As for the case of the vertical APMS (Chapter 3), the frontal cross-axis APMS under vertical WBV (0.5 m s^{-2} RMS) was conditioned with the aim to establish whether the drop in the coherence function below 4 Hz was attributable to some nonlinearity. Besides the input acceleration, the absolute value and the squared power of the acceleration time history were included as parallel inputs. Additional nonlinear functions were not considered in the model since preliminary tests showed that they did not increase the modelling accuracy.
Results on the sample evidenced that the increase in the multiple coherence function was too poor (Figure 6.10). Hereafter, Figure 6.11 sketches the conditioned frontal cross-axis APMSs of two subjects which exhibited the deepest drops in the ordinary coherence function.

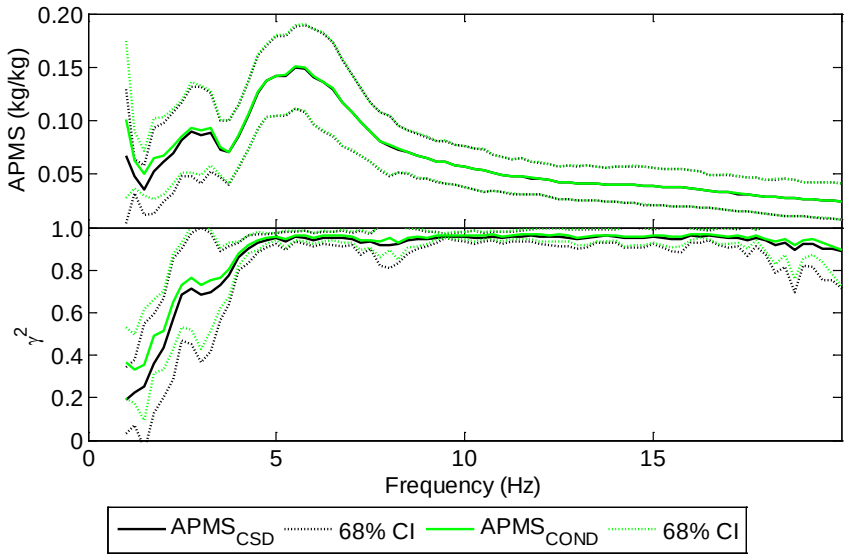

Figure 6.10 Conditioned normalized frontal cross-axis APMS for the sample population (vertical WBV).

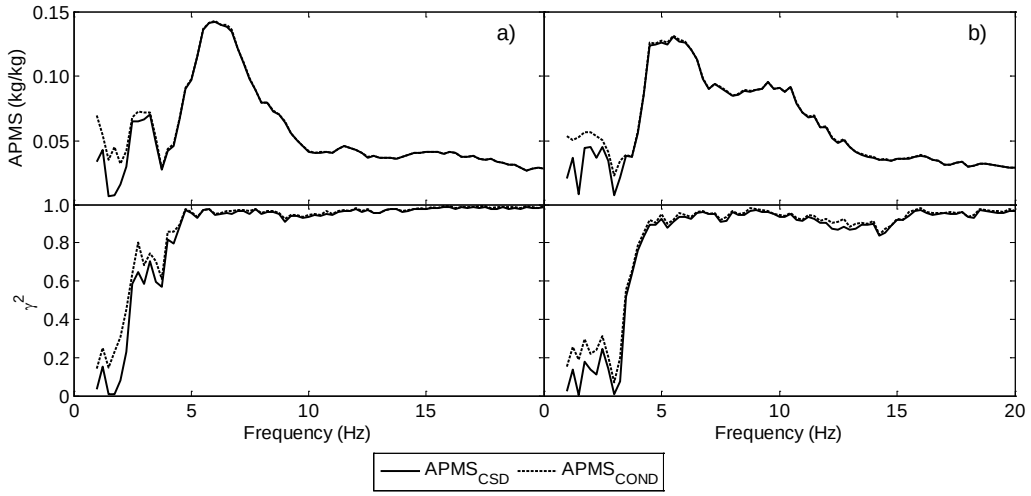

Figure 6.11 Conditioned normalized frontal cross-axis APMS: a) subject nr.3; b) subject nr. 4.

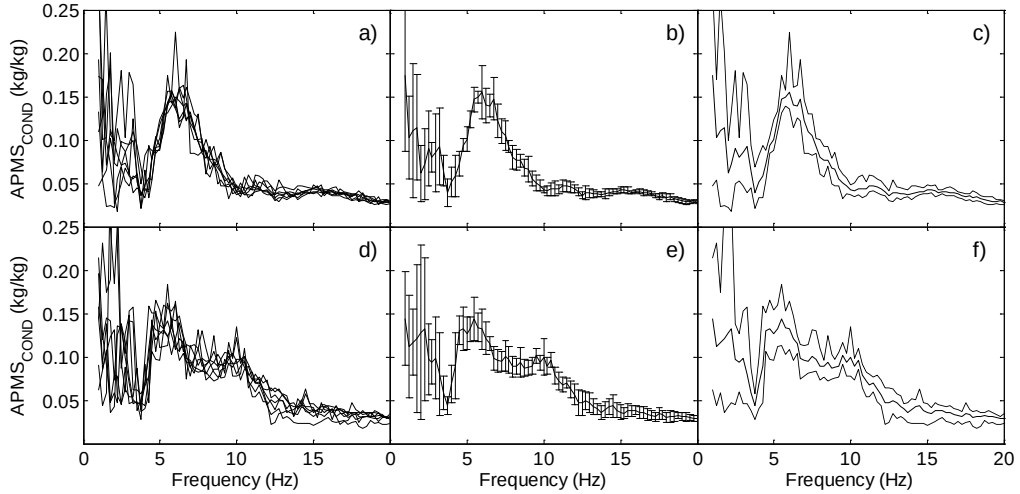

Figure 6.12 Normalized conditioned apparent mass (intra-subject variability): a), subject nr. 3, d), subject nr. 4; normalized apparent mass (mean and standard deviation): b), subject nr. 3, e), subject nr. 4; normalized apparent mass (upper and lower envelopes): c), subject nr. 3, f), subject nr. 4.

The stationarity of both the responses of Figure 6.11 was assessed by dividing the time history into sub-records and then by computing the conditioned apparent mass within each sub-interval. The statistical analysis performed on the resulting conditioned apparent masses are shown in Figure 6.12. For the frontal cross-axis APMS, the ordinary coherence function was low in magnitude where the apparent mass had large coefficients of variation and both the lower and the upper envelopes were misaligned (peaks and drops occurred at different frequencies). As already mentioned in Chapter 3, the low coherence may be associated with

low frequency motion during the tests and involuntary muscular actions, given that the nonlinearity in the response and the measurement noise were proven trivial.

6.5.1 Conditioned APMS matrix for the individual

The APMS matrix for the individual at 0.5 m s^{-2} RMS was conditioned with the aim to establish the extent of the nonlinearities. The input acceleration, the absolute value and the squared power of the acceleration time history were included as parallel inputs; additional nonlinear functions were neglected.

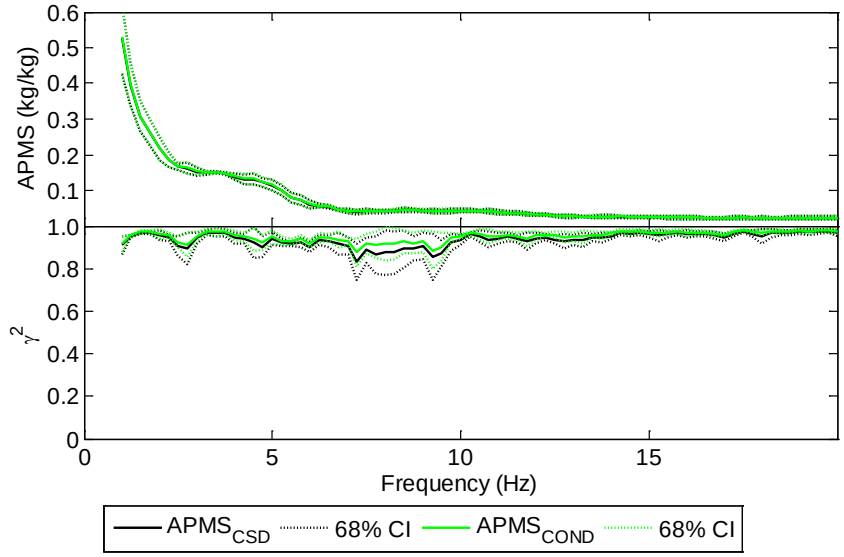

Figure 6.13 Conditioned normalized frontal direct APMS for the individual (frontal WBV).

In case of frontal WBV, the direct APMS (Figure 6.13) along with both the cross-axis APMSs (Figure 6.14 and Figure 6.15) exhibited few improvements by the addition of the nonlinear terms. The APMS magnitudes were not significantly changed since the variability of the mean values was compatible to the intra-subject uncertainty.

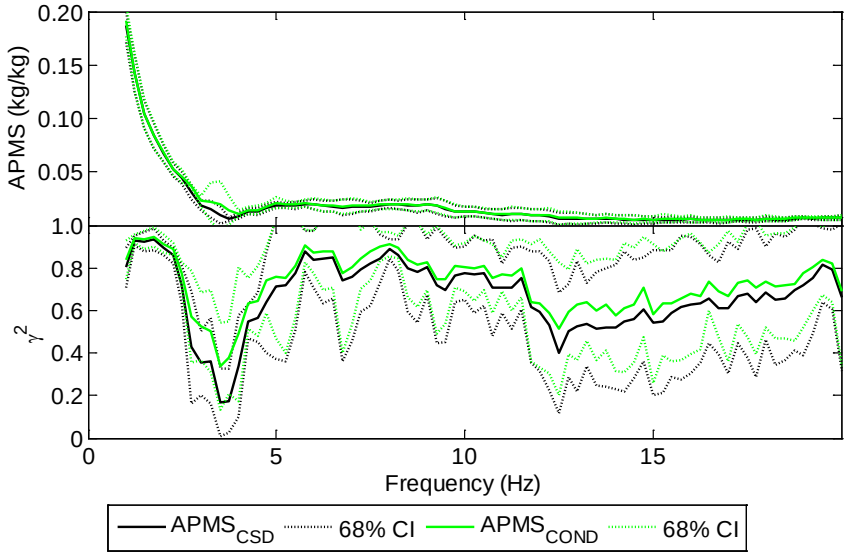

Figure 6.14 Conditioned normalized lateral cross-axis APMS for the individual (frontal WBV).

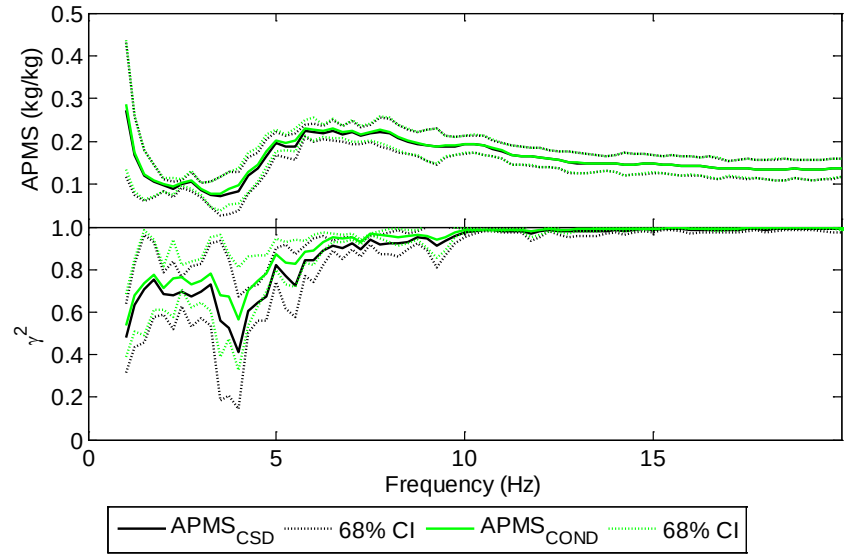

Figure 6.15 Conditioned normalized vertical cross-axis APMS for the individual (frontal WBV).

After conditioning the APMSs due to a lateral single-axis vibration, from Figure 6.16 to Figure 6.18, results were compatible to those derived using the linear estimators. For the frontal cross-axis APMS (Figure 6.17), the rising in the multiple coherence function did not reduce the drop in the ordinary coherence function. Conversely, an increase in both the conditioned APMS and the multiple

coherence function occurred for the vertical cross-axis APMS at about 7 Hz (Figure 6.18).

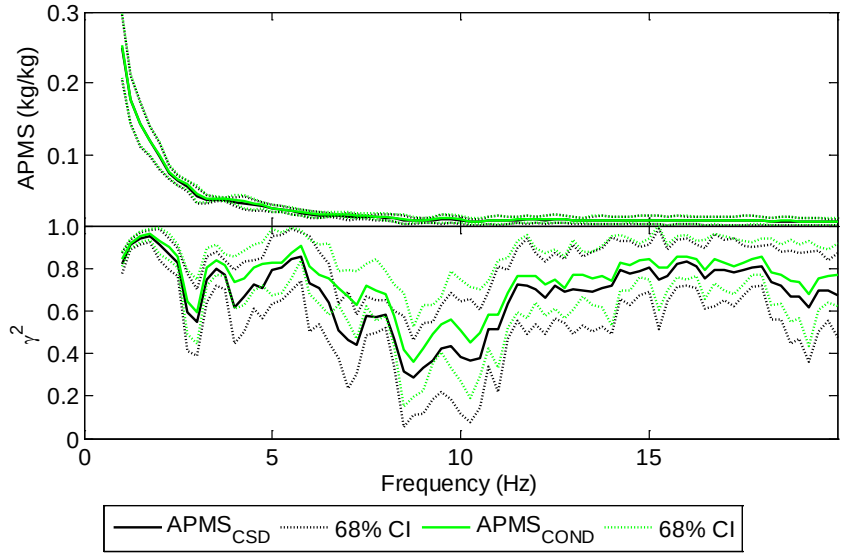

Figure 6.16 Conditioned normalized frontal cross-axis APMS for the individual (lateral WBV).

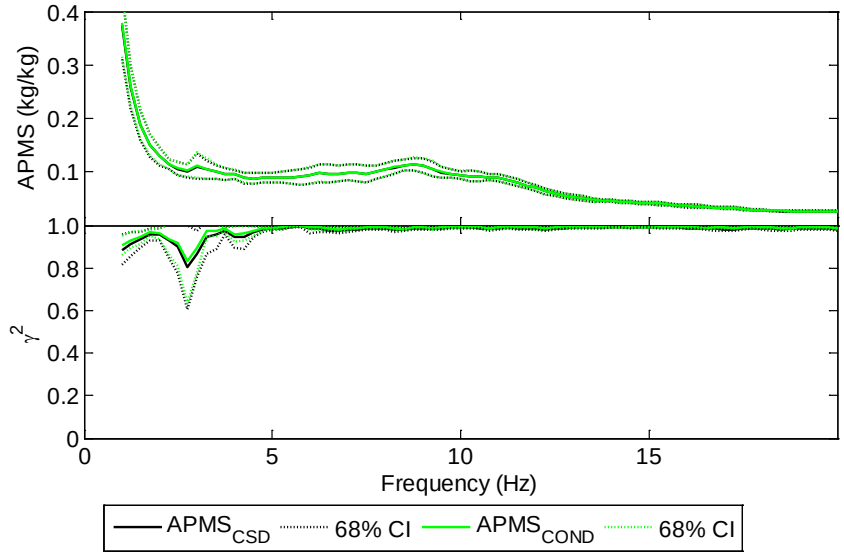

Figure 6.17 Conditioned normalized lateral direct APMS for the individual (lateral WBV).

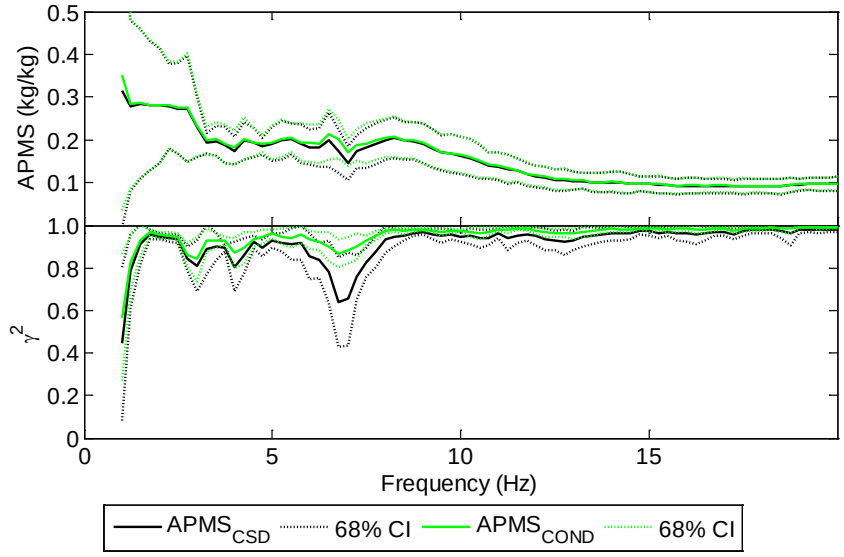

Figure 6.18 Conditioned normalized vertical cross-axis APMS for the individual (lateral WBV).

Finally, no remarkable improvements were noticed in the direct and the frontal cross-axis APMSs in case of vertical vibration. With regard to the lateral cross-axis APMS, an improvement in the response occurred below 4 Hz.

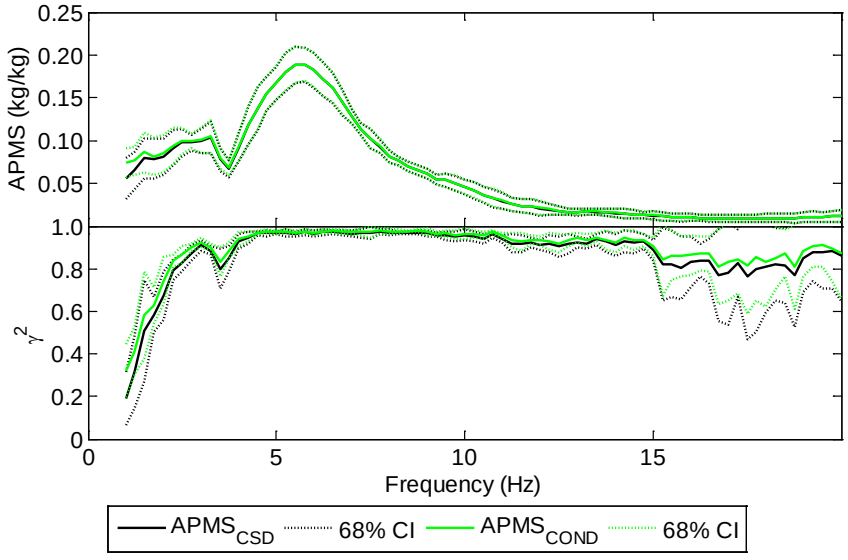

Figure 6.19 Conditioned normalized frontal cross-axis APMS for the individual (vertical WBV).

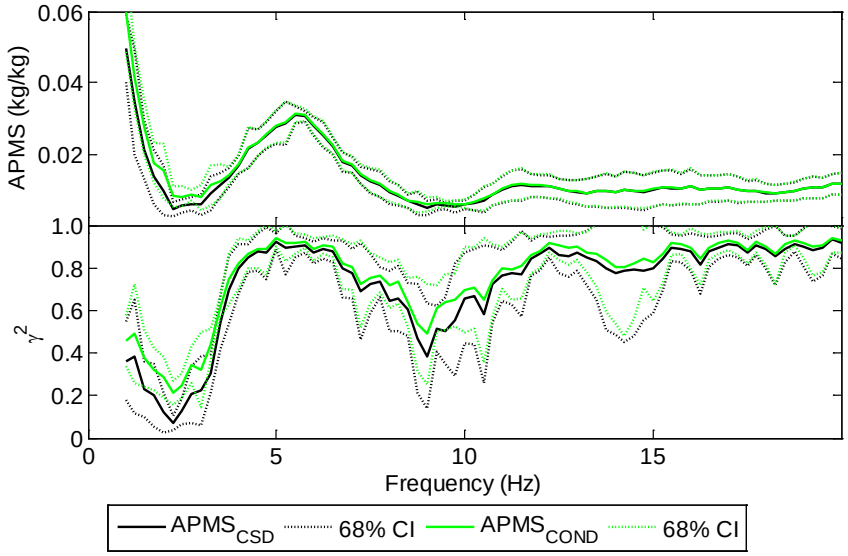

Figure 6.20 Conditioned normalized lateral cross-axis APMS for the individual (vertical WBV).

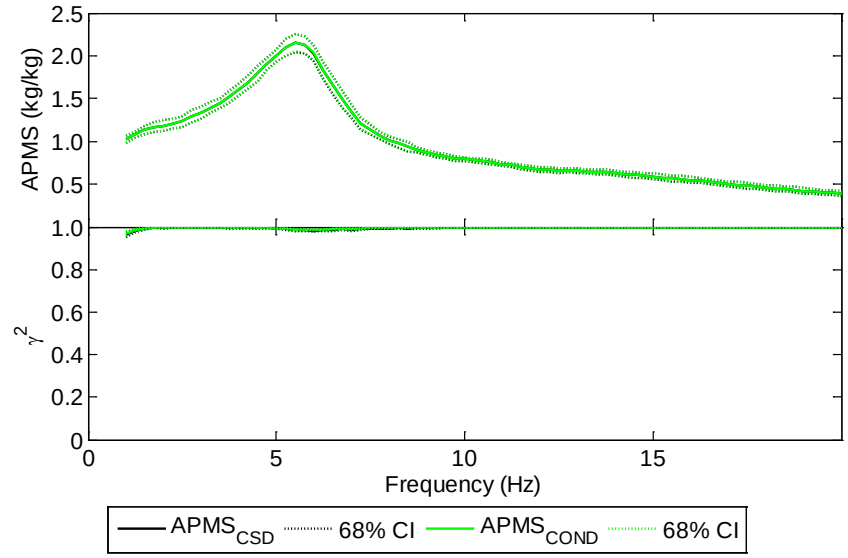

Figure 6.21 Conditioned normalized vertical direct APMS for the individual (vertical WBV).

6.6 Statistical analysis

6.6.1 Effect of vibration magnitude

As in Chapter 2, the effect of the vibration magnitude was assessed to establish whether the apparent mass matrix differed under the two tested acceleration levels (0.2 m s^{-2} and 0.5 m s^{-2} RMS). Both the t-student and Wilcoxon matched paired tests were applied frequency by frequency with the aim to test the medians and the means of the collected apparent masses.
The results on the apparent masses due to frontal WBV are shown in Figure 6.22. There were no significant statistical differences (p-value > 0.05) between all the apparent masses at the two vibration levels, except for the Wilcoxon test at 1 Hz for the lateral cross-axis apparent mass.

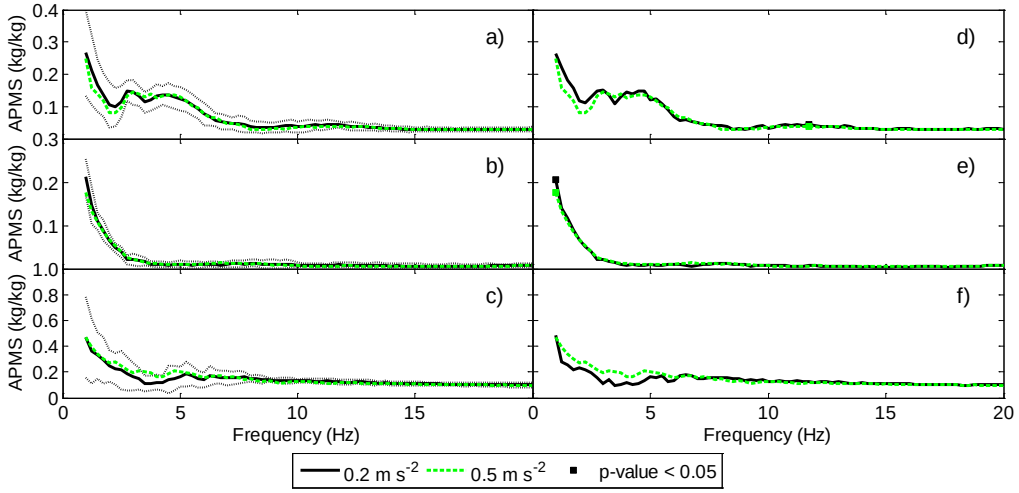

Figure 6.22 Results of the paired t-student test (a, b, c) and paired Wilcoxon signed rank test (d, e, f) for the APMSs taken under frontal WBV (x-axis: a), d); y-axis: b), e); z-axis: c), f)).

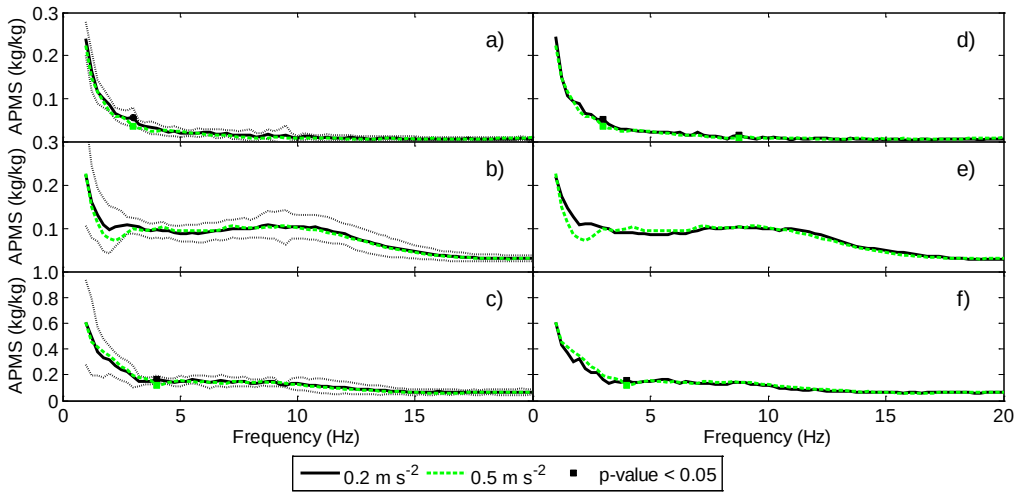

Figure 6.23 Results of the paired t-student test (a, b, c) and paired Wilcoxon signed rank test (d, e, f) for the APMSs taken under lateral WBV (x-axis: a), d); y-axis: b), e); z-axis: c), f)).

Figure 6.23 shows the results from the two tests on the apparent masses derived in case of lateral vibration. There were no differences in the direct lateral apparent masses and the two cross-axis apparent masses were almost identical. Few differences occurred in both the frontal and the vertical cross-axis apparent masses: at 3 and 9 Hz and at 4 Hz, respectively. Both the tests on the medians and on the means produced the same results.

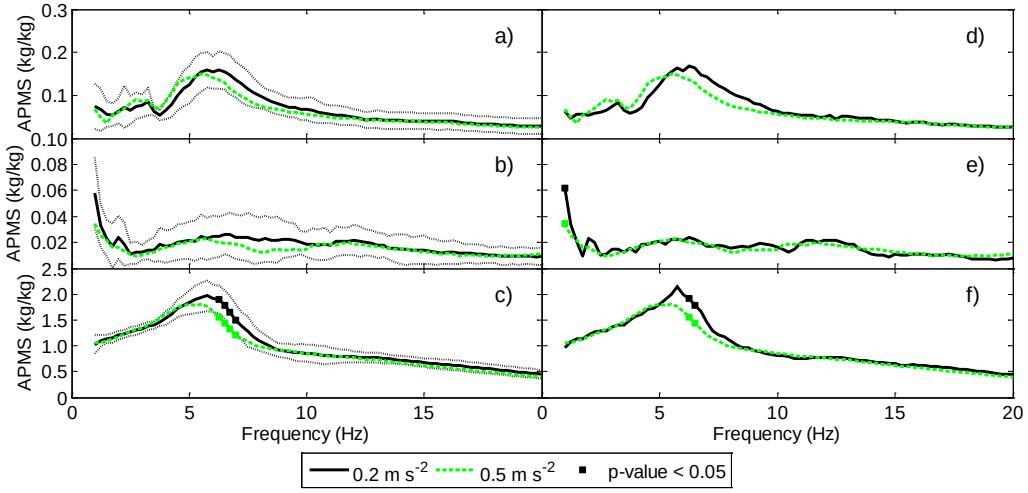

Figure 6.24 Results of the paired t-student test (a, b, c) and paired Wilcoxon signed rank test (d, e, f) for the APMSs taken under vertical WBV (x-axis: a), d); y-axis: b), e); z-axis: c), f)).

Under vertical WBV (Figure 6.24), the t-student test evidenced a difference between the two direct apparent masses within the range 6-7 Hz; even the paired Wilcoxon signed rank test showed the same result but within a narrower range of frequencies (6-6.5 Hz). In the other two directions the apparent masses at the two vibration levels where almost identical (p-value > 0.05).

6.6.2 Single subject

The APMS matrices at different acceleration levels were compared in order to assess whether a nonlinearity with respect to the vibration magnitude exists for single subjects. The APMS matrix of subject 2 (Table 6.2), measured at 0.2 m s^{-2} and 0.5 m s^{-2} RMS, was averaged over five repetitions under mono-axial WBV along the three coordinated axes. Even in this case, both the t-student and Wilcoxon matched paired tests were applied for having a frequency-by-frequency comparison between the APMSs.
Figure 6.25 shows the direct and the two cross-axis APMSs due to frontal WBV: there were no significant statistical differences (p-value > 0.05) between the APMSs at the two vibration levels. In facts, both the tests failed over narrow ranges of frequencies for which the APMS was even low in magnitude (i.e less than 5% of the static weight).

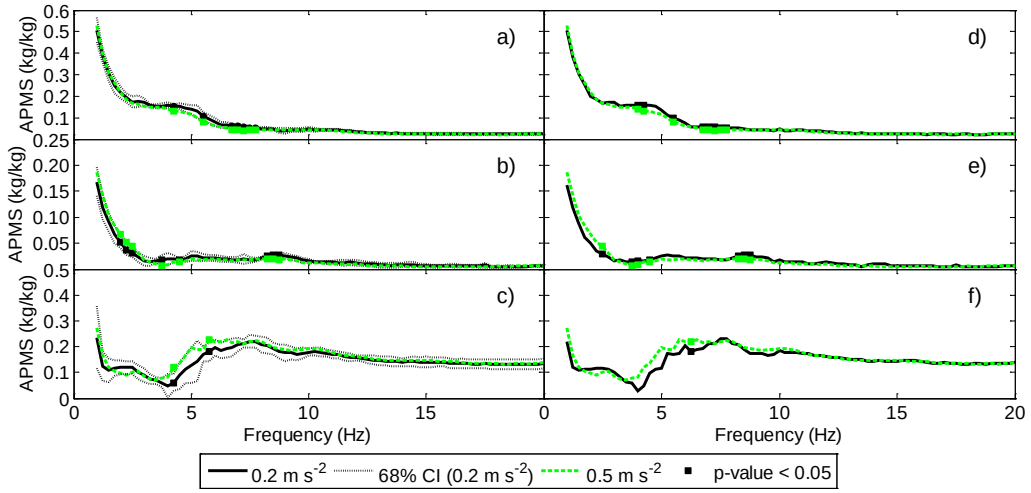

Figure 6.25 Results of the paired t-student test (a, b, c) and paired Wilcoxon signed rank test (d, e, f) for the APMSs of subject 2 under frontal WBV (x-axis: a), d); y-axis: b), e); z-axis: c), f)).

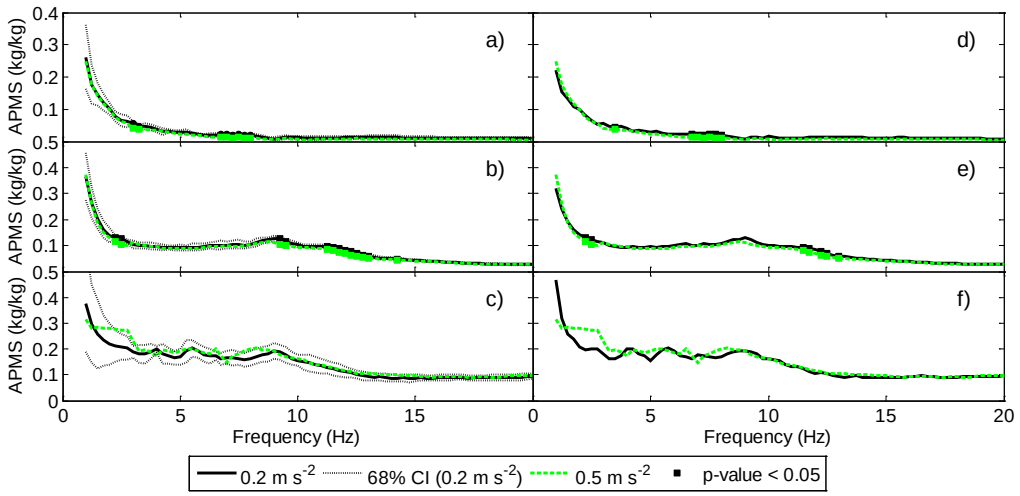

Figure 6.26 Results of the paired t-student test (a, b, c) and paired Wilcoxon signed rank test (d, e, f) for the APMSs taken under lateral WBV (x-axis: a), d); y-axis: b), e); z-axis: c), f)).

For the case of lateral WBV (Figure 6.26), both the cross-axis APMSs were almost identical. The only differences occurred in the direct lateral APMS for the range 11-14 Hz where both the tests gave the same results (the Wilcoxon over a narrower range of frequencies).

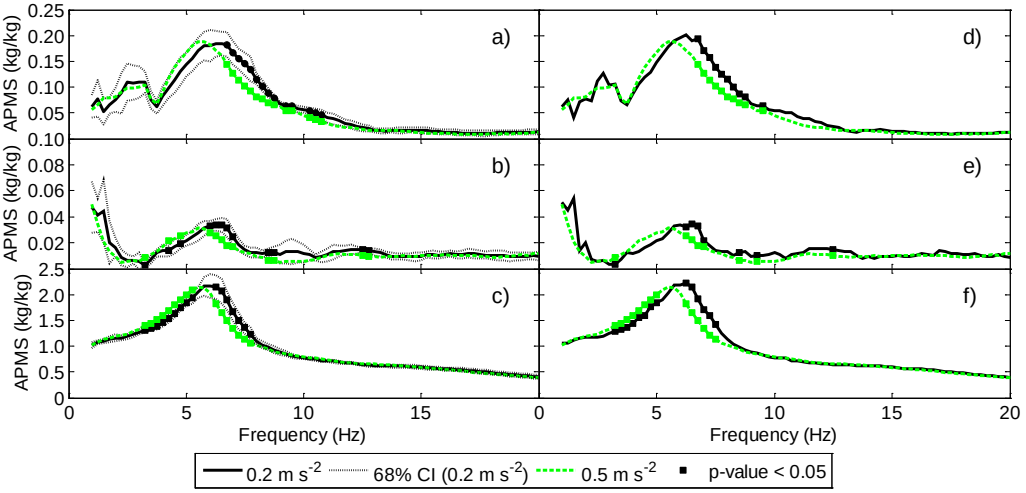

Figure 6.27 Results of the paired t-student test (a, b, c) and paired Wilcoxon signed rank test (d, e, f) for the APMSs taken under vertical WBV (x-axis: a), d); y-axis: b), e); z-axis: c), f)).

In Figure 6.27 (vertical WBV), both the frontal and the lateral cross-axis APMSs differed only in the range 7-10 Hz; conversely, the vibration magnitude was found

statistically significant (p-value > 0.05) between 3 Hz and 8 Hz for the direct vertical APMS.

6.6.3 Symmetry of the APMS matrix

The superposition principle is the widespread used property for establishing whether a system is linear or nonlinear. Nevertheless, such property cannot be directly verified and one should provide for alternative procedures based, for instance, on the harmonic distortion, homogeneity and reciprocity properties of the system response [62].
Basically, the harmonic distortion implies a change in the frequency content of the input signal. Linearity holds whenever both the harmonic input and output are at the same frequency. The homogeneity or FRF distortion check consists in examining the response of the system to different input magnitudes. Linearity holds whenever a change in the input magnitude produces a proportional change in the output amplitude or the FRFs perfectly match. This was the case of the previous paragraphs in which the responses at different acceleration magnitudes were compared by the use of matched paired statistical tests. The harmonic distortion and homogeneity are weaker conditions than the superposition principle and can be verified without any particular effort. Instead, reciprocity is the property by which the FRF at some point *j* due to an input at some other point *i* is equal to the FRF at *i* when the same input is applied to *j*, which implies a symmetric FRF matrix. Reciprocity is a necessary but not a sufficient condition for linearity. In general, when one of such properties breaks down nonlinearity occurs in the system [62].
In this study, the reciprocity property was considered and the APMS matrix derived in section 6.4 was analysed for checking whether it is symmetric or not.
As in the previous paragraphs, both the paired t-student and Wilcoxon tests on the means and medians were adopted for comparing, frequency-by-frequency, the extra-diagonal terms of the APMS matrix:

$$\left[M(\omega)\right] = \begin{bmatrix} M_{xx}(\omega) & M_{xy}(\omega) & M_{xz}(\omega) \\ M_{yx}(\omega) & M_{yy}(\omega) & M_{yz}(\omega) \\ M_{zx}(\omega) & M_{zy}(\omega) & M_{zz}(\omega) \end{bmatrix} \tag{6.2}$$

Comparisons were performed on both the vibration magnitudes (i.e. 0.2 m s^{-2} and 0.5 m s^{-2} RMS) for the following couples of FRFs:
1. M_{xy}-M_{yx};
2. M_{xz}-M_{zx};
3. M_{yz}-M_{zy}.

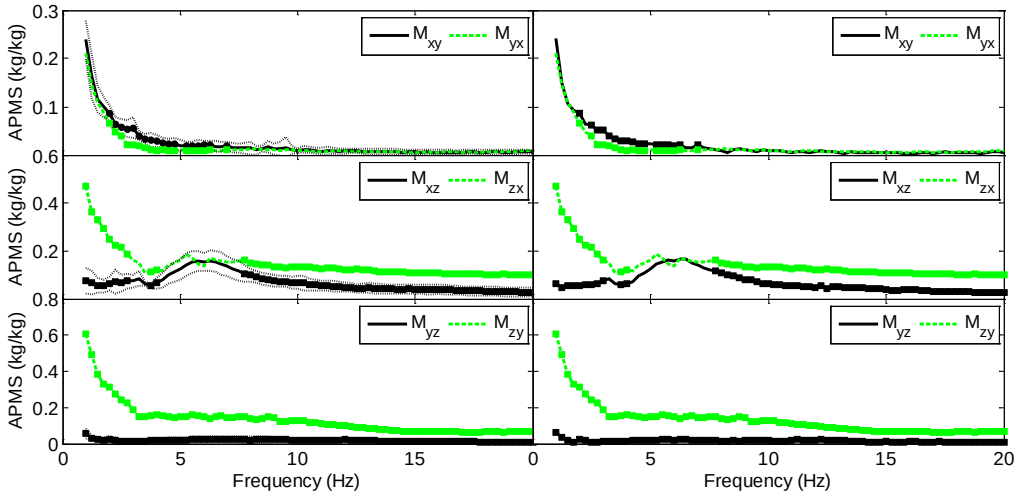

Figure 6.28 Results of the paired t-student test (on the left) and paired Wilcoxon signed rank test (on the right) for the extra-diagonal terms of the APMS matrix (0.2 m s^{-2} RMS): ■, p-value < 0.05.

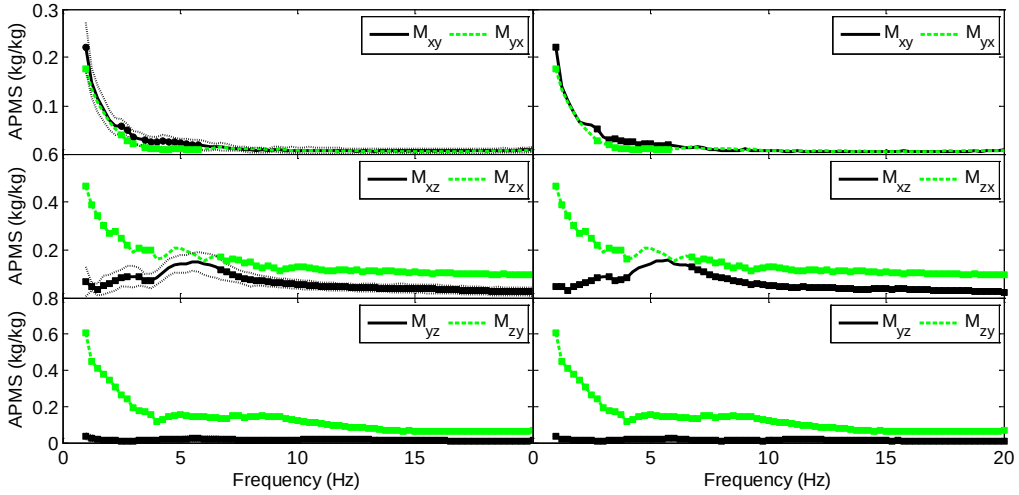

Figure 6.29 Results of the paired t-student test (on the left) and paired Wilcoxon signed rank test (on the right) for the extra-diagonal terms of the APMS matrix (0.5 m s^{-2} RMS): ■, p-value < 0.05.

Figure 6.28 and Figure 6.29 reports the results of the matched paired tests performed on the extra-diagonal terms of the APMS matrix. For the first couple M_{xy}-M_{yx}, statistical significant differences (i.e. p-value < 0.05) occurred in the range 2-6 Hz for both the tests and vibration magnitudes. On the contrary, both the couples M_{xz}-M_{zx} and M_{yz}-M_{zy} were statistically different (i.e. p-value < 0.05) over the whole range of frequencies. In this last case, both the tests on the means

and medians leaded to the same results, independently on the applied vibration magnitude.

6.7 Conclusions

6.7.1 APMS matrix

The apparent mass matrix was derived after exposing people to single-axis vibrations along the three orthogonal directions. Results agreed with previous findings in which the APMS was investigated within the range 0.1-5 Hz. In this study, it was found the same decreasing trend at lower frequencies but it was also explored the behaviour along the three axes within an extended range of frequencies (1-20 Hz).
A common vibration mode was evident under vertical WBV between the direct vertical and the frontal cross-axis APMSs. Such coupling was not evident for the APMSs in the other two directions of excitation. In addition, the human body was found much sensitive to vertical vibrations: the vertical cross-axis APMSs were always higher in magnitude than the corresponding direct APMSs.

6.7.2 Conditioned APMS matrix

The frontal cross-axis APMS (under vertical WBV) was conditioned with the aim to establish whether the drop in the coherence function below 4 Hz was attributable to some nonlinearity. After conditioning the transmitted forces, both the conditioned APMS and the multiple coherence function did not differ from the linear estimators. Hence, the drop in the coherence function was not attributable to some nonlinearity but further tests evidenced that the response was not stationary. As already reported in Chapter 3, the low coherence may be associated with low frequency motion during the tests and involuntary muscular actions. Consequently, the APMS matrix of an individual was conditioned with the same aim of proving the extent of the nonlinearity. The differences between the linear estimators and the conditioned quantities were found comparable to the intra-subject variability.

6.7.3 Effect of vibration magnitude

The effect of the vibration magnitude was investigated for both the APMSs of the sample population of eight subjects and of a single individual. The aim was to establish whether a scatter in the biometric data of the testing population makes less evident the nonlinearity due to an increased excitation level.

Within the sample population, it was found a perfect match between all the APMSs (both direct and cross-axis), except for the direct vertical APMS in which some differences occurred on the right side of the main resonance peak. These differences can be endorsed to minor changes in the modal parameters of the subjects. On the contrary, in case of the single individual, the APMS depends on the vibration magnitude: a reduction in both the resonance peak and frequency were evident. Fewer modifications were also found in the cross-axis APMSs but of less entity.
Finally, a nonlinearity with respect to the vibration magnitude was evident for the direct vertical APMS of a single individual rather than in the APMS of the sample population. In facts, if the APMS has low scatters for the individuals (i.e. 5% for the direct vertical APMS), a larger variability is expected for the APMS of the whole population where the uncertainty due to different biometric data is such to overlay magnitude dependent effects.

6.7.4 Reciprocity

The reciprocity property is an alternative procedure for checking nonlinearity. Hence, the extra-diagonal terms of the APMS matrix were compared by pairs and their differences were statistically checked (i.e. paired t-student and Wilcoxon tests). Significant statistical differences were found within the pairs M_{xz}-M_{zx} and M_{yz}-M_{zy} at both the vibration magnitudes. Thus, the APMS matrix was not symmetric and the reciprocity condition did not hold.

Chapter 7

Apparent mass matrix under dual-axis excitations

The same population of subjects was submitted to dual-axis WBVs. The resulting apparent mass matrix has been compared to that derived in case of mono-axial excitations. The effect of the secondary vibration magnitude has been evaluated with paired statistical tests (i.e. t-student and Wilcoxon matched paired tests) either for the sample or for a single individual.

7.1 Introduction

The biodynamic response under multi-axial excitations (i.e. both dual-axis and tri-axial) has been extensively investigated for the sitting posture but a complete comparison between all the terms of the apparent mass matrix has been never performed. Only the direct APMSs were compared with those derived in case of multi-axial excitations [16, 31, 58]. If the human body behaves linearly, a complete knowledge of the impedance matrix is mandatory for predicting the response under multi-axial excitations because the superposition principle holds. Tough linearity was generally assumed for deriving the response of the human body, the validity of the superposition principle was discussed only in case of dual-axis (correlated) WBV and for the seated person [16]. Results showed that the superposition principle did not hold, which implies a nonlinearity in the system. In addition, under multi-axial excitation, the body seemed to be sensitive to the overall vibration magnitude rather than the magnitude along the measuring direction from which deriving the response for each axis [31, 38, 40, 58].
Actually, there are no studies focused on the characterization of the response for the standing person under multi-axial (dual-axis) vibrations and nobody had proved the extent of the above mentioned findings even for the standing postures.

7.2 Experimental method

7.2.1 Apparatus

As mentioned in the previous chapter, the experimental setup was able to generate uncorrelated dual-axis excitations along two perpendicular directions. Similarly, subjects stood on the plate and, in case of emergencies, they were able to hang to a lateral metallic frame fixed to shaker’s base. The force plate was directly used to measure the transmitted forces, without any change, and both signals conditioning and acquisition were performed according to the same settings as for

mono-axial trials. Finally, signals were digitized and stored on a personal computer and the collected time histories were afterwards processed off-line.

7.2.2 Subjects

The eight subjects called for mono-axial trials (biometric data summarized in Table 6.2) were newly involved in this experimental session. The aim was to perform proper statistical comparisons between the responses taken under different conditions for the same population of subjects.

7.2.3 Stimuli

Subjects were exposed to Gaussian white noise signals along two axes per time of the basicentric reference system. Vibrations were provided in the range 1 - 20 Hz with combinations of two magnitudes of acceleration (0.2 m s^{-2} and 0.5 m s^{-2} RMS). Hence, the experiment matrix was composed by six trials (Table 7.1) for which an equivalent dual-axis magnitude was given as the vectorial summation of the two single-axis magnitudes.

Table 7.1 Experiment matrix for dual-axis trials.

Magnitudes (m s^{-2} RMS)			
x-axis	y-axis	z-axis	Overall
0.50	/	0.20	0.54 dual-axis
0.20	/	0.50	0.54 dual-axis
0.50	/	0.50	0.71 dual-axis
/	0.50	0.20	0.54 dual-axis
/	0.20	0.50	0.54 dual-axis
/	0.50	0.50	0.71 dual-axis

The input signals were synthetized each time, by changing the settings of the shakers' control software (the x- and y-axis were excited by a secondary shaker while the z-axis by the primary one). As usual, this practice should provide for more information with respect to the commonly used procedure in which the same acceleration waveforms were used in each session of trials [46]. Stimuli were randomly presented in order to prevent fatigue phenomena.

7.2.4 Postures

During the experiments, subjects stood on the force plate by adopting an upright posture with straight legs. Subjects kept their feet 25 cm apart, wearing their own shoes (the apparent mass is weak effected by the feet/plate interface [48]). The total exposure duration did not exceed 60 seconds for each configuration. In addition, subjects were advised to look straight to a fixed point during the trial and to maintain the same posture without any involuntary movement of the body.

7.2.5 Excitation procedure

All subjects were exposed to vibrations along two axes of the basicentric reference system. Excitations were simultaneous in order to derive both the direct and the two cross-axis APMSs in case of a secondary increasing vibration. As an example, the z-axis was excited at the maximum magnitude (0.5 m s^{-2} RMS) while the y-axis at the lowest magnitude (0.2 m s^{-2} RMS). Afterwards, the secondary vibration was increased to 0.5 m s^{-2} RMS being the z-axis acceleration at the same level. Such procedure was repeated either for the x- or the y-axis as primary directions with increasing z-axis vibrations. Since the secondary shaker acted along the transversal axis, exposures along the x-axis were obtained by inviting the subjects to turn themselves and then looking straight to the secondary shaker. Trials were presented randomly, without a prefixed order of presentation.

7.3 Data processing

The biomechanical response in the basicentric reference system was expressed in terms of the apparent mass (APMS), derived by the use of the cross-spectral density method (CSD). The resulting apparent masses ($APMS_{CSD}$) were provided with both the magnitude and the ordinary coherence function (all spectral quantities were presented with frequency resolution of 0.50 hertz). The inertial contribute due to the plate's mass was removed by mass cancellation in the time-domain; afterwards, the apparent masses were also normalized with respect to the subject's mass as done in the previous chapters. The mean behaviour of the sample was given by aggregating all individuals APMS in a unique matrix of mean quantities (i.e. magnitude and ordinary coherence function), each provided with a proper value of uncertainty (i.e. the standard deviation computed frequency-by-frequency).

7.4 Apparent mass matrix under dual-axis WBV

As already mentioned, the use of two independent controllers should provide for uncorrelated vibrations along two perpendicular directions. Such condition was assessed by computing the ordinary coherence functions between the driving accelerations.

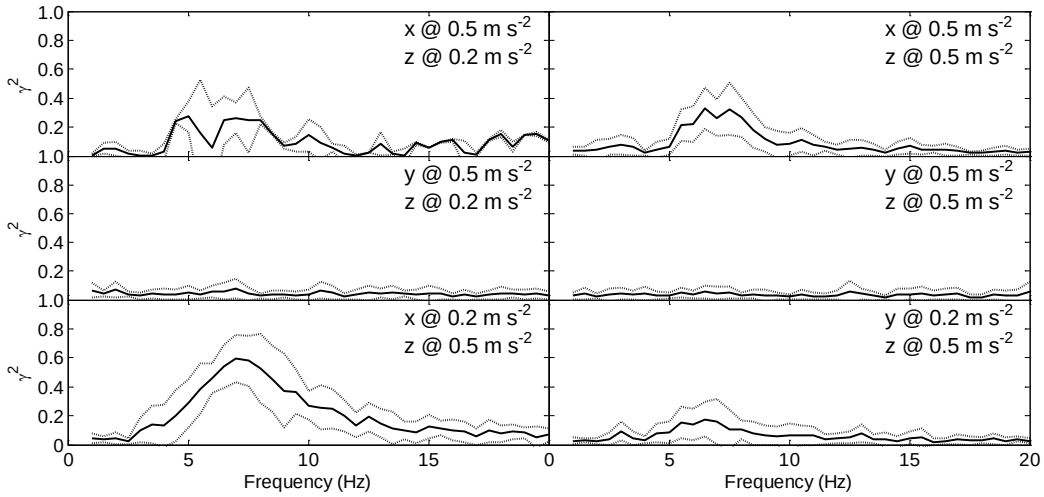

Figure 7.1 Coherence functions between the driving accelerations (sample population).

As shown in Figure 7.1, the ordinary coherence function had a maximum at approximately 7 Hz for the coupling between the x- and z-axis. Such peak was higher when both the accelerations had their maximum magnitude (0.5 m s^{-2} RMS). Instead, for the combined lateral and vertical vibrations the coherence was always below 0.2.

7.4.1 Frontal excitation

The direct frontal APMSs under combined x- and z-axis vibrations are shown in Figure 7.2. The APMSs were similar to each other: they decreased in magnitude till 2.5 Hz and then increased to a secondary minor resonance peak at 5 Hz. No differences occurred to their asymptotic value for frequencies higher than 10 Hz. The ordinary coherence function decreased in value as the vertical vibration increased; the reduction was maximum when both the x- and the z-axis vibrations were 0.5 m s^{-2} RMS in magnitude. However, around the secondary peak the coherence function maintained higher values, independently on the overall vibration. Despite the reduction in magnitude, the coherence function always tended to higher values for increasing frequencies. There were no significant

changes in the scatters across the subjects in both the APMSs and coherence functions.

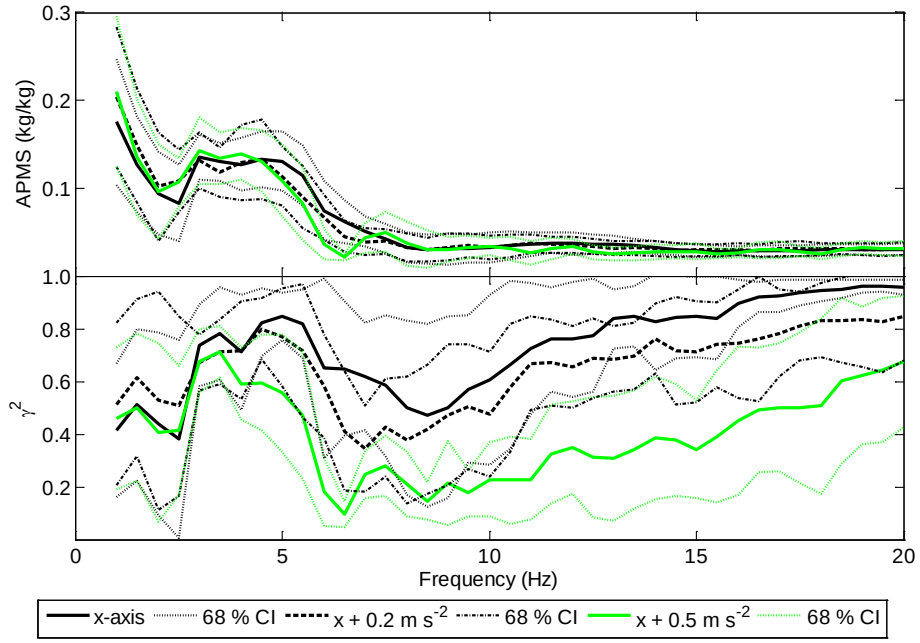

Figure 7.2 Dual-axis WBV (x-axis primary vibration): frontal direct APMS.

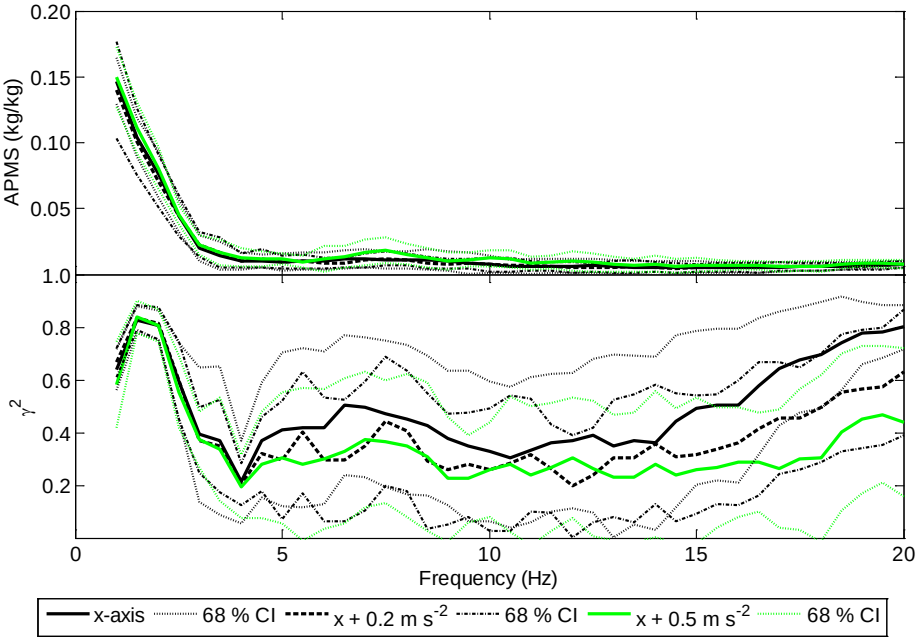

Figure 7.3 Dual-axis WBV (x-axis primary vibration): lateral cross-axis APMS.

The lateral cross-axis APMSs (Figure 7.3) did not change their shape under combined vibrations. The ordinary coherence function decreased in value as the vertical vibration increased; the reduction was always maximum when both the vibrations were equal in magnitude. As for the frontal APMS, a similar increasing trend was found in the coherence function towards higher frequencies.

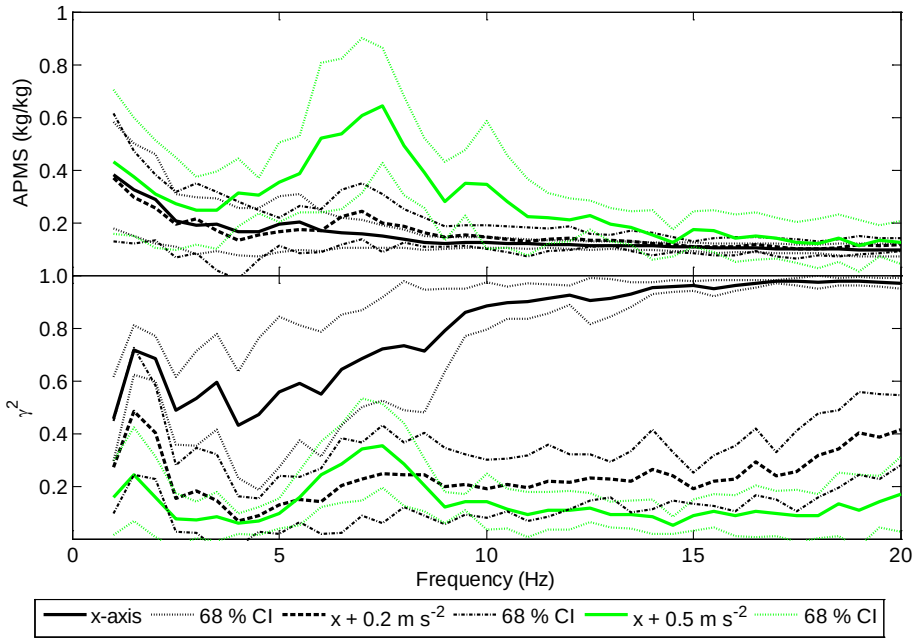

Figure 7.4 Dual-axis WBV (x-axis primary vibration): vertical cross-axis APMS.

As opposed to the previous two cases, the vertical cross-axis APMS seemed to change its shape as the secondary vertical vibration increased in magnitude. A peak of about 0.60 times the static mass rose at about 7 Hz accompanied by a large scatter (50%) across the subjects. As the vertical vibration increased, the ordinary coherence function reduced in value with a minimum at 0.5 m s^{-2} RMS along the z-axis. In correspondence of the peak, the coherence increased to values higher than those derived for the combined vibration with the lower magnitude.

7.4.2 Lateral excitation

The direct lateral APMS did not change in shape due to the addition of a vertical secondary vibration (Figure 7.5). It decreased from low frequencies to about 10% of the static mass then decreased asymptotically to 0.03. The ordinary coherence

function was marginally influenced by the vertical vibration even if it slightly reduced as the z-axis vibration increased in magnitude.

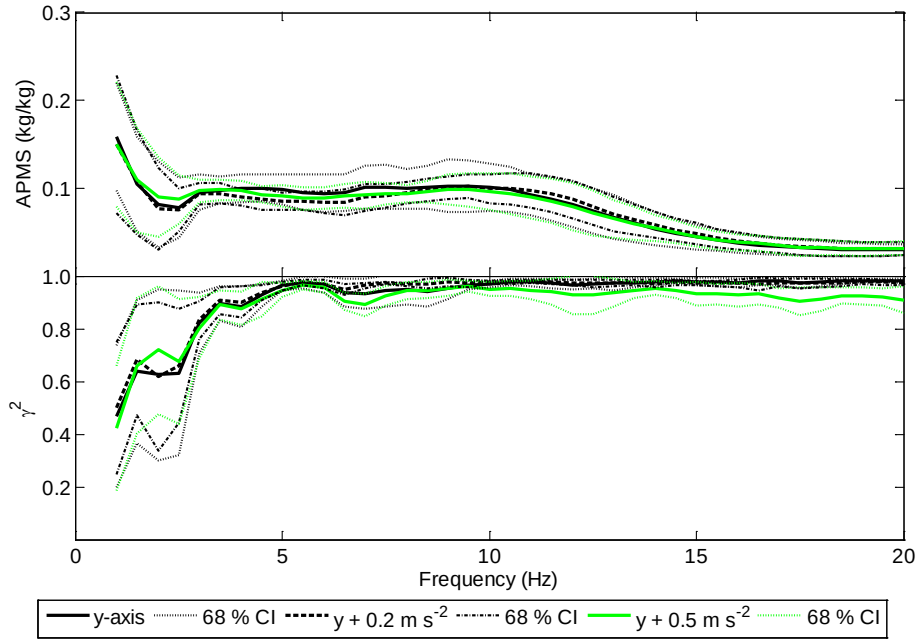

Figure 7.5 Dual-axis WBV (y-axis primary vibration): lateral direct APMS.

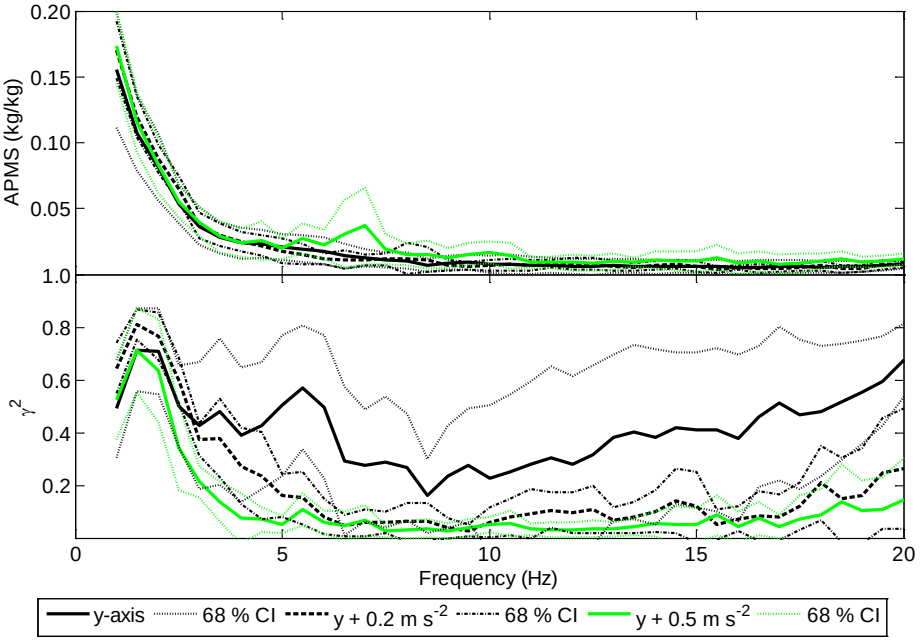

Figure 7.6 Dual-axis WBV (y-axis primary vibration): frontal cross-axis APMS.

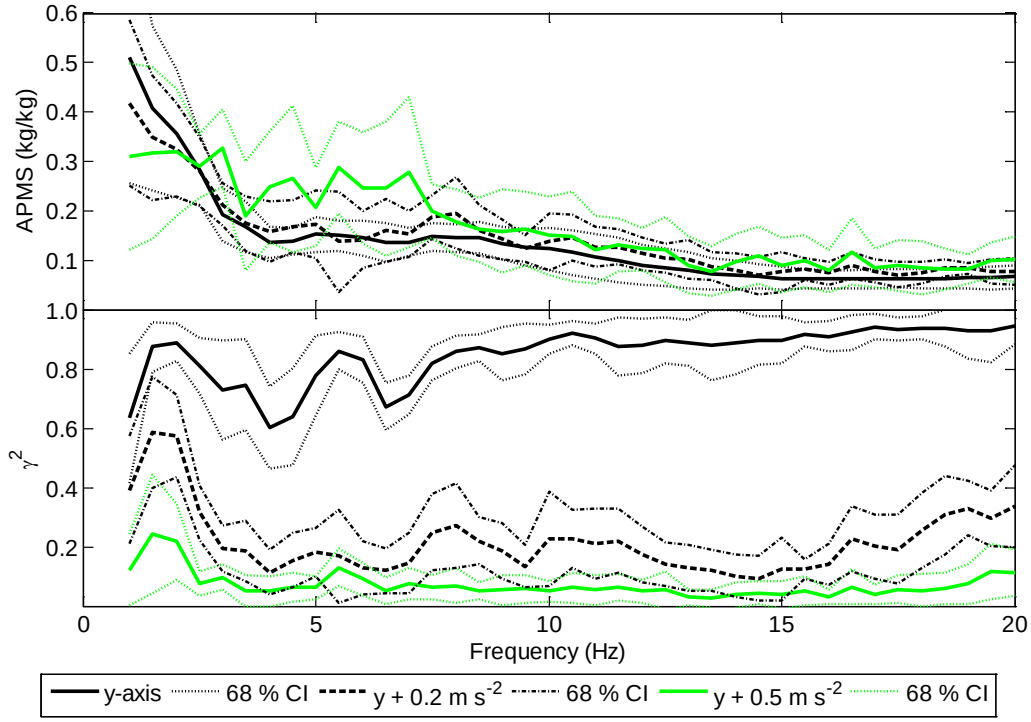

Figure 7.7 Dual-axis WBV (y-axis primary vibration): vertical cross-axis APMS.

The frontal cross-axis APMSs (Figure 7.6) were almost identical in shape within the investigated range of frequencies. The ordinary coherence function progressively reduced with a minimum at about 8 Hz; afterwards it increased in magnitude. The coherence of the direct frontal APMS was characterized by large scatters (about 60%); the variability reduced as the secondary vibration rose. Below 2 Hz, the coherence function of the three APMSs was almost identical in value.

There were no differences in shape between the vertical cross-axis APMSs (Figure 7.7): they all decreased in amplitude towards the same asymptotic value. For the only APMS with the highest z-axis vibration (0.5 m s^{-2} RMS), the magnitude passed from 0.15 to 0.25 in the range 4-8 Hz. A significant decrease in the ordinary coherence function was evident in case of combined frontal-vertical vibrations being the maximum values below 2 Hz

7.4.3 Vertical excitation

In Figure 7.8 are shown the vertical direct APMSs when increasing transversal vibrations (i.e x- and y-axis) add to the primary vertical vibration. Basically, the

direct APMSs did not change in shape and all exhibited a main resonance peak in the range 5-6 Hz with a peak amplitude twice the static mass. The ordinary coherence function reduced in value as the transversal vibration increased with a maximum reduction when both the primary and the secondary vibrations were equal in magnitude (0.5 m s^{-2} RMS). A reduction trend towards higher frequencies was also evident along with large scatters across the subjects.

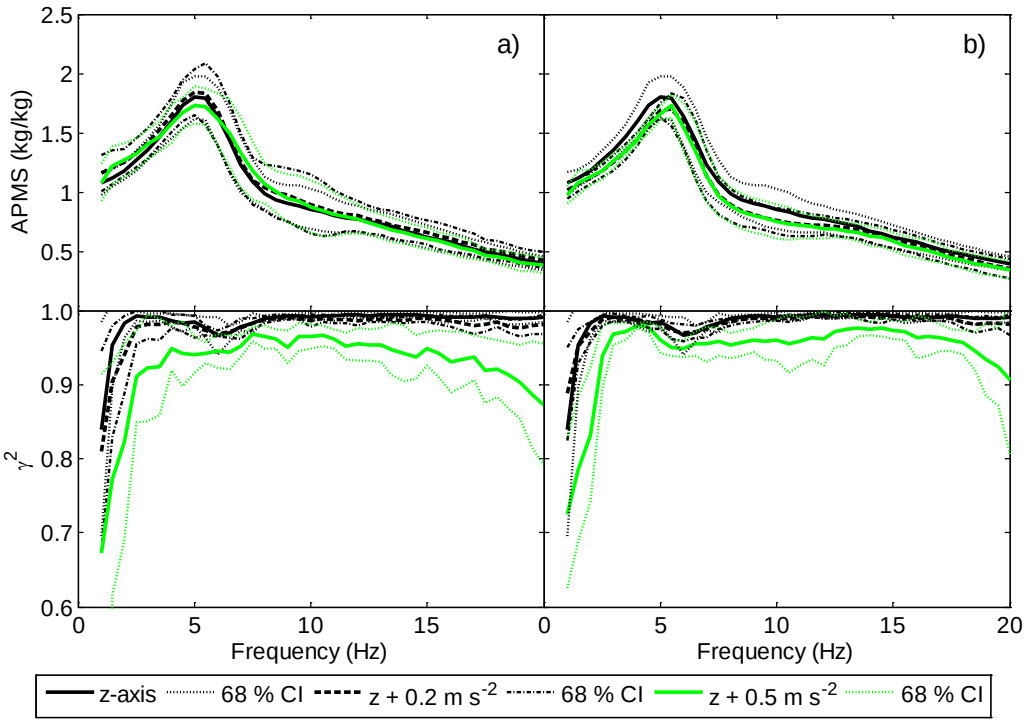

Figure 7.8 Dual-axis WBV (z-axis primary vibration): vertical direct APMS, a) combined z-axis and x-axis vibrations, b) combined z-axis and y-axis vibrations.

The corresponding frontal cross-axis APMSs are depicted in Figure 7.9. Even in this case all the APMSs had their main resonance peaks between 5 Hz and 6 Hz with amplitudes that seemed to change with increasing secondary vibrations. In facts, the mean amplitude reduced as the frontal excitation rose but increased for higher lateral excitations. As the transversal vibration increased, the ordinary coherence function reduced more evidently than that of the direct vertical APMS. The maximum reduction was reached when both the primary and the secondary vibrations were equal in magnitude (0.5 m s^{-2} RMS), especially for the x-axis transversal vibration. A reduction trend was also evident towards higher frequencies along with large scatters across the subjects.

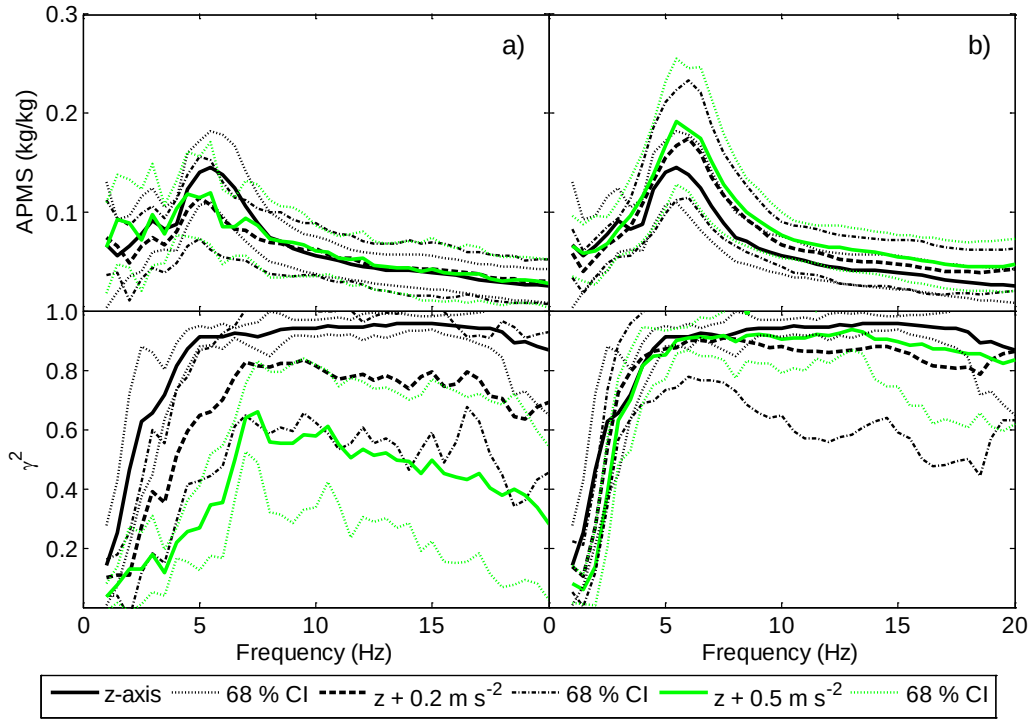

Figure 7.9 Dual-axis WBV (z-axis primary vibration): frontal cross-axis APMS, a) combined z-axis and x-axis vibrations, b) combined z-axis and y-axis vibrations.

The lateral cross-axis APMSs (Figure 7.10) had no significant changes and their amplitudes were always below 0.05. Though, in case of frontal secondary vibration, the drop at 8 Hz (pure z-axis) seemed to disappear and the mean APMS was constant in magnitude in the range 5-12 Hz. Conversely, the rises in the mean APMS increased in amplitude as the lateral vibration summed. As the transversal vibration increased, the lateral forces were less coherent to the vertical vibration. The ordinary coherence function reduced in value as the transversal vibration rose; such behaviour was dramatically evident for the case of lateral (y-axis) vibrations where the coherence dropped below 0.10.

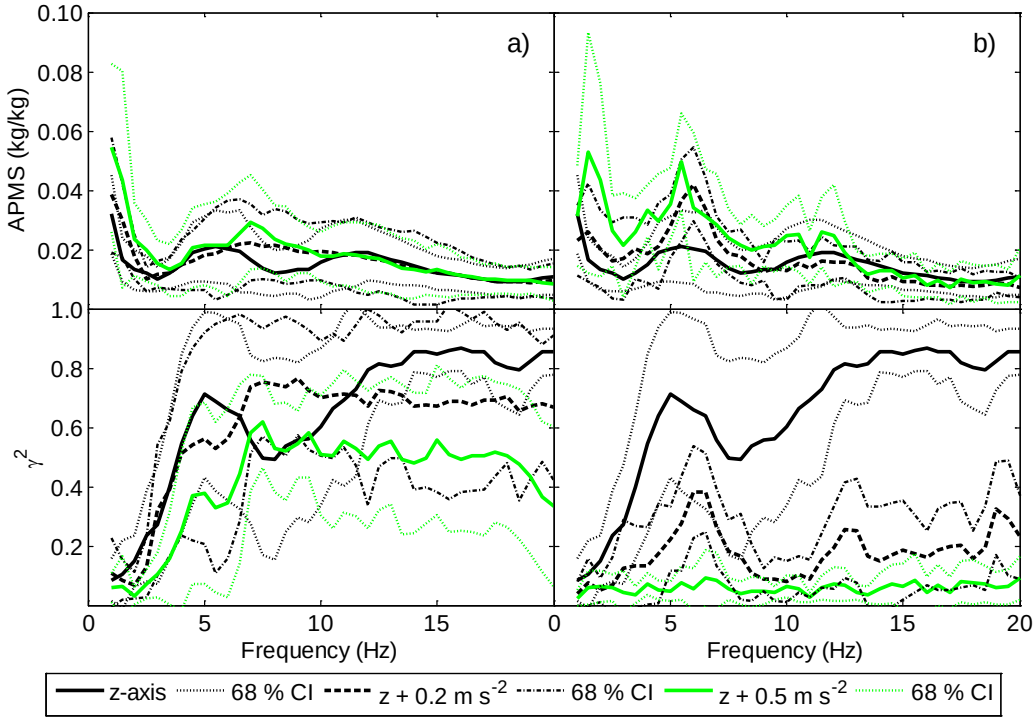

Figure 7.10 Dual-axis WBV (z-axis primary vibration): lateral cross-axis APMS, a) combined z-axis and x-axis vibrations, b) combined z-axis and y-axis vibrations.

7.5 Effect of the secondary axis of vibration

In order to establish whether a dual-axis excitation changes the APMS matrix, both the t-student and Wilcoxon matched paired tests were applied frequency by frequency. Results from the t-student test were graphically displayed as the mean APMS and the associated band of uncertainty (68% CI); instead, for the Wilcoxon test only the median APMSs were provided.

7.5.1 Frontal vibration

The effect of an increasing transversal vertical vibration (0.2 m s^{-2} and 0.5 m s^{-2} RMS) was checked on the direct frontal and both the cross-axis APMSs (Figure 7.11). Results from both the statistical tests showed that there were no significant differences (p-value > 0.05) either in the direct frontal APMS or in the lateral cross-axis APMS. With regard to the vertical cross-axis APMS, no differences were evidenced between the single-axis and the dual-axis "x + z (0.2 m s^{-2})" APMSs; conversely, the "x + z (0.5 m s^{-2})" was found completely different within

the range 4-16 Hz. When the vertical acceleration was 0.5 m s^{-2}, a huge peak rose at about 7 Hz which was completely absent in the previous two conditions.

7.5.2 Lateral vibration

The APMSs under combined lateral and vertical WBVs were almost identical (Figure 7.12). On the contrary, significant differences (p-value < 0.05) were found for the couple y-axis/y + z (0.5 m s^{-2}), between 4 Hz and 8 Hz. Such behaviour was also found between the "y + z (0.2 m s^{-2})" and the "y + z (0.5 m s^{-2})" APMSs but within a narrower range of frequencies.

7.5.3 Vertical vibration

The addition of a frontal secondary vibration did not change the shape of the APMSs along the three axis (Figure 7.13). Instead, if a lateral vibration occurred (Figure 7.14) significant differences were found in the frontal cross-axis APMS between the "z-axis" and the "z + y (0.5 m s^{-2})" AMPSs. No differences were identified within the couple "z-axis"/"z + y (0.2 m s^{-2})" and between the two APMSs taken under dual-axis vibration.
The mono-axial lateral cross-axis APMS differed from those under dual-axis vibrations. As the lateral vibration increased, the differences became more evident. Both the "z + y (0.2 m s^{-2})" and the "z + y (0.5 m s^{-2})" were statistically equivalent.
The direct vertical APMS was influenced by the lateral acceleration (Figure 7.13). In both cases, the mono-axial APMS differed from the dual-axis APMSs: significant differences were found across the left side of the resonance peak while the two dual-axis APMSs were equal in magnitude.

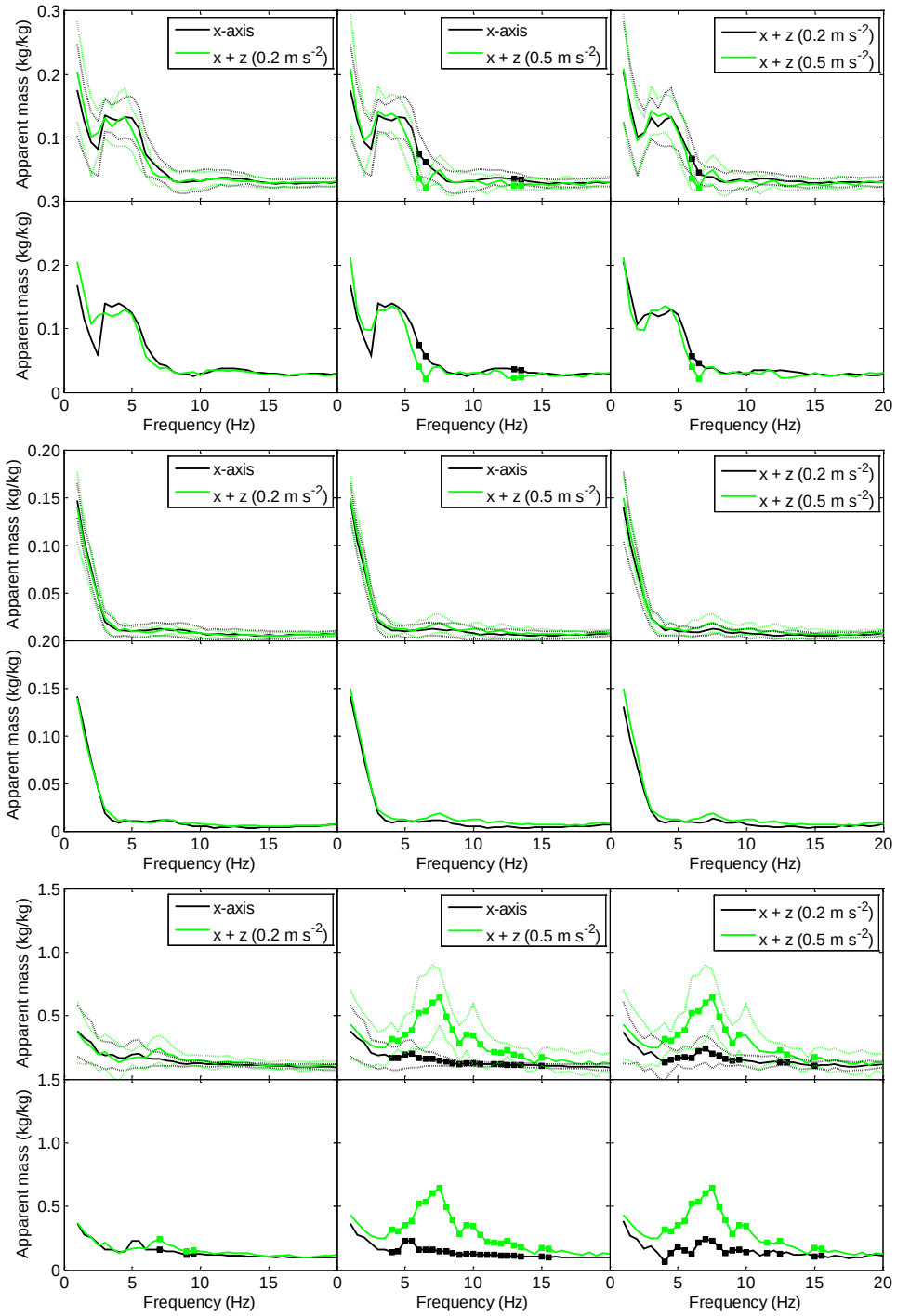

Figure 7.11 APMS under frontal-vertical WBV, results from the paired t-student test (rows 1-3-5) and paired Wilcoxon signed rank test (rows 2-4-6). Frontal in-line APMS (1-2), lateral cross-axis APMS (3-4), vertical cross-axis APMS (5-6); (■ p-value < 0.05).

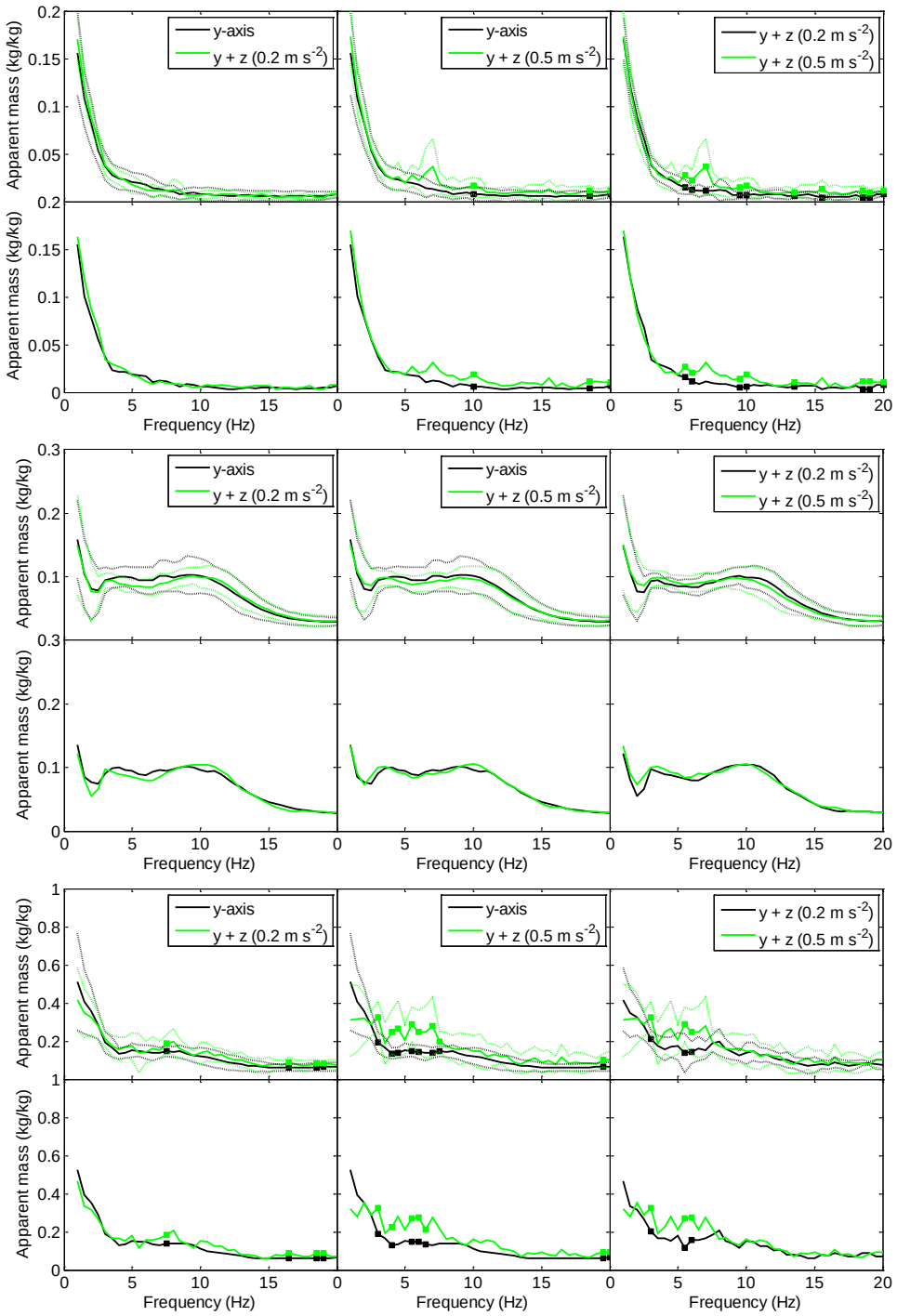

Figure 7.12 APMS under lateral-vertical WBV, results from the paired t-student test (rows 1-3-5) and paired Wilcoxon signed rank test (rows 2-4-6). Frontal cross-axis APMS (1-2), lateral in-line APMS (3-4), vertical cross-axis APMS (5-6); (■ p-value < 0.05).

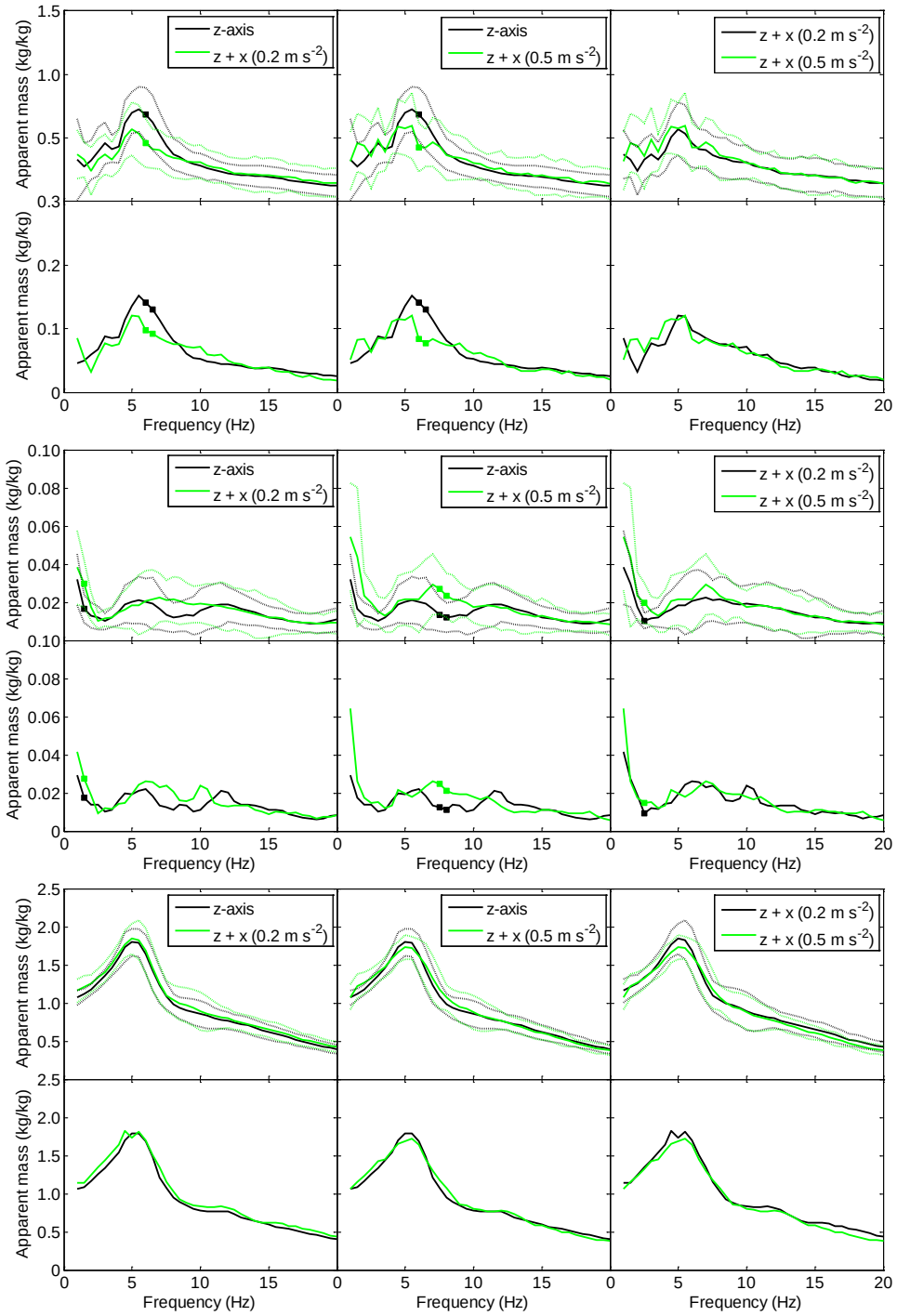

Figure 7.13 APMS under vertical-frontal WBV, results from the paired t-student test (rows 1-3-5) and paired Wilcoxon signed rank test (rows 2-4-6). Frontal cross-axis APMS (1-2), lateral cross-axis APMS (3-4), vertical in-line APMS (5-6); (■ p-value < 0.05).

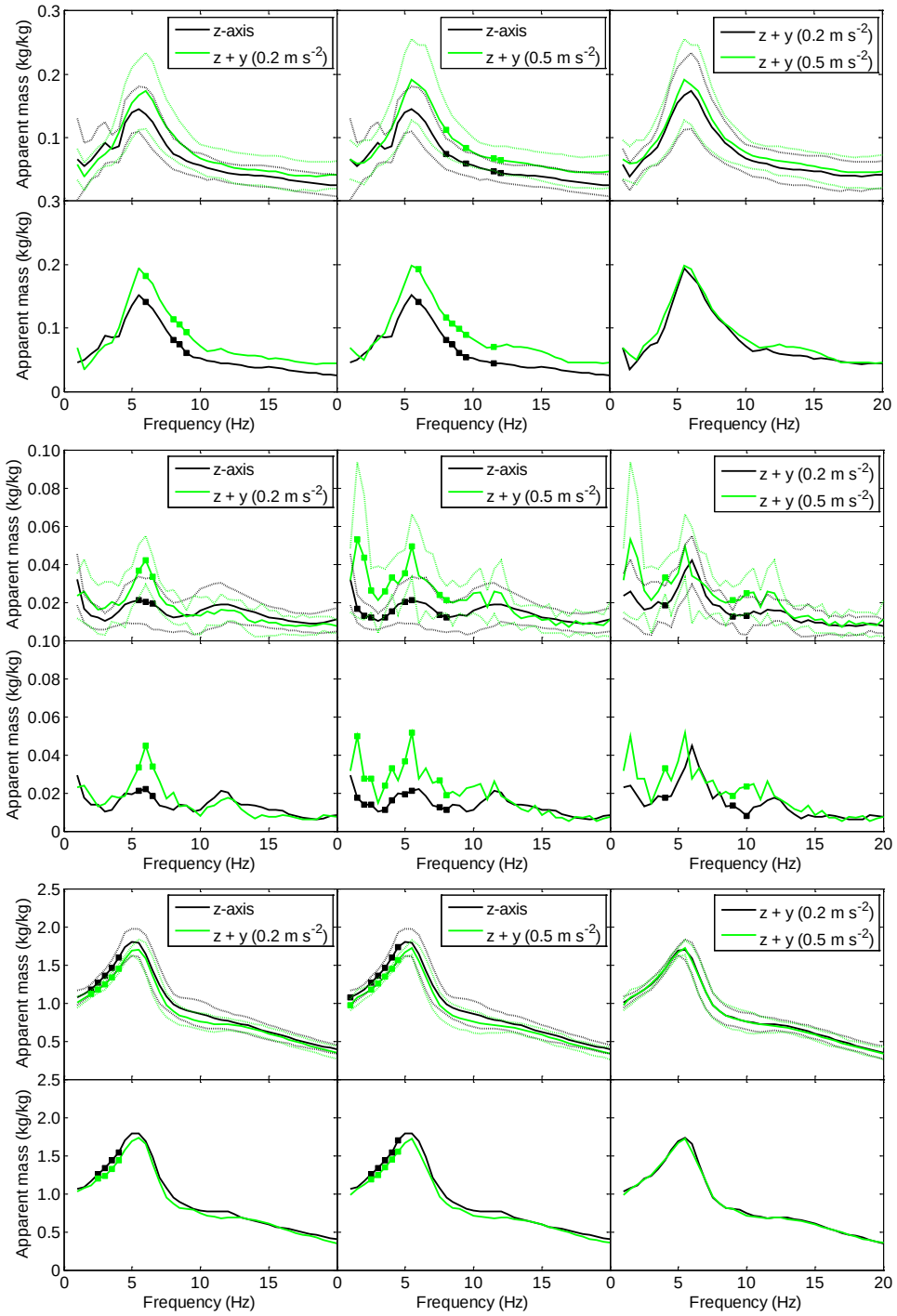

Figure 7.14 APMS under vertical-lateral WBV, results from the paired t-student test (rows 1-3-5) and paired Wilcoxon signed rank test (rows 2-4-6). Frontal cross-axis APMS (1-2), lateral cross-axis APMS (3-4), vertical in-line APMS (5-6); (■ p-value < 0.05).

7.6 Single person analysis

As for the case of the APMS matrix, subject 2 was selected to compare its responses under either mono-axial or dual-axis vibrations (i.e. 0.2 m s^{-2} RMS and 0.5 m s^{-2} RMS). The APMSs were averaged over five repetitions and both the t-student and Wilcoxon matched paired tests were applied to derive a frequency-by-frequency comparison. The ordinary coherence functions were computed for checking the correlation between the driving accelerations.

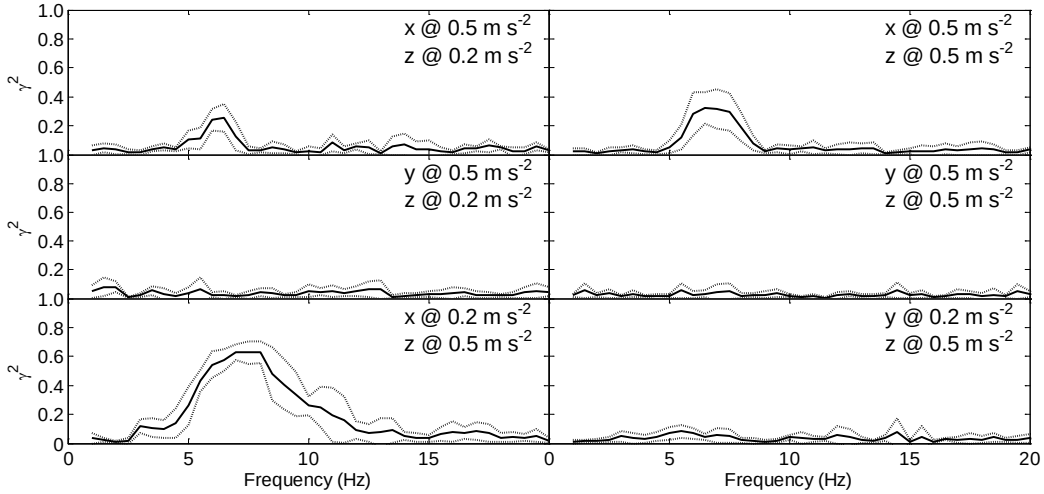

Figure 7.15 Coherence functions between the driving accelerations (single individual).

The ordinary coherence function had a peak at approximately 7 Hz when vibrations on the x- and the z-axis were combined. Similarly to Figure 7.1, the coherence rose when both the accelerations were 0.5 m s^{-2} RMS in magnitude. Instead, the coherence was always below 0.2 for combinations along the lateral and the vertical directions.

7.6.1 Frontal vibration

The addition of an increasing vertical vibration to the primary frontal vibration did not change the shape of the direct frontal and of the lateral cross-axis APMSs (Figure 7.16). On the contrary, the vertical cross-axis APMS changed deeply when both the magnitudes were equal: a huge resonance peak appeared at about 7 Hz and, consequently, there were significant differences in the range 5-10 Hz.

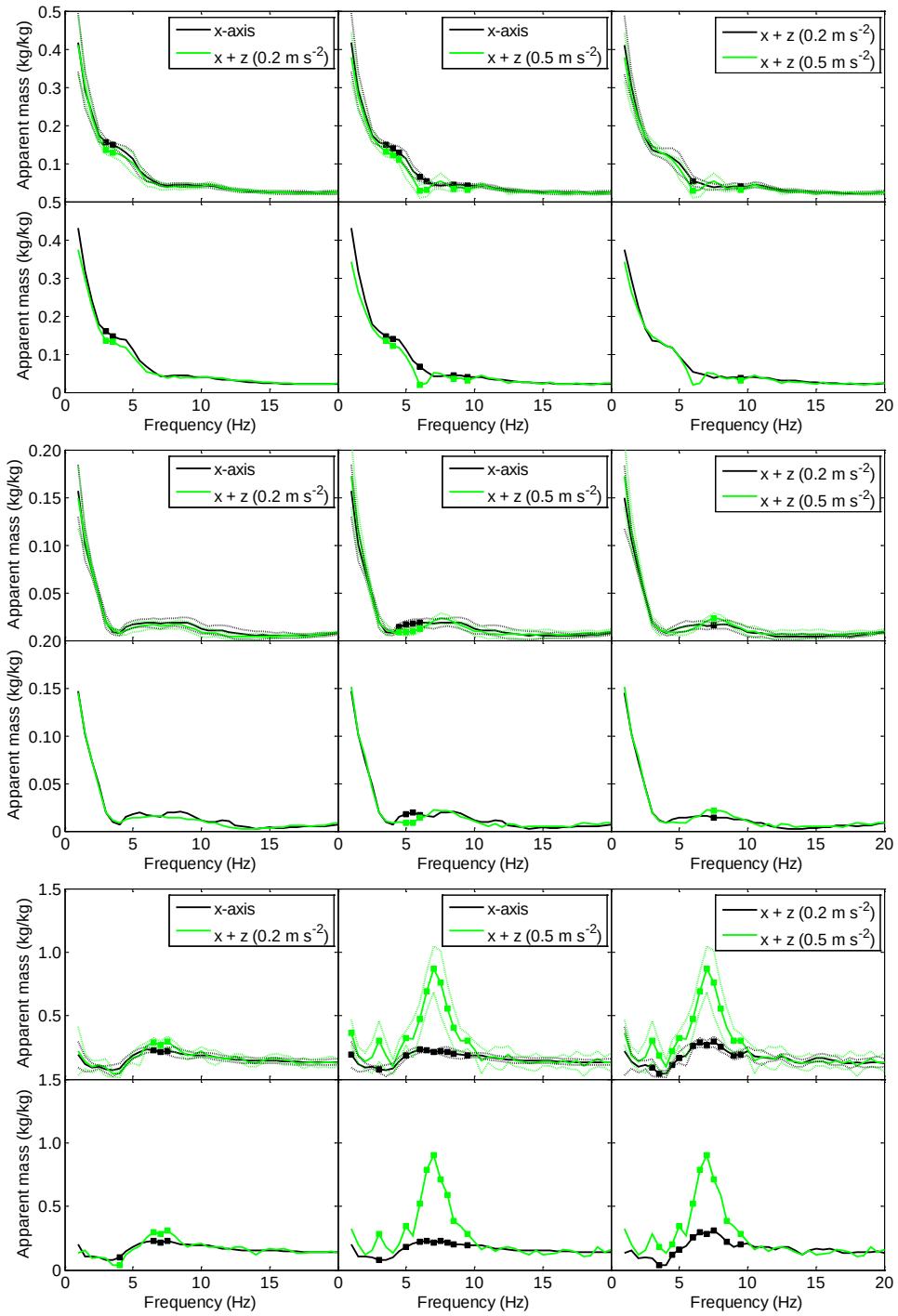

Figure 7.16 Individual's APMS under frontal-vertical WBV, results from the paired t-student test (rows 1-3-5) and paired Wilcoxon signed rank test (rows 2-4-6). Frontal direct APMS (1-2), lateral cross-axis APMS (3-4), vertical cross-axis APMS (5-6); (■ p-value < 0.05).

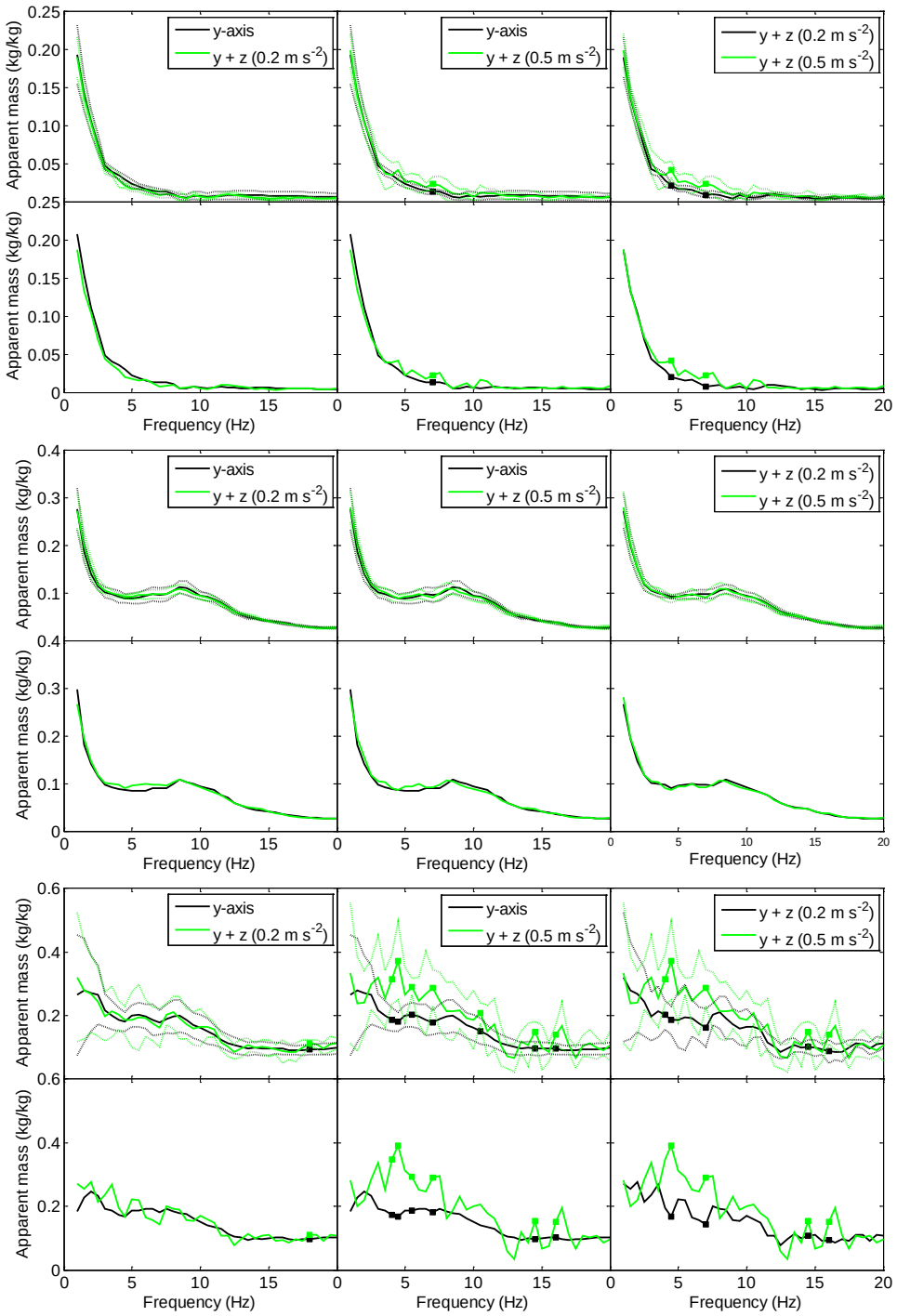

Figure 7.17 Individual's APMS under lateral-vertical WBV, results from the paired t-student test (rows 1-3-5) and paired Wilcoxon signed rank test (rows 2-4-6). Frontal cross-axis APMS (1-2), lateral direct APMS (3-4), vertical cross-axis APMS (5-6); (■ p-value < 0.05).

7.6.2 Lateral vibration

No differences occurred within the APMSs taken under combined lateral and vertical vibrations (Figure 7.17). An exception occurred for the vertical cross-axis APMS where the p-value was below 0.05 between 4 Hz and 7 Hz for the pair "y-axis"/"y + z (0.5 m s^{-2}).

7.6.3 Vertical vibration

In case of secondary frontal vibration, significant differences were evidenced between the mono-axial and the dual-axis APMSs, especially for the frequencies across the right slope of the main resonance peak. However, both the dual-axis APMSs were statistically equal (Figure 7.18). For the lateral cross-axis APMS, no differences were found except for frequencies above 15 Hz for the pair "z-axis"/"z + x (0.5 m s^{-2})". The direct vertical APMS was not effected by the secondary frontal vibration.
The frontal cross-axis APMS was not influenced by a lateral vibration; this was not the case of the lateral cross-axis APMS that increased in magnitude in both the dual-axis conditions (p-value < 0.05 below 11 Hz).
The direct vertical APMS changed in shape around the main resonance peak, where it decreased in amplitude. Other minor changes occurred in the region around 10 Hz and above 15 Hz (Figure 7.19).

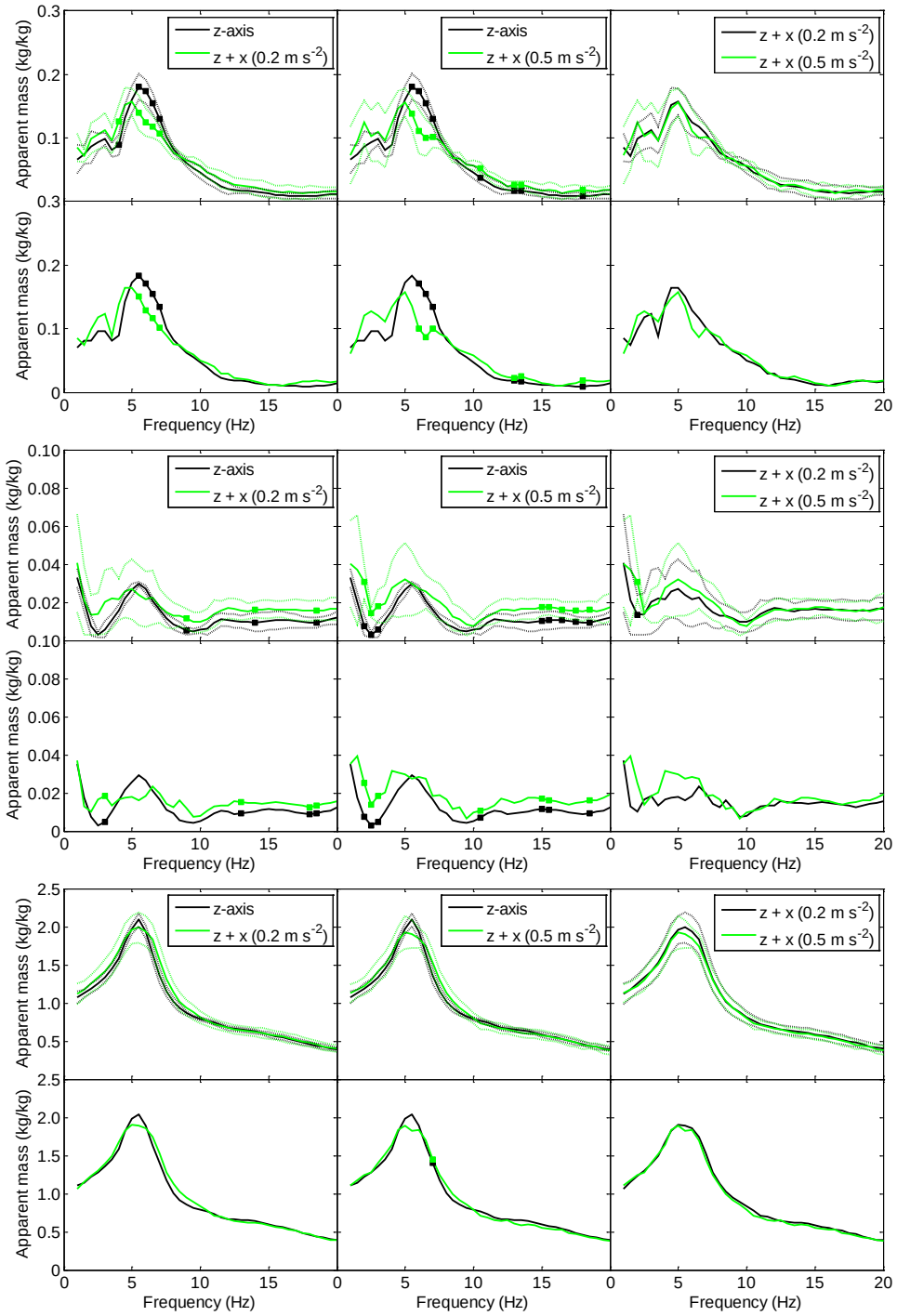

Figure 7.18 Individual's APMS under vertical-frontal WBV, results from the paired t-student test (rows 1-3-5) and paired Wilcoxon signed rank test (rows 2-4-6). Frontal cross-axis APMS (1-2), lateral cross-axis APMS (3-4), vertical direct APMS (5-6); (■ p-value < 0.05).

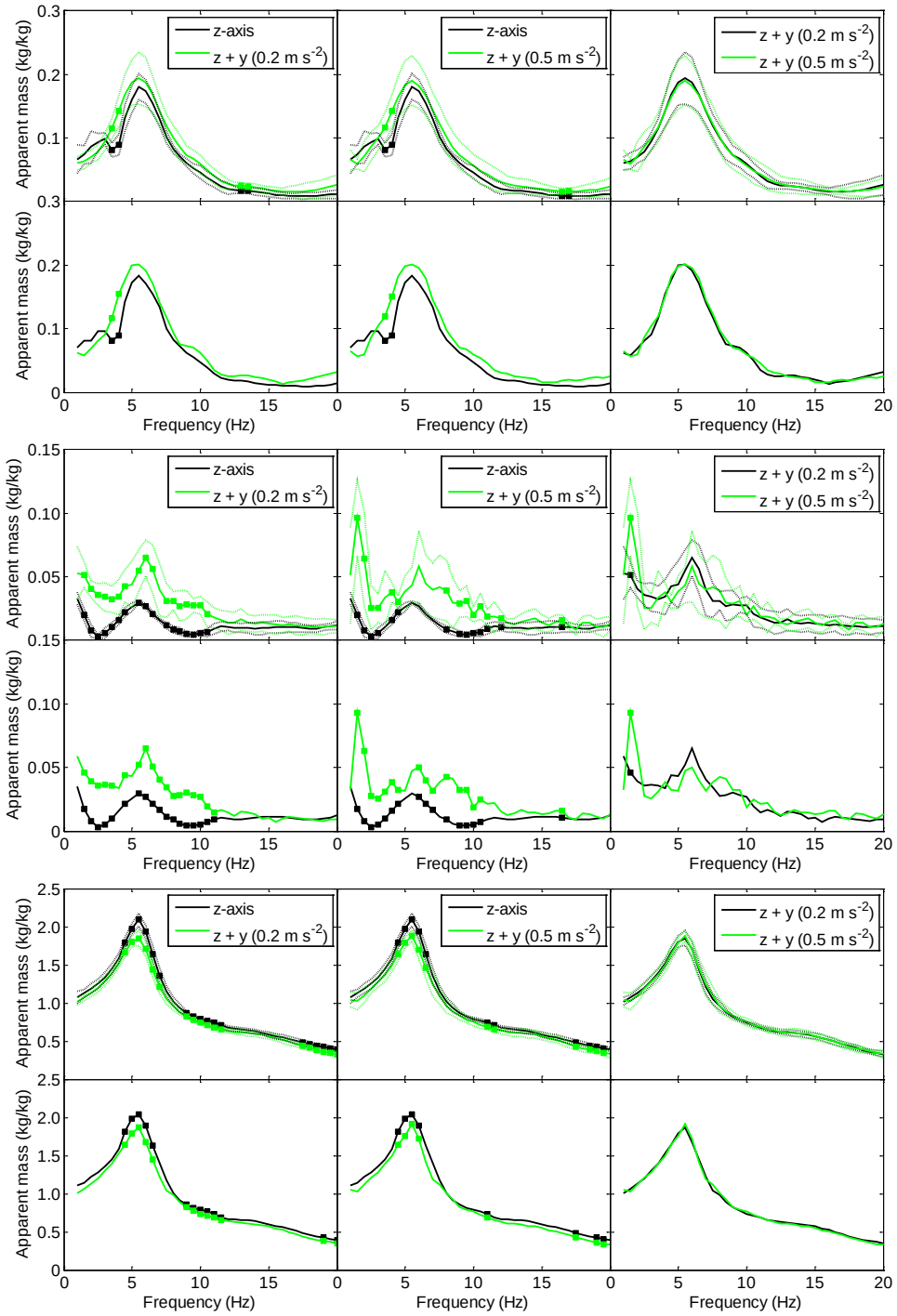

Figure 7.19 Individual's APMS under vertical-lateral WBV, results from the paired t-student test (rows 1-3-5) and paired Wilcoxon signed rank test (rows 2-4-6). Frontal cross-axis APMS (1-2), lateral cross-axis APMS (3-4), vertical direct APMS (5-6); (■ p-value < 0.05).

7.7 Conclusions

7.7.1 Effect of the secondary axis of vibration

Despite the ordinary coherence functions did not indicate uncorrelated inputs within the whole range of frequencies, results seemed to be not affected by unexpected resonances and the ordinary coherence functions between the transmitted forces and the accelerations were all congruent.
In case of combined frontal and vertical accelerations, the vertical cross-axis APMS exhibited a peak of about 60% of the static mass at 7 Hz. Such increase in amplitude was not in common to the direct frontal APMS and this may suggest changes in the response of the body due to a combination of accelerations of equal magnitude along the vertical and the frontal directions.
The effect of a combination between a lateral and a vertical acceleration or a vertical and a frontal acceleration did not produce significant changes, especially for the direct lateral and vertical APMSs. Conversely, if a lateral acceleration was summed to a vibration in the vertical direction, the cross-axis lateral APMS increased in magnitude while the direct vertical APMS reduced in amplitude for those frequencies below the main resonance.

7.7.2 Dual-axis vibrations on single individual

As for the case of the APMS matrix under mono-axial WBVs, the effect of the secondary vibration was investigated for both the APMSs of the sample population and for a single individual. The aim was to establish whether a scatter in the biometric data of the testing population makes less evident the nonlinearity due to an increased excitation level introduced by a transversal acceleration.
For the case of frontal-vertical excitation, results confirmed the rise of the main peak in the vertical cross-axis APMS; no differences were observed for the APMSs derived under lateral-vertical vibrations.
However, the individual's responses were found different from that of the sample in case of combined vertical-frontal and vertical-lateral vibrations. In the first case, the frontal cross-axis APMS reduced in amplitude at frequencies above the main peak of resonance but the direct vertical APMS did not change in shape. Conversely, when a lateral vibration occurred the nonlinearity with respect to the overall vibration was more evident in the individual rather than in the sample population.

Chapter 8

Conclusions and further developments

This doctoral dissertation was focused on the identification of the nonlinearities which affect the response of the human body exposed to whole-body vibrations. In particular, the study was oriented on the characterization of the response, expressed in terms of the apparent mass, of the standing people.
The research activity was carried out according to the following steps:

1. characterization of the apparent mass in case of vertical whole-body vibration;
2. identification of the nonlinearities;
3. design and realization of a suitable excitation system and setup for measuring the apparent masses in the basicentric reference system;
4. characterization of the full (three-by-three) matrix of apparent masses for the standing persons;
5. characterization of the response in case of multi-axial vibrations (no more than two axis contemporarily excited).

A summary of the main results gained throughout the chapters is provided as follows with the addition of some recommendations for further developments.

8.1 Vertical apparent mass

Nonlinearities in the human body response to vertical WBV were analysed using the conditioned output spectra and the multiple coherence functions. The contributions of the nonlinear terms to the apparent mass were negligible (i.e. the modelled nonlinear terms did not take part in the definition of the response) and the nonlinearity was associated to the variation of the modal parameters in time, due to low frequency motion during the tests and involuntary muscular actions.
Both in the standing and legs bent postures, the biodynamic response to vertical whole-body vibration was affected by the vibration magnitude for frequencies above 10 Hz, where the effect of modelling inaccuracy was less critical. The responses modelled with conditioned and linear models were very similar and differences between the ordinary and the multiple coherence functions were comparable to the intra-subject variability. According to our experience, the procedure for the identification of the origins of nonlinear effects consisted of the computation of the apparent mass using the Welch approach and the H_1 estimator of the transfer function. The ordinary coherence function had to be analysed without any procedure for the outliers' rejection; if the coherence was close to unity the linear model was valid, otherwise low coherence indicated that the system was nonlinear. The causes of the nonlinearity may be the variation of modal parameters during the test or the presence of nonlinear terms in the

response. The variation of modal parameters was evidenced by the analysis of FRF COV using the Welch approach while the presence of nonlinear terms was outlined by a difference between the conditioned and the conventional apparent mass.

8.2 APMS matrix

The full three-by-three APMS matrix was derived by exposing subjects to independent vibrations along the three orthogonal axis. Such task involved the design of either a dual-axis excitation system, made by the junction of two electrodynamic shakers, or a tri-axial force plate, for the measurement of the transmitted forces in the reference system. For each axis, both the direct and the cross-axis APMSs were computed by the use of linear estimators.
Basically, results agreed with previous findings reported in the literature but a full correspondence cannot be found since nobody have still never investigated the biodynamic response for the standing persons along the three directions and for such extended range of frequencies (1-20 Hz). At the current state-of-the art, the available studies were carried out under not homogenous conditions because they were focused on some postural peculiarity. In addition, there was no correspondence between the samples (i.e. different populations each time) and both the vibration levels and the frequency ranges were incompatible to each other (in case of vibrations in the xy-plane, the response was limited for frequencies below 5 Hz).
Generally, the normalized APMS decreased in amplitude towards higher frequencies, except for the case of vertical WBV where both the direct and the frontal cross-axis APMSs increased to a main resonance peak (at about 5-6 Hz) and then decreased to lower magnitudes. Such coupling may suggest a common vibration mode in the xz-plane but it did not occur under a reciprocal condition (i.e any resonance rose on both axis due to a frontal excitation). No more couplings were found between the direct and the cross-axis APMSs under excitations along the other axes.
Unexpectedly, along the vertical direction (z-axis) the human body was found more sensitive to vibrations. Independently on the excitation axis, the direct vertical APMS and both the vertical cross-axis APMSs were higher in magnitude than the corresponding direct APMSs. In facts, one would expect that the major inertial contribute occurs along the direction of excitation.
The effect of the vibration magnitude was investigated by comparing the APMS matrices taken at two magnitudes of vibration (i.e. 0.2 m s^{-2} and 0.5 m s^{-2} RMS). Comparisons were performed by applying both the t-student and the Wilcoxon matched paired tests, frequency by frequency, with the aim to test for equality the medians and the means of the apparent masses for the sample population.

Generally, no differences occurred within the APMSs being the vibration magnitude not a driving parameter for the modelling of the biodynamic response. Nevertheless, an exception occurred in the direct vertical APMS in which some differences rose across the main resonance peak. A reduction in both the amplitude and resonance frequency were evident in both the mean and median APMSs as the acceleration magnitude increased. Such finding was the typical result given in the literature and it was indicated as the main nonlinearity.
Secondly, the same statistical analysis were performed on the APMS matrices of a single individual. In this case, it was observed a more dependence of the response on the vibration magnitude. Many differences occurred at frequencies where the aggregate responses were found equal. This was the case of the APMSs derived due to vertical vibration. For both the cross-axis APMSs, the resonance peak tended to reduce its amplitude and frequency but for the direct vertical APMS the statistical tests evidenced a deeper modification of the modal parameters since differences rose within a wider range of frequencies.
Definitely, the comparison between the population and the individual's APMS matrices evidenced the more dependence of the individual's response on the vibration magnitude. This finding may depend on the scatter in the population's biometric data whose uncertainty introduced on the response is such to overlay magnitude dependent effects.

8.3 Conditioned APMS matrix

The frontal cross-axis APMS under vertical WBV was conditioned for assessing whether nonlinearities in the response occurred. Results from the linear estimators and the conditioned quantities were found similar. Further analysis evidenced that the drop in the coherence function was not attributable to some nonlinearity but the response was not stationary. Consequently, the APMS matrix of an individual was fully conditioned with the same aim of proving the extent of the nonlinearity. The differences between the linear estimators and the conditioned quantities were comparable to the intra-subject variability.

8.4 Dual-axis excitation

The APMS matrices in case of dual-axis excitations were characterized by exposing subjects contemporarily to independent vibrations along either a primary or a transversal directions (i.e. with increasing magnitudes of acceleration). Results from the sample population showed few differences in shape for the APMSs under frontal and lateral primary vibrations. An exception occurred for the vertical cross-axis APMS, where it significantly changed in shape when both the direct and the transversal vibrations were equal in magnitude. Conversely, when a vertical vibration was combined with single-axis horizontal

vibrations, significant changes in shape were obtained for the case of lateral secondary excitations. Both the direct vertical and the lateral cross-axis APMSs differed from single-axis to dual-axis exposures.
For the case of an individual, there were no differences from single-axis horizontal and dual-axis (horizontal and vertical) vibrations. When combining vertical and horizontal (secondary) accelerations, the dual-axis APMSs along each of the two directions of excitation changed in shape with respect to those derived under single-axis vibrations. In zy-plane, the lateral cross-axis APMS increased in magnitude but the direct vertical APMS also reduced in amplitude at resonance.
Results from the comparison between the APMSs taken under single-axis and dual-axis exposures confirmed that the biodynamic response was influenced by the addition of a secondary transversal acceleration. Such dependence cannot be extended either to all the directions of excitation or within a specific response path. It was found a marginal contribute of the overall magnitude of vibration since dual-axis APMSs were almost equal. As for the APMS under single-axis excitations, nonlinerity in the response due to the addition of a secondary vibration was more evident for the individual rather than in the sample population. Such behaviour may again depend on the variability in the population's biometric data whose uncertainty is such to overlay the effects due to the addition of extra-axis vibrations.

8.5 Further developments

The study on dual-axis excitations should be completed by the characterization of the missing combinations in the horizontal plane. Future works should also involve a wider range of vibration magnitudes in order to evaluate the extent of the results outlined in this study. Another important issue is the characterization of the APMS matrix in case of combined excitations on the three orthogonal axis. Afterwards, it should be outlined the importance of both the acceleration level (in terms of the single-axis and the overall magnitude) and the propagation path for the modelling of the biodynamic response for the standing people.
In addition, a better understanding of the key role of the uncertainty introduced by the variability in the biometric data of testing persons is required. This task should be easily solved by comparing the responses of the whole population with those of more individuals in order to assess whether the nonlinearities will be more evident or not.
Finally, the method for conditioning the apparent masses can be applied to any study focused on the analysis of the nonlinear behaviour of the human body (for instance, the study of the biodynamic response of sitting and recumbent subjects or of the hand-arm response to vibration).

Bibliography

[1] D. Hoy, P. Brooks, F. Blyth, R. Buchbinder, The epidemiology of low back pain, Best practice & research Clinical rheumatology, 24 (2010) 769-781.
[2] M. Bovenzi, F. Rui, C. Negro, F. D'Agostin, G. Angotzi, S. Bianchi, L. Bramanti, G. Festa, S. Gatti, I. Pinto, An epidemiological study of low back pain in professional drivers, Journal of Sound and Vibration, 298 (2006) 514-539.
[3] R. Buchbinder, F.M. Blyth, L.M. March, P. Brooks, A.D. Woolf, D.G. Hoy, Placing the global burden of low back pain in context, Best Practice & Research Clinical Rheumatology, 27 (2013) 575-589.
[4] K. Majid, E. Truumees, Epidemiology and natural history of low back pain, in: Seminars in Spine Surgery, Elsevier, 2008, pp. 87-92.
[5] D. Hoy, L. March, P. Brooks, A. Woolf, F. Blyth, T. Vos, R. Buchbinder, Measuring the global burden of low back pain, Best Practice & Research Clinical Rheumatology, 24 (2010) 155-165.
[6] Council Directive 2002/44/EC of the European Parliament and of the Council of 25 June 2002 on the minimum health and safety requirements regarding the exposure of workers to the risks arising from physical agents (vibration). *Official Journal of the European Communities* L 177/13, 6.7.2002, pp. 13-19.
[7] C. Hulshof, B.V. van Zanten, Whole-body vibration and low-back pain, International Archives of Occupational and Environmental Health, 59 (1987) 205-220.
[8] M. Bovenzi, C. Hulshof, An updated review of epidemiologic studies on the relationship between exposure to whole-body vibration and low back pain (1986–1997), International archives of occupational and environmental health, 72 (1999) 351-365.
[9] M. Bovenzi, I. Pinto, N. Stacchini, Low back pain in port machinery operators, Journal of sound and vibration, 253 (2002) 3-20.
[10] N.J. Mansfield, Impedance methods (apparent mass, driving point mechanical impedance and absorbed power) for assessment of the biomechanical response of the seated person to whole-body vibration, Industrial Health, 43 (2005) 378-389.
[11] ISO 2631-1:1997 "Mechanical vibration and shock - Evaluation of human exposure to whole-body vibration - Part 1: General requirements.".
[12] J.S. Bendat, A.G. Piersol, Engineering applications of correlation and spectral analysis, (1993).
[13] J.S. Bendat, A.G. Piersol, Random data: analysis and measurement procedures, Wiley, 2000.
[14] R. Lundström, P. Holmlund, L. Lindberg, Absorption of energy during vertical whole-body vibration exposure, Journal of biomechanics, 31 (1998) 317-326.

[15] P. Holmlund, R. Lundström, Mechanical impedance of the human body in the horizontal direction, Journal of sound and vibration, 215 (1998) 801-812.
[16] N. Mansfield, R. Lundström, The apparent mass of the human body exposed to non-orthogonal horizontal vibration, Journal of biomechanics, 32 (1999) 1269-1278.
[17] P. Holmlund, R. Lundström, L. Lindberg, Mechanical impedance of the human body in vertical direction, Applied Ergonomics, 31 (2000) 415-422.
[18] N.J. Mansfield, M.J. Griffin, Non-linearities in apparent mass and transmissibility during exposure to whole-body vertical vibration, Journal of biomechanics, 33 (2000) 933-941.
[19] P. Holmlund, R. Lundström, Mechanical impedance of the sitting human body in single-axis compared to multi-axis whole-body vibration exposure, Clinical biomechanics, 16 (2001) S101-S110.
[20] S. Rakheja, I. Haru, P.É. Boileau, Seated occupant apparent mass characteristics under automotive postures and vertical vibration, Journal of Sound and Vibration, 253 (2002) 57-75.
[21] N. Mansfield, M. Griffin, Effects of posture and vibration magnitude on apparent mass and pelvis rotation during exposure to whole-body vertical vibration, Journal of Sound and Vibration, 253 (2002) 93-107.
[22] N. Nawayseh, M. Griffin, Non-linear dual-axis biodynamic response to vertical whole-body vibration, Journal of Sound and Vibration, 268 (2003) 503-523.
[23] W. Wang, S. Rakheja, P.É. Boileau, Effects of sitting postures on biodynamic response of seated occupants under vertical vibration, International journal of industrial ergonomics, 34 (2004) 289-306.
[24] N.J. Mansfield, S. Maeda, Comparison of the apparent mass of the seated human measured using random and sinusoidal vibration, Industrial health, 43 (2005) 233-240.
[25] N.J. Mansfield, S. Maeda, Effect of backrest and torso twist on the apparent mass of the seated body exposed to vertical vibration, Industrial Health, 43 (2005) 413-420.
[26] N. Nawayseh, M. Griffin, Non-linear dual-axis biodynamic response to fore-and-aft whole-body vibration, Journal of Sound and Vibration, 282 (2005) 831-862.
[27] N. Nawayseh, M.J. Griffin, Tri-axial forces at the seat and backrest during whole-body vertical vibration, Journal of sound and vibration, 277 (2004) 309-326.
[28] Y. Huang, M.J. Griffin, Effect of voluntary periodic muscular activity on nonlinearity in the apparent mass of the seated human body during vertical random whole-body vibration, Journal of sound and vibration, 298 (2006) 824-840.

[29] N.J. Mansfield, S. Maeda, Comparison of the apparent masses and cross-axis apparent masses of seated humans exposed to single-and dual-axis whole-body vibration, Journal of sound and vibration, 298 (2006) 841-853.
[30] N. Mansfield, P. Holmlund, R. Lundström, P. Lenzuni, P. Nataletti, Effect of vibration magnitude, vibration spectrum and muscle tension on apparent mass and cross axis transfer functions during whole-body vibration exposure, Journal of biomechanics, 39 (2006) 3062-3070.
[31] N.J. Mansfield, S. Maeda, The apparent mass of the seated human exposed to single-axis and multi-axis whole-body vibration, Journal of biomechanics, 40 (2007) 2543-2551.
[32] S. Rakheja, S. Mandapuram, R.G. Dong, Energy absorption of seated occupants exposed to horizontal vibration and role of back support condition, Industrial health, 46 (2008) 550-566.
[33] W. Wang, S. Rakheja, P.É. Boileau, Relationship between measured apparent mass and seat-to-head transmissibility responses of seated occupants exposed to vertical vibration, Journal of Sound and Vibration, 314 (2008) 907-922.
[34] M.G.R. Toward, M.J. Griffin, Apparent mass of the human body in the vertical direction: Effect of seat backrest, Journal of Sound and Vibration, 327 (2009) 657-669.
[35] M. Toward, M. Griffin, Apparent mass of the human body in the vertical direction: Effect of a footrest and a steering wheel, Journal of Sound and Vibration, 329 (2010) 1586-1596.
[36] N. Nawayseh, M.J. Griffin, Power absorbed during whole-body vertical vibration: Effects of sitting posture, backrest, and footrest, Journal of Sound and Vibration, 329 (2010) 2928-2938.
[37] M.G.R. Toward, M.J. Griffin, Apparent mass of the human body in the vertical direction: Inter-subject variability, Journal of Sound and Vibration, 330 (2011) 827-841.
[38] S. Mandapuram, S. Rakheja, P. Marcotte, P.É. Boileau, Analyses of biodynamic responses of seated occupants to uncorrelated fore-aft and vertical whole-body vibration, Journal of Sound and Vibration, 330 (2011) 4064-4079.
[39] N. Nawayseh, M.J. Griffin, Power absorbed during whole-body fore-and-aft vibration: Effects of sitting posture, backrest, and footrest, Journal of Sound and Vibration, 331 (2012) 252-262.
[40] S. Mandapuram, S. Rakheja, P.É. Boileau, S. Maeda, Apparent mass and head vibration transmission responses of seated body to three translational axis vibration, International Journal of Industrial Ergonomics, 42 (2012) 268-277.
[41] G. Zheng, Y. Qiu, M.J. Griffin, Vertical and dual-axis vibration of the seated human body: Nonlinearity, cross-axis coupling, and associations between resonances in transmissibility and apparent mass, Journal of Sound and Vibration, 331 (2012) 5880-5894.

[42] R.R. Coermann, The mechanical impedance of the human body in sitting and standing position at low frequencies, Human Factors: The Journal of the Human Factors and Ergonomics Society, 4 (1962) 227-253.
[43] R.G. Edwards, K.O. Lange, A mechanical impedance investigation of human response to vibration, in, DTIC Document, 1964.
[44] T. Miwa, Mechanical impedance of human body in various postures, Industrial health, 13 (1975) 1-22.
[45] Y. Matsumoto, M. Griffin, Dynamic response of the standing human body exposed to vertical vibration: influence of posture and vibration magnitude, Journal of sound and vibration, 212 (1998) 85-107.
[46] G.H.M.J. Subashi, Y. Matsumoto, M.J. Griffin, Apparent mass and cross-axis apparent mass of standing subjects during exposure to vertical whole-body vibration, Journal of Sound and Vibration, 293 (2006) 78-95.
[47] Y. Matsumoto, M. Griffin, The horizontal apparent mass of the standing human body, Journal of Sound and Vibration, 330 (2011) 3284-3297.
[48] M. Tarabini, B. Saggin, D. Scaccabarozzi, D. Gaviraghi, G. Moschioni, Apparent mass distribution at the feet of standing subjects exposed to whole-body vibration, Ergonomics, 56 (2013) 842-855.
[49] Y. Matsumoto, M. Griffin, Mathematical models for the apparent masses of standing subjects exposed to vertical whole-body vibration, Journal of Sound and Vibration, 260 (2003) 431-451.
[50] G. Subashi, Y. Matsumoto, M. Griffin, Modelling resonances of the standing body exposed to vertical whole-body vibration: effects of posture, Journal of Sound and Vibration, 317 (2008) 400-418.
[51] D.C. Montgomery, G.C. Runger, Applied Statistics and Probability for Engineers, Wiley, 2002.
[52] M. Morioka, M.J. Griffin, Magnitude-dependence of equivalent comfort contours for fore-and-aft, lateral and vertical whole-body vibration, Journal of Sound and Vibration, 298 (2006) 755-772.
[53] G.J. Stein, P. Múcka, B. Hinz, R. Blüthner, Measurement and modelling of the y-direction apparent mass of sitting human body-cushioned seat system, Journal of Sound Vibration, 322 (2009) 454-474.
[54] J.S. Bendat, Nonlinear system techniques and applications, (1998).
[55] G. D'Antona, A. Ferrero, Digital signal processing for measurement systems: theory and applications, Springer, 2006.
[56] G.H. Golub, C. Reinsch, Singular value decomposition and least squares solutions, Numerische Mathematik, 14 (1970) 403-420.
[57] J.S. Bendat, Spectral techniques for nonlinear system analysis and identification, Shock and Vibration, 1 (1993) 21-31.
[58] B. Hinz, R. Blüthner, G. Menzel, S. Rützel, H. Seidel, H.P. Wölfel, Apparent mass of seated men—determination with single-and multi-axis excitations at different magnitudes, Journal of Sound and Vibration, 298 (2006) 788-809.

[59] M. Tarabini, B. Saggin, D. Scaccabarozzi, G. Moschioni, Hand-arm mechanical impedance in presence of unknown vibration direction, International Journal of Industrial Ergonomics, 43 (2013) 52-61.
[60] R.D. Sill, E.J. Seller, Accelerometer Transverse Sensitivity Measurement Using Planar Orbital Motion, in: 77th Shock and Vibration Symposium, 2006.
[61] M. Planitz, Inconsistent Systems of Linear Equations, The Mathematical Gazette, (1979) 181-185.
[62] G. Manson, K. Worden, M. Wood, Analysis of Reciprocity Breakdown in Nonlinear Systems, in: Journal of Physics: Conference Series, IOP Publishing, 2012, pp. 012031.